POST-PRINT

The Marine Isotope Stage 1 to 5 cryptotephra record of Tenaghi Philippon, Greece: Towards a detailed tephrostratigraphic framework for the Eastern Mediterranean region

Sabine Wulf[1,2,3], Mark Hardiman[3], Richard A. Staff[4,5], Andreas Koutsodendris[2], Oona Appelt[6], Simon P.E. Blockley[7], J. John Lowe[7], Christina J. Manning[7], Luisa Ottolini[8], Axel K. Schmitt[2], Victoria C. Smith[5], Emma L. Tomlinson[9], Polina Vakhrameeva[2], Maria Knipping[10], Ulrich Kotthoff[11,12], Alice M. Milner[7], Ulrich C. Müller[13], Kimon Christanis[14], Stavros Kalaitzidis[14], Polychronis C. Tzedakis[15], Gerhard Schmiedl[12,16], Jörg Pross[2]

[1] Senckenberg Research Institute and Natural History Museum, Senckenberganlage 25, D-60325 Frankfurt, Germany.
[2] Institute of Earth Sciences, Heidelberg University, Im Neuenheimer Feld 234-236, D-69120 Heidelberg, Germany.
[3] Department of Geography, University of Portsmouth, Buckingham Building, Lion Terrace, Portsmouth, PO1 3HE, United Kingdom.
[4] Scottish Universities Environmental Research Centre (SUERC), University of Glasgow, Rankine Avenue, Scottish Enterprise Technology Park, East Kilbride, G75 0QF, United Kingdom.
[5] Research Laboratory for Archaeology and the History of Art, University of Oxford, 1-2 South Parks Rd, Oxford, OX1 3TG, United Kingdom.
[6] Helmholtz Centre Potsdam, GFZ German Research Centre for Geosciences, Section 4.3 Chemistry and Physics of Earth Materials, Telegrafenberg, D-14773 Potsdam, Germany.
[7] Centre for Quaternary Research, Department of Geography, Royal Holloway, University of London, Egham, Surrey, TW20 0EX, United Kingdom.
[8] National Research Council of Italy (CNR)-Institute of Geosciences and Earth Resources (IGG), Unit of Pavia, Via A. Ferrata 1, 27100 Pavia, Italy.
[9] Department of Geology, Trinity College Dublin, The University of Dublin, Dublin 2, Ireland.
[10] Institute of Botany, University of Hohenheim, Garbenstraße 30, D-70593 Stuttgart, Germany.
[11] Center for Natural History, University of Hamburg, Bundesstraße 55, D-20146 Hamburg, Germany.
[12] Institute for Geology, University of Hamburg, Bundesstrasse 55, D-20146 Hamburg, Germany.
[13] Parlamentsstraße 32, D-60385 Frankfurt, Germany.
[14] Department of Geology, University of Patras, GR-26504 Rio-Patras, Greece.
[15] Environmental Change Research Centre, Department of Geography, University College London, Pearson Building, Gower Street, London WC1E 6BT, United Kingdom.
[16] Center for Earth System Research and Sustainability, University of Hamburg, Bundesstrasse 55, D-20146 Hamburg, Germany

* Corresponding author: sabine.wulf@port.ac.uk (S. Wulf)

Keywords: tephrochronology, last glacial-interglacial cycle, Tenaghi Philippon, Eastern Mediterranean region, peat record, Italian volcanism, Santorini eruptions

Abstract

The iconic climate archive of Tenaghi Philippon (TP), NE Greece, allows the study of short-term palaeoclimatic and environmental change throughout the past 1.3 Ma. To provide high-quality age control for detailed palaeoclimate reconstructions based on the TP archive, (crypto)tephra studies of a peat core 'TP-2005' have been carried out for the 0–130 ka interval. The results show that the TP basin is ideally positioned to receive tephra fall from both the Italian and Aegean Arc volcanic provinces. Two visible tephra layers, the Santorini Cape Riva/Y-2 (*c*. 22 ka) and the Campanian Ignimbrite (CI)/Y-5 (*c*. 39.8 ka) tephras, and six primary cryptotephra layers, namely the early Holocene E1 tephra from the Aeolian Islands (*c*. 8.3 ka), the Campanian Y-3 (*c*. 29 ka) and X-6 tephras (*c*. 109.5 ka), as well as counterpart tephras TM-18-1d (*c*. 40.4 ka), TM-23-11 (*c*. 92.4 ka) and TM-33-1a (*c*. 116.7 ka) from the Lago Grande di Monticchio sequence (southern Italy), were identified along with repeatedly redeposited Y-2 and CI tephra material. Bayesian modelling of the ages of seven of the primary tephra layers, 60 radiocarbon measurements and 20 palynological control points have been applied to markedly improve the chronology of the TP archive. This revised chronology constrains the age of tephra TM-18-1d to 40.90–41.66 cal ka BP (95.4% range). Several tephra layers identified in the TP record form important isochrons for correlating this archive with other terrestrial (e.g., Lago Grande di Monticchio, Sulmona Basin and Lake Ohrid) and marine (e.g., Adriatic Sea core PRAD 1-2 and Aegean Sea core LC21) palaeoclimate records in the Mediterranean region.

1. Introduction

In light of current anthropogenic climate change, detailed temporal-spatial reconstructions of past natural climate variability are required. This holds true particularly for the climatically highly sensitive Eastern Mediterranean region, which is currently experiencing increased frequency and intensity of droughts and heat waves (e.g., Giorgi and Lionello, 2008; IPCC, 2014). Past short-term climate change as evidenced in marine cores from the North Atlantic

(e.g., Shackleton et al., 2000) and ice cores from Greenland (e.g., NGRIP members, 2004) is also registered in Mediterranean palaeoclimate archives. However, the exact age relationships of climate signals recorded in these archives have remained difficult to decipher due to a lack of precise age control. Long key records from this region include the annually laminated archive from Lago Grande di Monticchio (e.g., Allen et al., 1999; Brauer et al., 2007; Martin-Puertas et al., 2014), the Sulmona and Fucino Basins in Italy (e.g., Giaccio et al., 2012, 2017b; Regattieri et al., 2017), and Lake Ohrid (e.g., Sadori et al., 2016; Wagner et al., 2017), Lake Prespa (e.g., Damaschke et al., 2013; Panagiotopoulos et al., 2014) and the Tenaghi Philippon peatland (e.g., Pross et al., 2015; Tzedakis et al., 2006) in the Balkan Peninsula. In addition, precise correlation of terrestrial records with marine records from the Adriatic, Ionian and Aegean Seas is notoriously difficult due to dating uncertainties stemming from unknown or regionally variable radiocarbon reservoir ages (e.g., Rohling, 1994; Siani et al., 2001). Precise land-sea correlations can, however, be obtained through using event markers such as volcanic ash (tephra) layers that are preserved in the respective sedimentary archives. Tephras from explosive eruptions are deposited synchronously, often over wide geographic areas, and provide independent chronological markers in geological archives when well dated (e.g., Thorarinsson, 1944; Lowe, 2011). The Eastern Mediterranean region is ideally suited for a tephrochronological approach due to (i) the frequent activity of high-explosive, volcanoes in central and southern Italy, the Aegean Arc (Greece), central and eastern Anatolia (Turkey), and the East Carpathians (Romania) during the Quaternary (Fig. 1a); (ii) distinctive glass chemical compositions of tephras derived from different volcanic sources that enable unambiguous identification; and (iii) wide tephra dispersal plumes transported by prevailing westerly, but also minor northerly and southerly, winds, leading to the stratigraphical layering of tephras derived from different source regions (e.g., Druitt et al., 1995; Federman and Carey, 1980; Keller et al., 1978; Narcisi and Vezzoli, 1999).

The Tenaghi Philippon (TP) peatland in NE Greece is situated in an ideal geographical position to record eruptions of Eastern Mediterranean volcanoes (Fig. 1), and has a long history of palaeoclimatic and environmental research that extends back to coring campaigns

during the 1960s (van der Wiel and Wijmstra, 1987a, 1987b; Wijmstra, 1969; Wijmstra and Smit, 1976; see review of Pross et al., 2015, and references therein). The millennial-scale-resolution pollen records generated from these early TP cores for the last *c*. 1.35 Ma revealed strong similarities with deep-sea oxygen isotope records (e.g., Tzedakis et al., 2006; van der Wiel and Wijmstra, 1987b; Wijmstra and Groenhart, 1983; Wijmstra and Young, 1992).

Because the core material recovered through the drilling efforts from the 1960s has long since deteriorated and also suffered from partially limited core recovery, the potential of the TP archive for the analysis of short-term climate and ecosystem variability has long remained untapped. Therefore, two new long cores (TP-2005 and TP-2009) were drilled in 2005 and 2009 (Pross et al., 2007, 2015). The excellent core recovery achieved during these later drilling campaigns allows high-resolution (i.e., decadal to centennial) analyses (e.g., Fletcher et al., 2013; Milner et al., 2012, 2013, 2016; Müller et al., 2011; Pross et al., 2009).

A full, state-of-the-art tephrostratigraphic record for the TP sediment sequence, (crypto)tephra analysis has been conducted on the upper 34 m of the TP-2005 core, encompassing the time interval of the last *c*. 130 ka (Marine Isotope Stages [MIS] 1 to 5/6). This core interval has been selected because it spans the last full glacial-interglacial cycle and reveals pronounced millennial-scale climate variability similar to those reported from other high-resolution, tephra-dated Eastern Mediterranean palaeoclimate archives. Hence, it offers the potential for distal correlation of palaeoclimate signals in this region using common tephra isochrons (see Section 6.4).

In this study, we present major and trace element geochemical data for visible and non-visible (crypto)tephras from the 1–34 m depth interval of the TP-2005 core. Where the new data are combined with previously published tephra data (e.g., Müller et al., 2011, Albert et al., 2015, Pross et al., 2015: see details in Section 3), the results allow refined correlation of individual tephra layers to their respective volcanic sources. Published ages for the assigned tephra eruptions, together with radiocarbon dates and palynological control points from the TP archive, lead to an improved age model for the TP sequence, while refinement of the tephra record allows more secure correlations with other high-resolution palaeoclimate archives. Our

results therefore provide additional critical anchor points to underpin the distal tephrostratigraphical framework of the Eastern Mediterranean region.

2. Regional setting

The TP site is situated in the Philippi peatland within the southeastern part of the Drama Basin in NE Greece (Fig. 1b). The Drama Basin (40–200 m a.s.l.; Fig. 1) formed as a low-elevation graben structure resulting from post-orogenic, arc-parallel extension that started in the late early or middle Miocene (Christanis, 1983; see Pross et al., 2015, for a discussion of its geological evolution). The basin is bordered by the Phalakron Range (2,232 m a.s.l.) to the north, the Menikion Range (1,956 m a.s.l.) to the west, the Pangaeon Range (1,956 m a.s.l.) to the south, and the Lekanis Mountains (1,150 m a.s.l.) to the east; to the southeast, the Symvolon Hills (477 m a.s.l.) separate the basin from the northern Aegean Sea. Today, several streams that discharge into the Angitis River and onward into the Strymon River drain the Drama Basin.

The Philippi peatland harbours nearly 200 m of limnotelmatic sediments, which make it the thickest known peat-dominated succession in the world (Christanis, 1987). A shallow unconfined aquifer exists at ~1–1.5 m below the surface in the central part of the basin (Georgakopoulos et al., 2001). Between 1931 and 1944, the Philippi peatland was drained for intensive agricultural cultivation, which has caused severe disturbances at the peat surface and subsidence that nowadays exceeds 7 m in the central part of the peatland (Christanis, 2016).

The regional climate is characterised by a typical Mediterranean seasonal regime modified by continental influence. During winter, anomalously cold and windy episodes occur that are triggered by southward outbreaks of polar air masses from the Russian High (Saaroni et al., 1996). Today's average annual precipitation amounts to 459 mm, with September being the driest (18 mm) and December being the wettest months (55 mm) (www.geoclima.eu). Moisture availability is mainly linked to the penetration of westerly storm tracks and Mediterranean cyclogenesis (Lionello et al., 2006; Xoplaki et al., 2004).

The TP site is located in a favourable downwind position with respect to the potential volcanic sources of tephra, *c*. 820–870 km east of alkaline Roman and Campanian, calc-alkaline Aeolian Island and peralkaline Pantelleria volcanoes (Italy), and *c*. 520–550 km north-northwest of calc-alkaline Aegean Arc volcanoes (e.g., Santorini, Nisyros, Yali, Kos) (Fig. 1a). Both the Italian and Aegean volcanic provinces are home to restless volcanoes that have explosively erupted during the Late Quaternary (e.g., Druitt et al., 1989, 1999; Keller et al., 1978; Narcisi and Vezzoli, 1999; Paterne et al., 1988; Sulpizio et al., 2003; Zanchetta et al., 2011). Widely dispersed trachyphonolitic and rhyolitic-dacitic tephras have been detected in numerous sedimentary archives in the Aegean-Levantine (e.g., Eastwood et al., 1999; Federman and Carey, 1980; Keller et al., 1978; Leicher et al., 2016; Margari et al., 2007; Satow et al., 2015; Vinci, 1985) and Black Sea regions (e.g., Çağatay et al., 2015; Kwiecien et al., 2008; Wulf et al., 2002), some with trajectories towards the TP site. Other potential Late Quaternary tephra sources that may have impacted the TP site include the Ciomadul volcanic complex in Romania (*c*. 600 km north of TP; e.g., Harangi et al., 2015; Karátson et al., 2016; Molnár et al., 2018) and Central Anatolia (e.g., Acigöl, Hasan Dagi, and Erciyes Dagi; *c*. 930 km east-southeast of TP; e.g., Kuzucuoglu et al., 1998; Sarikaya et al., 2017; Schmitt et al., 2011) (Fig. 1a). However, erupted calcalkaline (high-silica) rhyolites from both these provinces are normally dispersed either towards the east (e.g., Cullen et al., 2014; Wulf et al., 2016) or south (e.g., Hamann et al., 2010; Neugebauer et al., 2017) and therefore may not necessarily be registered in the TP sequence.

3 Previous tephra studies of the TP sequence

In the 1980s, short (<15 m long) cores from the Tenaghi Philippon basin were examined for their tephrostratigraphic potential. These efforts initially yielded four visible tephra horizons that were mineralogically characterised, and tephra ages were constrained by radiocarbon dates of over- and underlying sediments (Christanis, 1983). Two prominent tephra layers, labelled ‘unterer Tuffit’ and ‘oberer Tuffit’ by Christanis (1983), were tentatively correlated with Late Pleistocene Campanian and Santorini tephras that occur in deep-sea sediments in the Eastern

Mediterranean Sea, namely the Y-5 and Y-2 tephras, radiocarbon dated at TP to >28 ^{14}C ka BP and *c.* 14 ^{14}C ka BP, respectively. Christanis (1983) also mentioned a Holocene tephra (*c.* 3.6–4 ^{14}C ka BP) and a layer intercalated between the Y-5 and Y-2 tephras (*c.* 19 ^{14}C ka BP) of unknown origin. In a later study, St. Seymour et al. (2004) were the first to geochemically analyse three visible tephra horizons (PhT1, PhT2, PhT3) recovered from new cores from the marginal zone of the Philippi peatland (cores Ph1, Ph2 and Ph3; Fig.1), but in similar stratigraphic positions to those described by Christanis (1983). The major element glass compositions of the lowermost tephras PhT2 and PhT3 confirmed the correlations of Christanis (1983) with the Y-2/Cape Riva tephra from Santorini (*c*. 22 cal ka BP; Bronk Ramsey et al., 2015) and the Y-5/Campanian Ignimbrite (CI) eruption from Italy (39.85 ka; Giaccio et al., 2017a), respectively. The youngest visible tephra PhT1, dated to *c*. 13.0 ^{14}C ka BP, was found to be geochemically similar to the Y-2 tephra and therefore was tentatively assigned to an unknown eruption of Thera volcano, Santorini (St. Seymour et al., 2004). These results demonstrated that the TP site has received volcanic fall material from both Italian and Aegean Arc volcanoes. Hence, from a tephrostratigraphical perspective it can be considered a key archive for linking Central and Eastern Mediterranean palaeoclimate records.

The first studies on visible tephra layers of the newly drilled TP-2005 core (Pross et al., 2007) geochemically identified the Y-2 tephra (PhT2, ‘oberer Tuffit’) and CI/Y-5 (PhT3, ‘unterer Tuffit’) at 7.61 m and 12.87 m core depth (Müller et al., 2011; Lowe et al., 2012), but failed to detect the ~13.0 ^{14}C ka PhT1 tephra previously described by St. Seymour et al. (2004). Initial cryptotephra studies on the 4–19 m interval of the TP-2005 core were performed within the RESET project (Lowe et al., 2015), and as part of the results, Albert et al. (2015) highlighted the identification of the Campanian Y-3 tephra (29 cal ka BP; Bronk Ramsey et al., 2015). Furthermore, a preliminary account of cryptotephra findings from the 6–15 m interval of the TP-2005 core (MIS 2-4) was provided by Pross et al. (2015). Recent cryptotephra studies at Heidelberg University focused on TP-2005 core sections from 1-4 m (Middle-late Holocene) and 19-34 m (MIS 5) depth. In order to provide a complete tephrostratigraphy for the entire MIS 1 to MIS 5 interval, data and results of all (crypto)tephra studies conducted on the TP-

2005 core are either newly presented or reviewed in this paper.

4 Material and methods

The deep core TP-2005 was drilled in April 2005 in the southern part of the Philippi peatland (coordinates: 40°58'40"N, 24°13'42"E, 40 m a.s.l., Fig. 1c) using a non-rotating probe driven by a pneumatic hammer system on a WIRTH Eco l drill rig (Pross et al., 2007, 2015). It extends from the surface to 60 m depth and represents a sedimentary sequence that spans the Late Holocene to MIS 9c continuously (base at *c*. 312 ka; Fletcher et al., 2013). The core material was used to generate the first high-resolution (decadal- to centennial-scale) pollen record from the TP archive (Fletcher et al., 2013; Milner et al., 2012, 2013, 2016; Müller et al., 2011; Peyron et al., 2011; Pross et al., 2009, 2015; Schemmel et al., 2017) (Fig. 2).

Age control of the upper 15 m of the TP-2005 sequence, as currently published, is based on 20 radiocarbon ages and inclusion of the age estimates for the two visible Y-2 and Y-5/CI tephra layers (Müller et al., 2011; Pross et al., 2009); beyond the range of ^{14}C dating, the age control was based on either tuning to the NGRIP oxygen isotope curve (MIS 4; Müller et al., 2011) or alignment of the TP pollen data with marine core MD95-2042 from the Iberian Margin (MIS 5; Milner et al., 2012, 2016).

4.1 Preparation of tephra samples

Detailed cryptotephra analyses were carried out for the depth interval from 1 to 34 m of the TP-2005 core, spanning the period from the late Holocene (MIS 1; *c*. 2.8 cal ka BP) to the transition from the Penultimate Glacial (MIS 6) to the Last Interglacial (MIS 5e) (*c*. 130 ka BP). The uppermost metre of the TP peat sequence (<2.8 cal ka BP) was not considered for tephra sampling because it is compromised by anthropogenic disturbances, notably oxidation and self-combustion of the mire surface due to intense drainage and cultivation of the peatland (Kalaitzidis and Christanis, 2004). The core interval from 4 to 19 m was analysed at Royal Holloway, University of London (RHUL, UK). The core intervals from 1 to 4 m and from 19 to 34 m were analysed at Heidelberg University (Germany). In addition, the core interval between

4.9 and 5.3 m was resampled in Heidelberg in order to extract further glass shards from detected tephra layers for geochemical analyses.

The investigated sediments consist almost entirely of decomposed fen peat and peaty muds with two layers of lake marl at depths of 12.55–12.64 m and 32.00–33.00 m. The sequence was continuously subsampled in 10-cm-sections for initial cryptotephra scans. Samples in which tephra glass shards were detected were re-examined in 1-cm increments for isochron refinement. The preparation procedures for cryptotephra scanning followed slightly different methods at the RHUL and Heidelberg laboratories, which, however, did not impact upon the quality and comparability of data.

In a first step, samples were dried at 105°C for 12-24 hours and weighed, then combusted in a muffle furnace for 4 hours at 550°C and subsequently treated overnight with *c.* 15% H_2O_2 solution (Heidelberg) to remove organic matter. Carbonates were dissolved by a 7.5–10% HCl solution. The residues were sieved to yield 25–125µm (RHUL) and 20–100 µm (Heidelberg) grain-size fractions, to which a density flotation procedure was applied based on the protocols of Turney (1998) and Blockley et al. (2005). At RHUL, the residual samples of the light (2.0–2.55 g/cm^3) and heavy fractions (>2.55 g/cm^3) were mounted onto slides using Euparal^{TM} or Glycerol. The samples in Heidelberg were transferred into rectangular plastic lids using Ethanol and dried prior to inspection for glass shards under a transmitted light microscope. Counts of detected glass shards were based on the replicated 1-cm interval samples and are expressed as 'shards per g dry weight (shards/g_{dwt})'.

Where the number of glass shards was very low, individual shards were extracted with a 5 µl gas chromatography syringe fitted with a 110 µm diameter micromanipulator needle, transferred onto a resin stub and covered with Specifix^{TM} resin (RHUL). Alternatively, glass shards were handpicked with a single-hair brush into a single-hole aluminium stub and embedded in Epofix^{TM} resin (Heidelberg) prior to sectioning and polishing for geochemical analyses. Samples with very high tephra-shard concentrations were directly sprayed and mounted onto stubs. Identified tephra layers were labelled using the mean isochron depth in the TP-2005 core in meters below the surface (e.g., TP05-7.61).

In order to test potential correlations with the tephra samples from TP, medial-distal tephras (samples TM-18-1d, TM-18-4, TM-18-9e and TM-27; Wulf et al., 2006, 2012; Wutke et al., 2015) were sampled from the lacustrine sediment record of Lago Grande di Monticchio (southern Italy; Fig. 1) and geochemically re-analysed with the same instrument as the potential TP tephra correlatives. In addition, juvenile material from the proximal Cape Tripiti pumice fall deposits, which correspond to the 26 ka marine Y-4 tephra (Fabbro et al., 2013), was sampled by R. Gertisser (Keele University, UK) at Cape Tripiti at the southern coast of Therasia Island, Santorini (coordinates: 36.41401°N, 25.3439°E) and provided for geochemical analysis.

4.2 Geochemical analyses

4.2.1 Electron probe microanalyses (EPMA)

Single tephra glass shards were analysed for their major element compositions using a JEOL JXA8600 wavelength-dispersive (WDS) electron microprobe at the Research Laboratory for Archaeology and the History of Art, University of Oxford, UK (RHUL samples from 7 to 19 m), a CAMECA-SX51 (WDS) instrument at the Institute of Earth Sciences at Heidelberg University (Heidelberg samples from 4.9 to 5.3 m and 19 to 34 m), and a JEOL JXA8500F at the GFZ Potsdam (Heidelberg samples from 1 to 4 m and tephra TP05-31.255) (Supplement 1). The instrument at Oxford used an accelerating voltage of 15 kV, a 6 nA beam current and a defocused 10 µm beam. Count times for elements were 10 seconds for Na, 30 seconds for Si, Al, K, Ca, Fe, Mg, Ti and Mn, and 60 seconds for P and Cl. The instrumental setup for the Heidelberg instrument was 15 kV, 10 nA and a 10 µm beam; count times were 10 seconds for all elements. The probe at GFZ Potsdam used a 15 kV voltage, a 10 nA beam current and a 10 µm beam with count times of 20 s for the elements Fe, Cl, Mn, Ti, Mg, and P, and 10 s for F, Si, Al, K, Ca, and Na. A range of MPI-DING glasses including GOR128-G, GOR132-G, ATHO-G and StHs6/80 (see Jochum et al., 2006) and natural Lipari obsidian (Hunt and Hill, 1996; Kuehn et al., 2011), were employed as secondary glass standards for all instruments in order to maintain inter-laboratory consistency of analytical data (Supplement 1). Major element

geochemical data were recalculated on a volatile-free basis to 100 wt% (normalised data) for comparison with potential proximal and distal tephra correlatives. In this respect, tephras TM-18-1d, TM-18-4, TM-18-9e, and TM-27 from the Lago Grande di Monticchio record and the Santorini Cape Tripiti pumices were additionally analysed with the Oxford and GFZ instruments (see Supplement 2).

4.2.2 Laser-Ablation Inductively Coupled Plasma-Mass Spectrometry (LA-ICP-MS)

The trace elemental composition of the coarser-grained TP tephras from the core interval corresponding to MIS 2–4 (i.e., TP05-7.07, TP05-7.26, TP05-7.61, TP05-9.70, TP05-9.78, and TP05-12.87) and Monticchio tephra samples TM-18-1d, TM-18-4 and TM-18-9e were measured using LA-ICP-MS apparatus at the Department of Earth Sciences, RHUL, applying an Agilent 7500ce coupled to a Resonetics 193 nm ArF excimer laser-ablation system (RESOlution M-50 prototype) with a two-volume ablation cell (Müller et al., 2009; Tomlinson et al., 2010). The laser was deployed to analyse single circular 'spot' samples, with spot sizes varying between 25 and 54 µm; larger spot sizes were always used if possible to increase precision (see Section 3.4.10). The repetition rate was 5 Hz and the count time 40 s (200 pulses) on samples and 20 s on gas blanks (background) before and after each measurement. The elements measured were Sc, Ti, V, Ni, Rb, Sr, Y, Zr, Nb, Ba, La, Ce, Pr, Nd, Sm, Eu, Gd, Dy, Er, Yb, Lu, Ta, Pb, Th, and U. Secondary standards included the MPI-DING glasses GOR128-G, ATHO-G and StHs6/80, while NIST-612 was used as the internal calibration standard. Si values imported from EPMA-WDS analyses were used as the internal standard for unknowns and GeoRem values for standards (Jochum et al., 2006). Data reduction was performed manually using a Microsoft Excel macro, which allowed removal of data that were affected by microcrystals or vesicle components. All LA-ICP-MS trace element data are summarised in Supplements 1 and 2.

4.2.3 Secondary Ion Mass Spectrometry (SIMS)

Trace elemental compositions of finer-grained (<25 µm) cryptotephra samples were obtained

by SIMS analyses (Supplement 1). Individual glass shards from the RHUL tephra samples (i.e., TP05-7.07, TP05-9.23, TP05-9.38, TP05-9.51, TP05-13.34, TP05-13.54, and TP05-14.50) were measured at the Institute of Geosciences and Earth Resources (IGG)-CNR, Unit of Pavia, Italy, using a CAMECA IMS 4f ion probe with a current intensity of 0.5–0.7 nA and a spot diameter of 5–8 μm. The width of the energy slit was 50 eV and the voltage offset applied to the sample accelerating voltage (+ 4500 V) was -100 V. The filtered secondary ions were extracted and focused under an ion image field of 25 μm. We used the largest contrast diaphragm (400 μm) and field aperture (1800 μm) at a mass resolving power of ~600 (M/ΔM). A waiting time of 450 s was necessary to obtain steady-state sputtering conditions, and four acquisition cycles using the following count times per cycle were performed: Li (5 s), Be (5 s), Si (2 s), K (2 s), Sc (5 s), Ti (4 s), V (5 s), Cr (5 s), Rb (5 s), Sr (5 s), Y (5 s), Zr (5 s), Nb (5 s), Cs (8 s), Ba (8 s), La (10 s), Ce (10 s), Nd (10 s), Sm (15 s), Dy (20 s), Er and Yb (15 s each), Th and U (20 s each). Standards used for calibration and interference correction were the following: NIST-SRM 610 (Pearce et al., 1997), BCR-2G (USGS), BB basalt glass (inner CNR-IGG standard), and WY1 basaltic glass (CEA/CNRS - CE/Saclay, France) (for details of the reference concentrations assumed see Supplement 1).

Cryptotephras processed in Heidelberg (i.e., TP05-5.075, -19.915, -25.195, -25.465, -27.915, -32.225 and -32.265) and glass shards from the visible Campanian Ignimbrite layer at 12.87 m core depth were analysed at Heidelberg University using both a CAMECA IMS 3f and CAMECA 1280-HR (HIP) ion probe with a respective 5 nA/1 nA current intensity and a spot diameter of 10–5 μm. The width of the energy slit was 50 eV and the voltage offset applied to the sample accelerating voltage (+ 10 kV) was -105 V/-75 V. Pre-sputtering time was 120 s/30 s, and five acquisition cycles with the following count times per cycle were obtained: Si (2 s/0.5 s), Rb (5 s/3 s), Sr (5 s), Y (5 s/3 s), Zr (5 s/3 s), Nb (5 s/6 s), Ba (5 s), La (5 s/6 s), Ce (5 s/6 s), Th (20 s/10 s) and U (20 s/12 s). The NIST-SRM 612 glass standard was used as an internal (primary) standard for both SIMS instruments alongside secondary reference materials such as the rhyolitic ATHO-G and the andesitic StHs6/80-G glass standards (Jochum et al., 2006).

4.2.4 Bayesian chronological modelling

In order to refine the age-depth model for the TP-2005 core the Bayesian statistical software OxCal ver. 4.3 (Bronk Ramsey, 2017) was applied. Poisson-process deposition sequences ('P_Sequences') were utilised for successive core sections (Bronk Ramsey, 2008; Bronk Ramsey and Lee, 2013). A model averaging approach ('variable k') was applied to the section for which contiguous (5 cm resolution) ^{14}C data were available (i.e., 12.87–14.80 m core depth, *c.* 39 to 48 cal ka BP; Staff et al., in prep.), whereas a conservatively low rigidity (k=10) was applied to the core sections with fewer dated levels, allowing increased uncertainty ranges between dated core depths. The IntCal13 calibration curve (Reimer et al., 2013) was used for all radiocarbon data, and objective outlier analysis was applied (Bronk Ramsey, 2009b; Bronk Ramsey et al., 2010). Median modelled ages were imported into the program AnalySeries 2.0.8 (Paillard et al., 1996) in order to plot the TP-2005 palaeo-proxy data on the new time scale (Supplement 3) and to provide new age estimates of identified tephras (Table 1).

5. Results: Description and correlation of tephras

Two visible tephras and 40 cryptotephra layers have been identified in the 1–34 m interval of core TP-2005 (Fig. 2). With the exception of three cryptotephra layers for which shards could not be extracted, all tephra layers have been characterised in terms of their major element glass composition. Trace compositional glass data were obtained from the two visible tephras and from a total of 24 cryptotephra layers using either LA-ICP-MS or SIMS analysis; two tephras (i.e., TP05-7.07 and TP05-12.87) were analysed using both techniques in order to test the compatibility of LA-ICP-MS and SIMS data.

The chemical data repeatedly revealed the presence of redeposited components from the Y-2 and/or Y-5/CI visible tephra layers (7.61 m and 12.87 m depth) in most cryptotephra layers. Only six layers revealed distinctive geochemical features that enabled confident allocation to primary tephra fallout. The new mean age estimates derived from Bayesian modelling, pollen-based stratigraphical positions, glass shard concentrations, geochemical compositions and source correlations of all detected tephra layers are described below in stratigraphic order from

top to base of TP-2005.

5.1. MIS 1 (Holocene) tephras

TP05-2.625 and TP05-3.375 (*c*. 5.67 and 6.53 cal ka BP)

The youngest cryptotephras, TP05-2.625 and TP05-3.375, are tightly constrained layers confined to 2.62–2.63 m and 3.37–3.38 m core depth, with glass shard peak concentrations of 95 and 12 shards/g_{dwt}, respectively (Fig. 3a). The major-element glass compositions of both cryptotephras are trachyphonolitic with narrow concentration ranges of 61.5–62.4 wt% SiO_2, 18.8–19.6 wt% Al_2O_3, 3.0–3.3 wt% FeO, 1.8–2.5 wt% CaO, and alkali (K_2O/Na_2O) ratios of 1.7–3.2 (TP05-2.625) and 1.1–1.5 (TP05-3.375) (Fig. 4a). This alkaline composition suggests a Campanian (Italian) source, more specifically within the Campi Flegrei (CF) volcanic field. Widespread mid-Holocene tephras from this region are only known from the Astroni sequence, Agnano Monte Spina and Averno 1 eruptions (Di Vito et al., 1999; referred to hereafter as the 'AAA' cluster). They form a geochemically relatively homogenous cluster of tephra layers dated to *c*. 4.1–4.6 cal ka BP and *c*. 5.1–5.4 cal ka BP in proximal tephra deposits (Smith et al., 2011), and have been previously described from distal sites in the southern Adriatic Sea (Siani et al., 2004) and in Lake Shkodra in Albania/Montenegro (Sulpizio et al., 2010a). Other widely dispersed tephras from the Campanian province include the phonolitic Avellino (3945 ± 20 cal yr BP; Sevink et al., 2011) and older Mercato tephras (8,535 ± 90 cal yr BP; Zanchetta et al., 2011) from Mount Vesuvius, both identified in lake records from the Balkans (Damaschke et al., 2013; Leicher et al., 2016; Sulpizio et al., 2010a, 2010b). However, despite some similarities in silica and CaO concentrations none of the TP cryptotephra chemistries match the major-element composition of Holocene CF (Smith et al., 2011) or Vesuvian tephras (Tomlinson et al., 2015) (Fig. 4a). Instead, they fully fall within the compositional field of the Campanian Ignimbrite (CI) that occurs as a thick layer in TP sediments *c.* 9-10 m further down-core. Therefore, we interpret cryptotephras TP05-2.625 and TP05-3.375 as re-deposited CI tephra material most likely through anthropogenically induced erosional processes (see Section 6.1). Thus, these layers cannot serve as marker horizons for the TP-2005 sequence.

TP05-5.075 (*c*. 8.26 cal ka BP)

TP05-5.075 (5.05–5.10 m depth) is an early Holocene cryptotephra with low glass shard concentrations (12 shards/g_{dwt}) that immediately precedes the palynologically and organic geochemically defined 8.2 ka climatic event (Pross et al., 2009; Schemmel et al., 2016) (Fig. 3a). The major element composition of five glass shards is bimodal between alkaline trachyphonolitic (n=4) and calc-alkaline rhyolitic (n=1). The trachyphonolitic component is similar to that of cryptotephra TP05-3.375 and is characterised by concentration ranges of 60.8–62.2 wt% SiO_2, 18.8–20.6 wt% Al_2O_3, 2.6–3.3 wt% FeO, 1.9–2.1 wt% CaO, and alkali ratios of 1.0–1.3 (Fig. 4a). SIMS trace elemental data display a rather heterogeneous composition with 271–343 ppm Rb, 33–44 ppm Sr, 9–49 ppm Y, 187–563 ppm Zr, 42–97 ppm Nb, 23–381 ppm Ba, 40–106 ppm La, 52–197 ppm Ce, 10–45 ppm Th, and 4–15 ppm U. The geochemical data suggest a Campanian origin. During the early Holocene, violent eruptions of Somma-Vesuvius and the CF produced several tephra deposits, notably the widespread Mercato tephra (Vesuvius; 8,535 ± 90 cal yr BP; Zanchetta et al., 2011), which has also been detected in sediments from Lake Ohrid (Leicher et al., 2016), and CF tephra deposits at Fondi di Baia (9,610 ± 85 cal yr BP; Smith et al., 2011) and Pigna San Nicola (9,367 ± 166 cal yr BP; Di Vito et al., 1999; Smith et al., 2011). Comparisons of major element glass data obtained from these tephras yield a tentative correlation with the Fondi di Baia eruption, although this cannot be confirmed by trace-element data (Fig. 4a). Instead, the best chemical match of all analysed trachyphonolitic glass shards is with Campanian Ignimbrite compositional data (Fig. 4a), suggesting again the impact of secondary re-deposition processes.

The rhyolitic glass component of cryptotephra TP05-5.075 has concentrations in SiO_2 of 76.7 wt%, in FeO of 1.55 wt%, in CaO of 0.68 wt%, in Cl of 0.45 wt%, and an alkali ratio of 1.3. Hence, it shows a good match with the glass composition of the Gabellotto-Fiumebianco pumices from Lipari, Aeolian Islands (Fig. 4b). These deposits represent the proximal equivalent of the marine E1 tephra (e.g., Albert et al., 2017), which has been identified in Tyrrhenian (Paterne et al., 1988), Adriatic (7,770 ± 70 ^{14}C yr BP; Siani et al., 2004) and Ionian

deep-sea sediments (7,810 ± 45 ^{14}C yr BP; Caron et al., 2012) within early Holocene sapropel S1. The calibrated age of the E1 tephra at 8,270 ± 96 cal yr BP (Caron et al., 2012) is in excellent agreement with the stratigraphic position of the rhyolitic component of cryptotephra TP05-5.075 right below the 8.2 ka climatic event, implying that it reflects primary deposition.

In summary, the 5-cm-thick sediment segment across which cryptotephra TP05-5.075 occurs contains both a re-deposited CI component and low concentrations of a primary fall of the E1 tephra. Due to the lack of reproducibility of chemical data at higher resolution (viz. 1-cm sample increments), it was impossible to further constrain the positions of the reworked and primary tephra components. Therefore, a mean depth of 5.075 m has been adopted for the E1 tephra isochron in the TP-2005 core.

5.2 MIS 2 tephras

TP05-7.07, TP05-7.26 and TP05-7.61 (*c*. 18–22 cal ka BP)

TP05-7.61 is one of two visible tephra layers occurring diffusively throughout the 7.46–7.61 m interval (Fig. 3a). This primary fallout layer sits within MIS 2, just after a sharp increase and contraction in total tree pollen percentages (up to *c*. 20%). A cryptotephra component appears above the visible layer for a further 16 cm (Fig. 3a). Major and trace element glass compositions of TP05-7.61 reveal a homogenous calc-alkaline rhyolitic composition with narrow geochemical ranges of 70.9–72.0 wt% SiO_2, 14.1–14.7 wt% Al_2O_3, 2.7–3.3 wt% FeO, 4.8–5.6 wt% Na_2O, and 2.8–3.1 wt% K_2O (Fig. 5), a homogeneity that is also apparent in trace-element concentrations of Zr (289**–**322 ppm), Rb (104**–**109 ppm), Sr (72**–**80 ppm), and Th (14.5**–**16.7 ppm). Based on major element data, the visible TP05-7.61 tephra layer in core TP-2005 has previously been assigned by Müller et al. (2011) to the Cape Riva eruption of Thera volcano, Santorini (22,024 ± 321 cal yr BP; Lee et al., 2013; Bronk Ramsey et al., 2015, and references therein) and its marine distal equivalent, the Y-2 tephra (e.g., Keller et al., 1978; Wulf et al., 2002). Our trace elemental data support this correlation. The TP05-7.61/Y-2 tephra is likely identical to the *c*. 4 cm thick PhT2 tephra previously identified by St. Seymour et al. (2004) in previous short cores Ph1, Ph2 and Ph3, and most likely to the Upper Tephra (‘obere

Tuffitlage', *c*. 13,900 ^{14}C yr BP), generally found between depths of 3.2 and 8.7 m in numerous short cores from across the Philippi peatland (Christanis, 1983). Therefore, TP05-7.61 forms a valuable tephrochronological marker in the TP-2005 core dating to 22,024 ± 321 cal yr BP.

Two further dispersed cryptotephra layers (>10,000 shards/g_{dwt}) of identical rhyolitic major and trace element glass compositions appear at depths of 7.07 m and 7.26 m in the TP-2005 core (Figs. 3a, 5). They most likely represent re-deposited material of the underlying primary TP05-7.61/Y-2 tephra. However, it is worth noting that the shard concentration in these layers is much higher than in the majority of the cryptotephra layers detected in the TP-2005 sequence (see Figs. 3, 7). St. Seymour et al. (2004) described a visible tephra layer, PhT1, with a geochemical affinity to Y-2 in a similar stratigraphic position only a few decimeters above the primary PhT2/Y-2 tephra. The PhT1 layer has been radiocarbon-dated in core Ph2 to *c*. 10,152 ± 57 ^{14}C yr BP (11,735 ± 325 cal yr BP) and thereby assigned to a potentially younger, as yet unknown eruptive event from Thera (Santorini) volcano (St. Seymour et al., 2004). This correlation, however, was based solely on comparison with a conventional radiocarbon age of 12,950 ± 756 ^{14}C yr BP obtained from carbonized plant remains in a palaeosol directly overlying the Cape Riva ignimbrites at a proximal site on Santorini (Pichler and Friedrich, 1976). To date, there is no field, geochemical or additional geochronological evidence for an early Holocene/Lateglacial tephra from Thera volcano that approximates the Cape Riva/Y-2 glass composition (e.g., Druitt et al., 1999, 2015). The only distal tephra originating from Santorini with an early Holocene age has been reported from SE Aegean Sea core LC21 (cryptotephra LC21-2.005; Satow et al., 2015; Fig. 1). The major and trace element glass composition of this tephra, however, is more similar to that of the 3.6 ka Minoan/Z-2 tephra than to the Cape Riva/Y-2 tephra (Fig. 5). Consequently, we interpret tephra PhT1 not as a primary fallout deposit, but as a result of post-depositional recycling of PhT2/Y-2 material (see Section 6.1), which may correlate with either the TP05-7.07 or the TP05-7.26 cryptotephra layers.

TP05-8.90 and TP05-8.96 (*c*. 27.6 and 27.7 cal ka BP)

TP05-8.90 and TP05-8.96 are two cryptotephra layers with negative glass shard distribution skews over 4-5 cm wide intervals and low shard peak concentrations of 275 and 65 shards/g_{dwt}, respectively. Both tephra layers sit within early MIS 2 in an interval of low, but increasing total tree-pollen percentages (*c*. 2.7–8.1 %; Fig. 3a). Unfortunately, geochemical data could not be obtained from these layers due to problems of reproducibility during subsampling for geochemical analyses.

5.3 MIS 3 tephras

TP05-9.23, TP05-9.38, TP05-9.51, TP05-9.70 and TP05-9.78 (*c*. 28.2–29.2 cal ka BP)

This cluster of five cryptotephra deposits comprises one primary cryptotephra layer (TP05-9.70) and redeposited tephra material. The primary layer TP05-9.70 sits within a MIS 3 interval of low (*c*. 8 %) total tree pollen percentages (Figs. 2, 3b). It shows a highly positive distribution skew with a peak of ca. 2060 shards/g_{dwt} and a vertical stratigraphic spread of glass shards over 8 cm (Fig. 3b). Glass chemical data reveal a bi-modal mixed geochemical population of both alkaline trachytic and sub-alkaline rhyolitic composition in a 2:1 ratio, respectively (Fig. 5). Major elements in the main, trachytic component range from 60.1–62.7 wt% SiO_2, 18.1–18.7 wt% Al_2O_3, 2.8–3.8 wt% FeO, and 2.2–2.8 wt% CaO with alkali ratios of 2.1–2.8. Trace element concentrations also show a heterogeneous composition with ranges of 211–307 ppm Zr, 300–347 ppm Rb, 92–116 ppm Ce, 49–63 ppm La, 145–1601 ppm Ba, 314–845 ppm Sr, 32–48 ppm Nb, 22–28 ppm Y, and 17–26 ppm Th. Glass shards of the same trachytic major and trace element compositions are also found in three cryptotephra layers up to 47 cm above tephra TP05-9.70, i.e., in TP05-9.23 (56 shards/g_{dwt}), TP05-9.38 (1258 shards/g_{dwt}) and TP05-9.51 (1028 shards/g_{dwt}) (Fig. 3b). Both the major and trace element compositions of the trachytic component of TP05-9.70 and of the overlying cryptotephras best match that of the Y-3 tephra from the Campi Flegrei (29,059 ± 178 cal yr BP; Bronk Ramsey et al., 2015) as previously recognized by Albert et al. (2015) (Fig. 5). Because it has the highest shard count, we define TP05-9.70 as the primary fallout layer and consider the overlaying cryptotephras TP05-9.23, TP05-9.38 and TP05-9.51 as re-deposited material derived from the primary layer.

Consequently, TP05-9.70 is considered a reliable isochron dating to 29,059 ± 178 cal yr BP.

The rhyolitic component of TP05-9.70 is rather homogenous, with major element concentration ranges of 71.3–71.5 wt% SiO_2, 14.4–14.6 wt% Al_2O_3, 2.9–3.3 wt% FeO, 1.6–1.8 wt% CaO, 5.1–5.5 wt% Na_2O, and 2.9–3.0 wt% K_2O, and trace element values of 309–336 ppm Zr, 106–112 ppm Rb, 59-62 ppm Ce, 29-31 ppm La, 489-491 ppm Ba, 76–82 ppm Sr, 11-12 ppm Nb, 50-52 ppm Y, and 14.7–15.0 ppm Th. Both the major and trace element glass compositions are identical to a single glass shard in the overlying tephra TP05-9.51 and to rhyolitic cryptotephra TP05-9.78 (952 shards/g_{dwt}) that directly underlies and merges into the primary TP05-9.70/Y-3 tephra. Comparisons of glass data from rhyolitic volcanic centres in the Eastern Mediterranean region that were active during MIS 3 (e.g., Santorini, Nisyros, Yali, Acigöl, and Lipari) strongly suggest a Santorini provenance for the TP05-9.78 tephra (Fig. 5). Considering the timing of tephra deposition at TP at *c*. 29 cal ka BP, a potential source eruption could be the Cape Tripiti/Y-4 eruption of Santorini (*c*. 26 ka BP; Fabbro et al., 2013; Schwarz, 2000). However, the glass chemical composition of Cape Tripiti/Y-4 differs significantly from that of TP05-9.78, with lower SiO_2 (68.8–71.4 wt%) and higher FeO (2.9–4.6 wt%) and CaO (1.8–2.6 wt%) values as well as slightly different trace-element concentrations (Fig. 5). The good chemical match with the Cape Riva/Y-2 tephra (Fig. 5), however, is inconsistent with the stratigraphic position of TP05-9.78, more than two meters below the visible TP05-7.61/Y-2 tephra. Such a displacement of primary tephra material could result from post-depositional processes (see Section 6.1).

TP05-12.87 (*c*. 39.7 cal ka BP)

TP05-12.87 (12.64–12.87 m depth) is the lowermost and thickest visible tephra layer in the TP-2005 sequence. There is also a cryptotephra component that is distributed over a 20 cm interval above the primary layer. Total tree-pollen percentages immediately below and above the visible tephra are *c*. 5 % and 1.4 %, respectively, indicating deposition well after the onset of Heinrich Stadial H4 (Fig. 3b). Glass shards of TP05-12.87 reveal a phonotrachytic composition with ranges of 60.0–62.3 wt% SiO_2, 18.1–18.9 wt% Al_2O_3, 0.3–0.5 wt% TiO_2, 2.7–

4.1 wt% FeO, 0.2–0.9 wt% MgO, 1.6–2.8 wt% CaO, and bimodal alkali ratios of 1.1–1.3 and 2.5–3.7. Trace element concentrations also show a heterogeneous composition with large ranges of 176–678 ppm Zr, 276–477 ppm Rb, 84–251 ppm Ce, 44–133 ppm La, 13–662 ppm Ba, 18–563 ppm Sr, 28–126 ppm Nb, 19–56 ppm Y, and 13–55 ppm Th.

TP05-12.87 corresponds stratigraphically to the lower tephra ('untere Tuffitlage') of Christanis (1983) and to tephra PhT3 of St. Seymour et al. (2004); it has been previously correlated in the TP-2005 sequence by Müller et al. (2011) and Lowe et al. (2012) with the Campanian Ignimbrite (CI) eruption of the Campi Flegrei, Italy, (39.85 ± 0.14 ka; $^{40}Ar/^{39}Ar$; Giaccio et al., 2017a). This attribution is supported by our new trace element data (Figs. 5, 6). TP05-12.87 therefore provides a valuable independent marker for calibrating the TP-2005 chronology.

TP05-13.25 to TP05-14.50 (6 layers, *c*. 40.1–46.7 cal ka BP)

Below the visible Campanian Ignimbrite deposit, a total of six cryptotephra layers were detected between 13.25 and 14.50 m core depth (Fig. 3b). TP05-13.25, TP05-13.28 and TP05-13.34 form three tightly clustered peaks between 13.22 and 13.35 m depth, and all sit within a period of elevated total tree pollen percentages (*c*. 30–40 %) (Figs. 2, 3b). TP05-13.25 is a well-constrained layer with a negative distribution skew between 13.22 and 13.26 m and a maximum peak of 1311 shards/g_{dwt}. TP05-13.28 is confined to a 3-cm-thick interval with a peak of 1455 shards/$g_{dwt.}$ TP05-13.34 shows the strongest cryptotephra peak below the visible CI layer at 3092 shards/g_{dwt}. The geochemical glass compositions of all three cryptotephra layers are alkaline phonotrachytic with ranges of 60.4–62.2 wt% SiO_2, 18.2–19.0 wt% Al_2O_3, 0.32–0.46 wt% TiO_2, 2.4–3.6 wt% FeO, 0.27–0.79 wt% MgO, and 1.5–2.8 wt% CaO, and bimodal alkali ratios of 1.0–1.5 and 2.5–3.8 (Fig. 6). SIMS trace element concentrations of TP05-13.34 show a less homogenous composition with ranges of 263–793 ppm Zr, 305–431 ppm Rb, 116–275 ppm Ce, 65–160 ppm La, 42–136 ppm Ba, 17–292 ppm Sr, 39–136 ppm Nb, 29–63 ppm Y, and 23–70 ppm Th (Fig. 6).

Cryptotephra TP05-13.54 forms a 5-cm-thick horizon with a peak of *c*. 1582 shards/g_{dwt}.

TP05-13.92, in turn, is a tightly (3-cm-thick) constrained cryptotephra with a peak of ca. 2038 shards/g_{dwt}. TP05-13.54 and TP05-13.92 are situated within periods of low tree-pollen percentages (*c*. 6 % and 1.4–7.9 %, respectively; Fig. 3b). Both cryptotephras have heterogeneous trachyphonolitic major and trace element glass compositions that are indistinguishable from the overlying triple-cryptotephra set (Fig. 6, Supplement 1).

The lowermost cryptotephra TP05-14.50 has a diffuse shard distribution between 14.46 and 14.54 m core depth, with a maximum shard count of *c*. 40 shards/g_{dwt}, and lies in a period of low total tree percentages (*c*. 3–6 % total tree pollen). It has a homogenous trachytic geochemical glass composition with relatively low alkali ratios of 1.0–1.3, which overlaps with that of the five overlying cryptotephras (Fig. 6).

Glass compositions of all six cryptotephras that precede the CI suggest an origin from the Campi Flegrei in southern Italy, and best match the major and trace element composition of tephra TP05-12.87/CI. Only cryptotephra TP05-13.34 reveals an additional different component that more closely resembles the composition of the medial-distal tephra TM-18-1d in the Lago Grande di Monticchio sediment record (Fig. 6). TM-18-1d has a major element affinity to the CI, but differs in trace element composition by having higher concentrations in Y (50–64 ppm), Zr (618–795 ppm), Nb (115–143 ppm), La (116–148 ppm), Ce (227–281 ppm), Th (47–64 ppm), and U (17–22 ppm), and lower values in Rb (447–636 ppm), Sr (4–20 ppm), and Ba (4–95 ppm) (Supplement 2). At Lago Grande di Monticchio, TM-18-1d is dated by annual layer counting to 37,360 varve yr (Brauer et al., 2007). It precedes the deposition of the CI in this record by approximately 590 years (Wutke et al., 2015). Given that the $^{40}Ar/^{39}Ar$ age for the CI eruption is 39.85 ± 0.14 ka (Giaccio et al., 2017a), the varve age of TM-18-1d can be considered too young, and therefore this date should be used with caution.

In summary, all six pre-CI cryptotephras appear to consist of re-deposited CI material that was moved from the primary fall layer to lower peat levels by post-depositional processes (see Section 6.1). Only tephra TP05-13.34 contains some glass shards that are slightly more distinctive, and which we tentatively correlate with tephra TM-18-1d at Lago Grande di Monticchio. Due to the uncertain varve age of this tephra in the Monticchio record, cryptotephra

TP05-13.34 is not included as a chronological marker for the TP-2005 age model.

5.4 MIS 4 tephra

TP05-17.91 (*c*. 65.1 ka)

TP05-17.91 is a tightly constrained cryptotephra layer with a glass shard concentration peak of 749 shards/g_{dwt} that occurs in the middle of MIS 4 where there is a slight increase in relatively low tree-pollen percentages (to *c*. 12 %; Fig. 3b). Unfortunately, it was not possible to extract glass shards from this tephra for geochemical analyses at this stage, and hence the volcanic source is yet unknown.

5.5 MIS 5 tephras

TP05-19.915 to TP05-25.135 (8 layers, *c*. 74 – 95.6 ka)

Eight cryptotephra layers occur between 19.91 and 25.15 m depth, showing mainly tight (within 1-2 cm wide intervals) glass shard distributions with the following peak concentration values: 144 shards/g_{dwt} (TP05-19.915), 76 shards/g_{dwt} (TP05-21.045), 64 shards/g_{dwt} (TP05-22.065), 73 shards/g_{dwt} (TP05-23.055), 217 shards/g_{dwt} (TP05-24.055), 234 shards/g_{dwt} (TP05-24.915), 22 shards/g_{dwt} (TP05-25.085), and 83 shards/g_{dwt} (TP05-25.135). Only the lowermost cryptotephras (TP05-25.085 and TP05-25.135) show rather dispersed distributions over 5- and 4-cm-wide intervals, respectively (Fig. 7). Cryptotephras TP05-19.915, TP05-21.045 and TP05-22.065 sit within the palynologically defined MIS 5a interval, which records abrupt increases of temperate tree pollen (to *c*. 50–70 %). TP05-23.055 and TP05-24.055 occur at the end and the beginning of MIS 5b, respectively, in intervals that are characterised by short-term increases in temperate tree pollen percentages (*c*. 50 %). The preceding layers TP05-24.915, TP05-25.085 and TP05-25.135 were deposited during late MIS 5c, within a period of increased temperate tree pollen (*c*. 55–80 %) (Figs. 2, 7). All eight cryptotephra layers show similar heterogeneous phonotrachytic compositions that are characterised by ranges in concentrations of 59.7–64.2 wt% SiO_2, 17.8–20.8 wt% Al_2O_3, 2.6–3.8 wt% FeO, and 1.5–3.0 wt% CaO, and bimodal alkali ratios of 1.0–1.5 and 1.7–3.3 (Fig. 8a+b). SIMS trace element

data from cryptotephras TP05-22.065, TP05-24.055 and TP05-25.135 confirm this heterogeneity and strongly suggest a correlation of all layers with the Campanian Ignimbrite (Figs. 8a+b, 9). Two single glass shards extracted from cryptotephras TP05-21.045 and TP05-22.065 are rhyolitic, with the same compositional field as the Cape Riva/Y-2 tephra (Fig. 8a). The overall chemical evidence and the fact that most of the TP tephras occur within the top 10 cm of individual core segments suggests that they all consist of re-distributed material from the overlying visible CI and Y-2 tephras and thus cannot be used as tephrochronological markers. The remobilization of tephra material is here most likely due to drilling procedures (see Section 6.1).

TP05-25.195 (*c*. 95.8 ka)

Cryptotephra TP05-25.195 is a well-constrained, stratigraphically normally distributed cryptotephra layer (39 shards/g_{dwt}) that occurs between 25.18 and 25.20 m depth. It sits in the middle of MIS 5c within an interval of decreased temperate tree pollen (*c*. 50 %) (Figs. 2, 7). Major element glass compositions indicate a heterogeneous trachytic chemistry with concentration ranges of 60.2–62.9 wt% SiO_2, 18.2–20.1 wt% Al_2O_3, 2.6–4.2 wt% FeO, and 1.7–2.9 wt% CaO, and bimodal alkali ratios of 1.0–1.5 and 1.6–3.5 (Fig. 8b, Table 2). Trace element glass compositions confirm this heterogeneity with concentration ranges of 235–392 ppm Rb, 18–582 ppm Sr, 19–54 ppm Y, 170–638 ppm Zr, 25–113 ppm Nb, 14–770 ppm Ba, 39–118 ppm La, 75–217 ppm Ce, 12–47 ppm Th, and 4–16 ppm U. Most major and associated trace element glass compositions match that of the CI (Figs. 8b, 9a), implying that there is also re-deposited material in this core section. However, a minor component (2 glass shards) deviates from the CI composition and plots within the geochemical field of the prominent MIS 5c tephra TM-23-11/POP1 (Fig. 8b). This tephra derives from a yet unknown Campanian eruption; it has been described from the Sulmona Basin (POP1) and Lago Grande di Monticchio (TM-23-11) records in central and southern Italy, respectively (Giaccio et al., 2012; Wulf et al., 2006), and correlated with marine tephras C-22 in the Tyrrhenian basin (Paterne et al., 2008) and PRAD-2517-2525 in the Adriatic Sea (Bourne et al., 2010, 2015). The TM-

23-11/POP1 tephra is dated in Sulmona by $^{40}Ar/^{39}Ar$ to 92.4 ± 4.6 ka (Giaccio et al., 2012) and in Monticchio by annual layer counting to 96,210 ± 4,810 varve yr (Martin-Puertas et al., 2014), respectively. Our results strongly suggest an allocation of TP05-25.195 to TM-23-11/POP1, which leads us to integrate the $^{40}Ar/^{39}Ar$ age of this tephrochronological marker into the new TP age model.

TP05-25.465 to TP05-27.035 (5 layers, c. 96.7–105.4 ka)

Another five cryptotephra layers have been identified in peat-dominated lithologies between 25.46 and 27.04 m core depth, corresponding to the middle to early phase of the MIS 5c interval. They are tightly constrained in the core, with shard peaks of ca. 956 shards/g_{dwt} (TP05-25.465), 41 shards/g_{dwt} (TP05-26.055), 8 shards/g_{dwt} (TP05-26.35), 34 shards/g_{dwt} (TP05-26.915), and 110 shards/g_{dwt} (TP05-27.035). The glass shards of cryptotephras TP05-25.465, TP05-26.055, TP05-26.915 and TP05-27.035 are dominated by a heterogeneous phonotrachytic composition with concentration ranges of 59.7–65.4 wt% SiO_2, 16.4–20.6 wt% Al_2O_3, 2.7–3.6 wt% FeO, and 1.6–2.8 wt% CaO, and bimodal alkali ratios of 1.0–1.5 and 2.2–3.1. Major element data and additional trace element data available for TP05-25.465 strongly suggest a correlation of the phonotrachytic glass component in all four cryptotephras with the CI (Figs. 8b,c, 9a). A minor rhyolitic component found in tephras TP05-25.465 and TP05-26.915 best matches the Y-2 composition (Fig. 8b, c). Within this reworked material, an additional minor, but distinctive alkaline glass composition is evident, i.e., TP05-25.465 contains a phonotrachytic glass with CaO concentrations of 1.4 wt% and an alkali ratio of 0.9, which are both lower than in the CI (Supplement 1). However, to date no Campanian tephra of comparable composition has been described for this time interval, thus preventing a firm tephra assignment. Furthermore, cryptotephras TP05-26.35 and TP05-26.915 both exhibit a single trachytic glass composition with concentrations in SiO_2 of 61.9–62.2 wt%, FeO of 2.7–3.0 wt%, CaO of 1.7–1.9 wt%, and low alkali ratios of 0.7–0.8 (Fig. 8c, Supplement 1). This composition best matches the chemistry of the primary X-6 tephra deposited one meter further down-core in the TP-2005 sequence. The composition of another single glass shard in

cryptotephras TP05-26.915 and TP05-27.035 slightly resembles the composition of the Campanian X-5 tephra (106.2 ± 1.3 ka $^{40}Ar/^{39}Ar$; Regattieri et al., 2015) (Fig. 8c), but a firm correlation cannot be established at this point due to the lack of trace element data.

In summary, out of the five cryptotephras discussed here only TP05-25.465 may relate to a primary eruption at *c*. 97.5 ka, which is of a yet unknown, but likely Campanian origin. Therefore, to date no tephrochronological tie-point for the TP age model is available from this part of the TP-2005 core.

TP05-27.915 and TP05-27.995 (*c*. 109.4–109.7 ka)

Cryptotephras TP05-27.915 and TP05-27.995 form tightly constrained normal and reversed distributed layers with peak glass shard concentrations of 92 and 128 shards/g_{dwt}, respectively. They are positioned in the middle (TP05-27.995) and at the onset (TP05-27.995) of MIS 5d and C24, a cold period that is characterised by sharp declines in total (*c*. 30 %) and temperate tree-pollen percentages (*c*. 5 %; Figs. 2, 7). Both cryptotephras are phonotrachytic in composition, which suggests a Campanian origin. The major element chemistry is heterogeneous with concentration ranges of 60.2–64.9 wt% SiO_2, 18.3–20.6 wt% Al_2O_3, 2.7–3.6 wt% FeO, and 1.1–2.6 wt% CaO, and bimodal alkali ratios of 0.75–0.95 and 1.1–3.1 (Fig. 8c, Table 2). The bimodality of alkali ratios ($Na_2O>K_2O$ and $K_2O>Na_2O$) implies the presence of two distinct tephra components, which likely derive from different eruptions. Larger glass shards with $K_2O>Na_2O$ values and trace element compositions of 350–451 ppm Rb, 20–550 ppm Sr, 19–53 ppm Y, 172–676 ppm Zr, 26–131 ppm Nb, 20–648 ppm Ba, 42–118 ppm La, 76–220 ppm Ce, 13-48 ppm Th, and 4-19 ppm U suggests a correlation with re-deposited CI tephra material (Figs. 8c, 9b). The second component with $Na_2O>K_2O$ is restricted to smaller glass shards (<50 µm) and best matches the composition of the late Last Interglacial X-6 tephra. The X-6 tephra is a widespread tephra marker in the central-eastern Mediterranean that derived from a Plinian and co-ignimbritic plume from the Campanian region, but the specific centre is yet unknown (see e.g., Albert et al., 2012; Bourne et al., 2015; Giaccio et al., 2012; Keller et al., 1978; Leicher et al., 2016; Lucchi et al., 2008; Sulpizio et al., 2010b; Wulf

et al., 2012). X-6 is characterised by a typical bimodal peralkaline and low-K-alkaline chemistry, of which the latter is partly indistinguishable from the CI composition (Fig. 8c, Table 2, Supplement 2). The X-6 tephra has been precisely dated for the Sulmona Basin (POP4 tephra) and Lago Grande di Monticchio locations (TM-27) by $^{40}Ar/^{39}Ar$ methods using sanidine to 109.5 ± 0.9 ka (Regattieri et al., 2017) and by annual layer counting to 109,370 ± 5,469 varve yr (Martin-Puertas et al., 2014; Wulf et al., 2012), respectively. When compared to the tephrostratigraphic record from Lago Grande di Monticchio, cryptotephra TP05-27.915 shows the best fit to the X-6 tephra, which accords with its stratigraphic position in the middle of the C24 stadial, and therefore it is considered a useful isochron layer with an age of *c*. 109.5 ka.

TP05-31.255 (*c*. 120.9 ka)

Cryptotephra TP05-31.255 is a well-constrained layer between 31.24 and 31.26 m core depth, with a low glass shard peak concentration of 11 shards/g_{dwt} at 31.255 m depth. The tephra occurs in the middle of MIS 5e in an interval of high percentages of total tree (*c*. 97 %) and temperate tree taxa percentages (*c*. 78 %; Figs. 2, 7). TP05-31.255 has a heterogeneous trachyphonolitic glass composition with concentration ranges of 61.4–63.0 wt% SiO_2, 18.7–19.8 wt% Al_2O_3, 2.9–3.6 wt% FeO, and 1.1–2.5 wt% CaO, and low alkali ratios of 0.8–1.5. Trace element compositions of two larger glass shards show ranges in values of 282–382 ppm Rb, 33–92 ppm Sr, 21–46 ppm Y, 230–519 ppm Zr, 36–90 ppm Nb, 26–60 ppm Ba, 45–95 ppm La, 87–172 ppm Ce, 14–34 ppm Th, and 6–11 ppm U (Fig. 9). These shards can be confidently correlated with the CI, once again suggesting downward tephra remobilization in this core interval. The majority of TP05-31.255 major element chemical data, however, plots into the discrimination field of tephra TM-33-1a from Lago Grande di Monticchio (Martin-Puertas et al., 2014; Wulf et al., 2012) (Fig. 8d). This tephra has been assigned to the Punta Imperatore deposits on Ischia (116 ± 2.9 ka to 123 ± 3.8 ka K/Ar; Gillot et al., 1982) and is likely dated more accurately by annual layer counting to 116,700 ± 5,835 varve yr (Martin-Puertas et al., 2014). We use the varve age for integrating tephra TP05-33.255 into the new TP-2005 age model.

TP05-31.95 (*c*. 123.8 ka)

This cryptotephra has very low glass shard concentrations (7 shards across a 10-cm-thick interval) and occurs during early MIS 5e at the onset of a slight decline in total tree pollen (*c*. 91 %; Figs. 2, 7). TP05-31.95 shows both alkaline and calcalkaline glass compositions. The alkaline glass population is bimodal trachyphonolitic with one component (consisting of two shards) showing concentration ranges of 63.0–63.7 wt% SiO_2, 18.2–18.7 wt% Al_2O_3, 2.7–2.9 wt% FeO, and 1.8–2.0 wt% CaO, and alkali ratios of 1.3–1.4 (Fig. 8d). The second component (consisting of four shards) mainly differs in higher values of Al_2O_3 (18.8–19.3 wt%) and lower values of SiO_2 (62.1–62.7 wt%), CaO (0.7–1.3 wt%) and alkali ratios (0.7–1.1). Both compositions have a Campanian affinity and show similarities to Eemian tephras TM-33-1a, TM-33-2a and TM-37a recorded at Lago Grande di Monticchio (Wulf et al., 2012) but also to the Campanian Ignimbrite (Fig. 8d). However, due to the lack of trace element data for both the TP05-31.95 and the potentially correlative Monticchio tephras, it is not possible to make a firm correlation. The calcalkaline glass population (two shards) is rhyolitic, approximating both the major and trace element compositions of the Y-2 tephra from Santorini (Figs. 8d, 9b). The rhyolitic component in addition to the potential CI material suggests drilling-related tephra remobilization processes in this part of the TP-2005 sequence (see Section 6.1).

TP05-32.225 and TP05-32.265 (*c*. 124.9 and 125.1 ka)

Cryptotephras TP05-32.225 and TP05-32.265 are two closely spaced, tightly constrained layers with low glass peak concentrations of 13 and 21 shards/g_{dwt}, respectively. They are positioned within early MIS 5e in an interval of very high tree-pollen percentages (*c*. 95 %; Figs. 2, 7). Glass chemical compositions of both tephras are dominated by a relatively homogenous trachytic composition with concentration ranges in SiO_2 of 60.6–64.3 wt%, Al_2O_3 of 17.5–20.1 wt%, FeO of 2.8–3.3 wt%, and CaO of 1.7–2.1 wt%, and alkali ratios of 0.9–1.5 (Fig. 8d). Additional SIMS trace element data of a total of eight shards reveal values of 342–498 ppm Rb, 19–29 ppm Sr, 51–56 ppm Y, 616–731 ppm Zr, 105–135 ppm Nb, 13–26 ppm

Ba, 110–126 ppm La, 203–235 ppm Ce, 42–50 ppm Th, and 16–18 ppm U, strongly suggesting a correlation with the CI (Fig. 8d, 9b). TP05-32.225 has an additional rhyolitic component that approximates the Santorini Y-2 composition (Fig. 8d). Since no other large eruptions with similar compositions are known to have occurred from these centres during this time period, we consider both the trachytic and rhyolitic glass components as reworked tephra material, which may not be used as time markers for the TP chronology.

TP05-32.53 (*c*. 126.2 ka)

TP05-32.53 (32.52–32.54 m depth) is the deepest cryptotephra in the investigated core interval. It is a tightly constrained layer with a low glass shard concentration (2 shards/g_{dwt}, >10 shards in the 10-cm-thick scanning sample) that lies within early MIS 5e (*c*. 122.4–130 ka BP), where tree-pollen percentages are high (*c*. 87 %; Figs. 2, 7). Major element glass data reveal a heterogeneous phonotrachytic composition with concentration ranges of 60.1–62.6 wt% SiO_2, 18.8–20.2 wt% Al_2O_3, 2.8–3.5 wt% FeO, and 1.7–2.5 wt% CaO, and bimodal alkali ratios of 1.0–1.4 and *c*. 2.8 (Fig. 8d). The trace element composition of two glass shards with values of 372–398 ppm Rb, 23–24 ppm Sr, 48 ppm Y, 578–600 ppm Zr, 100–102 ppm Nb, 21–23 ppm Ba, 99 ppm La, 183–187 ppm Ce, 36 ppm Th, and 13–17 ppm U suggest a correlation of this glass population with the CI (Fig. 9b). One single glass shard shows a slightly more distinctive phonotrachytic composition with a lower CaO value of 1.3 and an alkali ratio of 0.7. The data indicate a Campanian origin, but the eruption cannot be further constrained at this time.

6. Discussion

6.1 Re-deposition of tephra shards

Our results show that in addition to *in situ* cryptotephras a considerable number of the recorded cryptotephra layers in the TP-2005 core contain secondary glass shards from the Campanian Ignimbrite and/or the Y-2 tephra. This suggests a complex history of re-deposition of tephra shards, with cross contamination between tephra layers. In the TP-2005 sequence, thick,

macroscopically visible layers represent the Campanian Ignimbrite and the Y-2 tephra at 7.61 and 12.87 m depth, respectively. Based on the stratigraphic positions of CI and Y-2 tephra material throughout the core sequence (Fig. 10), three main processes of tephra displacement are thought to be involved:

1) Post-depositional movement of tephra particles

Some of the reworked CI and Y-2 material is found stratigraphically close to the visible primary tephra layers. In the case of the TP05-7.61/Y-2 tephra, primary material has been displaced as much as *c*. 58 cm up-core (cryptotephra layers TP05-7.07 and TP05-7.26) and up to *c*. 220 cm down-core (cryptotephra layers TP05-9.23 to TP05-9.78) with respect to the visible layer. Reworked shards from the CI, in turn, were detected up to *c*. 167 cm below the primary deposit (cryptotephra layers TP05-13.25 to TP05-14.50), but are absent from the overlying lake marls and peat. This re-distribution is likely due to post-depositional movement of tephra material. Several experimental studies on peat deposits have shown that tephra shards can be moved vertically after deposition on a peat bog surface (e.g., Bjarnason, 1991; Payne and Gehrels, 2010; Payne et al., 2005). In lightly compacted peat, downward displacement is mainly by gravitational sinking, rainfall percolation and root penetration, particularly during times of a lowered water table, whilst upward displacement can result from vigorous plant growth or a rising water table (Payne and Gehrels, 2010). The scale of vertical tephra movement likely depends on the density and porosity of the surface peat and on the size of the tephra shards (Payne and Gehrels, 2010; Payne et al., 2005). These mechanisms might explain the vertical movement of most of the displaced Y-2 and CI tephra material within the subsurface of the Philippi peatland. The rather surprising extent to which Y-2 shards have been displaced both up-core and down-core suggests substantial fluctuations in the depth of the local water table leading to secondary re-deposition of tephra shards in the Philippi peatland. In contrast, tephra material derived from the CI is displaced exclusively down-core, possibly because the subsequent deposition of dense lake marls prevented upward movements when the water table was rising.

2) Secondary deposition of tephra particles

The re-distribution of CI tephra material in the 2–5 m section of the TP-2005 core (cryptotephra layers TP05-2.625, TP05-3.375 and TP05-5.075) is unlikely to reflect the displacement processes inferred above due to the long, vertical distance to the primary CI deposit (>7.5 m). Instead, they may be explained by secondary re-deposition resulting from anthropogenic exploitation of unconsolidated sediments and soils around the margins of the peat basin, leading to a release of tephra shards, which are then transported by wind or water to the peat surface into the basin (e.g., Payne and Gehrels, 2010). Other disturbance mechanisms that could lead to erosion and remobilisation of buried tephras include earthquake activity, natural fires, self-combustion or peat cutting (Payne and Gehrels, 2010). At TP, human agro-pastoral activities at the margin of the basin have been detected in sediments dating from *c*. 8.4 cal ka BP (Glais et al., 2016), suggesting that erosional and re-depositional processes may have played a role in this area since the onset of the Neolithic. Furthermore, drainage of the TP basin in 1931–1944 caused severe subsidence of the peatland resulting in the flooding of large areas and in the destruction of crop yields, which necessitates frequent deepening of the modern ditches and channels in the basin (e.g., Christanis, 2016).

3) Coring-related displacement of tephra particles

The third type of tephra displacement is associated with coring processes, particularly in the deeper part of the TP-2005 core. It is evidenced by the repeated occurrence in particular of CI, but also of Y-2 material at the tops and the ends of individual 1-m-long core segments between 17 and 34 m depth (Table 1). This repeating pattern most likely relates to the core-driving mechanism during drilling: When the core barrel is retracted, loose sediment (including tephra components) can slump into, and accumulate at the bottom of the borehole. In the next core segment recovered, these reworked sediments form a displaced top layer of variable thickness, which has to be rejected for pollen and tephra sampling. Between individual core retrievals small tephra shards can be gravitationally forced with water into lower peat levels as

a result of the load of the borehole water column. The latter was maintained constantly at a depth of 0–2 m below surface in order to avoid peat expansion at the bottom of the hole. The only exception was for the recovery of cores between 29 and 31 m depth, when the water level was minimized to *c*. 20 m depth below surface; these cores do not contain reworked tephra material. The distribution of re-mobilised CI and Y-2 tephra shards (Table 1) suggests that their penetration depth is not only a function of the load of the water column, but also of the loading residence time (i.e., the time interval between successive core recoveries). Core segments recovered within a routine time of 15–25 minutes generally exhibit evidence of reworked shards only in the uppermost 10 cm (e.g., cryptotephra layers TP05-21.045, Table 1), while longer time gaps of *c*. 45–60 minutes appear to result in displaced tephra shards being forced to depths of 20 cm or more into the top part of the subsequent core segment (e.g., cryptotephra layers TP05-32.225 and TP05-32.265).

Glass shard peak concentrations in top and basal samples affected by coring-related displacement of Y-2 and CI tephra particles in the 17–34 m interval is lower than 250 shards/g_{dwt} (Fig. 10, Table 1). However, two exceptions are cryptotephras TP05-17.91 and TP05-25.465, which exhibit significantly higher concentrations of 749 and 956 shards/g_{dwt} (Fig. 10). These tephras most likely contain a primary tephra component that adds to the reworked CI and Y-2 material.

In terms of the reliability of the palynological results, we do not expect pollen grains to be displaced by water into deeper peat levels, since pollen grains are more adhesive and substantially less dense than tephra shards (*c*. 1 g/cm^3 [e.g., van Hout and Katz, 2004] compared with glass-shard densities of >2 g/cm^3). Also, the concentration of *in situ* pollen grains would greatly exceed the number of any potentially re-deposited pollen grains and hence have only a negligible, if any impact on pollen spectra from the respective sections.

6.2 Revision of the TP-2005 age model

As described in the previous section, distinguishing between primary and re-deposited tephra material requires careful analysis of geochemical datasets, including trace-element

determinations, and independent stratigraphic control, which in this case is provided by high-resolution pollen stratigraphy. Integration of these data has enabled identification of six primary cryptotephras (TP05-5.075, TP05-9.70, TP05-13.34, TP05-25.195, TP05-27.915 and TP05-31.255), along with two visible tephras (CI and Y-2) the ages of which have previously been determined elsewhere by radiometric methods and/or varve chronology and can therefore be incorporated into a revised age model for the TP-2005 core.

Prior to this study, the chronology for the 1–34 m interval of the TP-2005 sequence has been established: (i) for the upper 15 m by radiocarbon dating, tephrochronology (visible Y-2 and CI tephras) and alignment of the Lateglacial to early Holocene pollen curve from the core with marine core SL152 (Müller et al., 2011; Pross et al., 2009); (ii) for the temperate tree pollen data between 15 and 19 m depth by alignment with the NGRIP oxygen isotope curve (Müller et al., 2011); and (iii) for the 19–34 m depth interval, by alignment with the pollen curve of marine core MD95-2042 from the Iberian Margin (Milner et al., 2012, 2016). Here we present a revised age model for the TP-2005 sequence that incorporates the ages of the additional primary tephra layers identified in the present study.

The timing of the eruptions to which the primary tephra layers reported here have been assigned are well constrained by a variety of approaches (Table 1). The ages of the youngest tephra correlatives (E1, Y-2 and Y-3) are based on radiocarbon dates obtained from marine sediments (E1; Caron et al., 2012), proximal volcanic deposits (Y-2; Bronk Ramsey et al., 2015, and references therein) and distal terrestrial sites (Y-3; Bronk Ramsey et al., 2015, and references therein). The original ^{14}C dates obtained for these eruptions have been calibrated using the Marine13 or IntCal13 calibration curves (Reimer et al., 2013) prior to their integration into the revised TP-2005 age model (Fig. 11). The corresponding tephra calendar ages, which are given in cal yr BP (1950) and include a 2σ error range, are 8,270 ± 96 cal yr BP for the E1 eruption, 22,024 ± 642 cal yr BP for Y-2, and 29,059 ± 356 cal yr BP for Y-3. The age of the visible tephra layer TP05-12.87 is well constrained by a new, precise $^{40}Ar/^{39}Ar$ date of the Campanian Ignimbrite (CI) eruption at 39.85 ± 0.14 ka (before AD 2015, 2σ error) ka (39,785 ± 140 cal yr before AD 1950; Giaccio et al., 2017a).

The tephra correlatives of the MIS 5 cryptotephras TP05-25.195, TP05-27.915 and TP05-31.255 have been dated both radiometrically and by varve chronologies, but these are not always in statistical agreement and have different precisions (Fig. 11b). For the integration of the ages of cryptotephras TP05-25.195 and TP05-27.915 into the new age model, preference is therefore given to the $^{40}Ar/^{39}Ar$ sanidine ages of the tephra correlatives POP1 (92.4 ± 4.6 ka, 2σ; Giaccio et al., 2012) and POP4 (X-6; 109.5 ± 0.9 ka, 2σ; Regattieri et al., 2017) rather than the varve-based ages of the respective Lago Grande di Monticchio tephra equivalents (96,210 ± 4,810 and 109,370 ± 5,470 varve yr, respectively; Martin-Puertas et al., 2014). For TP05-31.255, we use the Monticchio varve age of tephra TM-33-1a at 116,700 ± 5,825 varve yr (Brauer et al., 2007; Martin-Puertas et al., 2014) because of its higher precision compared with the wider range of the corresponding K/Ar dates (116 ± 2.9 ka to 123 ± 3.8 ka; Gillot et al., 1982) obtained from the proximal 'Punta Imperatore' deposits from Ischia.

In a first step towards constructing a revised age-depth model for the MIS 1–5 interval of the TP-2005 core, the above-mentioned tephra ages were compared with the previous chronologies established by Müller et al. (2011) and Milner et al. (2016). Figure 11a shows a comparison of all MIS 1–3 tephra ages (this study) with the former tephra-supported radiocarbon chronology for the uppermost *c*. 15 m of the TP-2005 sequence. The radiocarbon chronology is based on 17 AMS ^{14}C dates of bulk peat samples and three dates of snail shell fragments from the uppermost middle-late Holocene section (Müller et al., 2011), which have been re-calibrated here using the more recent IntCal13 calibration curve (Reimer et al., 2013) and incorporated into a Poisson-process ('P_Sequence') depositional model using the OxCal 4.3 program (Bronk Ramsey, 2008, 2009a). The comparison shows that most radiometric tephra ages agree with the radiocarbon chronology within 2σ error ranges. The only exception is in the early Holocene (Fig. 11a); here, a mean temporal deviation of 870 years can be observed between the published age of the E1/TP05-5.075 tephra (8,270 ± 96 cal yr BP; Caron et al., 2012) and the ^{14}C-interpolated age in the TP core (9,140 ± 695 cal yr BP). This deviation can be explained by an enhanced hard-water effect within the TP basin during the wet early Holocene period (Pross et al., 2009), although based on our data this hard-water effect

appears slightly less pronounced than the ~1000–1200 years originally proposed.

However, our new tephrochronological results for the MIS 5 interval of the TP-2005 core suggest that a more thorough revision of the former, pollen-based chronology of Milner et al. (2016) may be necessary (Fig. 11b). The original age model used ten age-control points at mid-transitions for the onset and end of the MIS 5 interglacial (Pangaion), interstadials (Doxaton-Drama and Elevtheroupolis) and stadials (Lydia I and II) to correlate the total tree pollen curves of cores TP-2005 and MD95-2042 (Milner et al., 2016) (Fig. 11b). According to this chronology, the cryptotephras TP05-25.195/TM-23-11, TP05-27.915/TM-27 and TP05-31.255/TM-33-1a would have mean ages of *c*. 98.8, 112.6 and 122.4 ka, respectively. These mean ages deviate systematically from the tephra-based ages derived from both the above-mentioned radiometric or Monticchio varve chronologies by >2600 years at the beginning of MIS 5c and by up to *c*. 5700 years during MIS 5e (Fig. 11b).

In view of these age discrepancies, we established a revised age-depth model for the MIS 1 to MIS 5 interval of TP-2005, integrating independent ^{14}C and tephra age estimates with those based on tuning with other high-resolution, well-dated proxy records in those core sections for which independent dates are not available (Figs. 11c, d, e; Supplement 3):

- For the uppermost 13 m (<40 cal ka BP), four imported tephra radiometric ages, twelve AMS-^{14}C dates based on snail fragments and bulk peat from Müller et al. (2011), and one ^{14}C age from pollen concentrates (Pross et al., 2009) have been included. In addition, the ages of five palynological tie points with marine core SL152 (Kotthoff et al., 2008a, b) were used instead of the reservoir-age affected radiocarbon dates obtained from early Holocene bulk peat samples (*c*. 7–11 cal ka BP; Pross et al., 2009). Radiocarbon dates from the glacial part of the record, however, do not appear to suffer from this reservoir-age effect, with radiocarbon age estimates corresponding well with independent ages of the visible TP05-7.61 (Y2) and TP05-12.87 (CI) tephra layers (see Albert et al., 2015 for details).
- The ~40–50 cal ka BP section is based on 44 new AMS-^{14}C dates of bulk peat samples (Supplement 3; Staff et al., in prep.) that substantially increase the temporal resolution of the previous radiocarbon chronology of Müller et al. (2011).

- The early MIS 3–MIS 5b interval (*c*. 50–90 ka) does not yet have independent time control, and hence recourse has been made to alignment of the TP pollen record with other well-dated proxy records that are considered to offer the best control points for this long time interval. Previous research has suggested that vegetation response to North Atlantic climate change was rapid and effectively synchronous across southern Europe (Roucoux et al., 2001; Sánchez Goñi et al., 2002; Tzedakis et al., 2002), which may justify a direct alignment of the TP pollen curve with other Mediterranean vegetation records. However, the 50–90 ka chronologies of the two available high-resolution pollen records, Lago Grande di Monticchio in southern Italy (Allen et al., 1999; Brauer et al., 2007) and marine core MD95-2042 from the Iberian margin (Sánchez Goñi et al., 1999), either exhibit large uncertainties (Lago Grande di Monticchio; Wulf et al., 2012) or are tuned to the NGRIP oxygen isotope record (MD95-2042; Sánchez Goñi et al., 2013, 2017). Since the ages of the onsets of Greenland Interstadials (GI) 9 to 12 in the NGRIP oxygen isotope record (Svensson et al., 2008) are within 2σ dating uncertainties of radiometrically-obtained ages for abrupt increases in total tree pollen concentrations (Fig. 12), tuning of the MIS 4–5 pollen record from TP directly to the NGRIP oxygen-isotope record is considered reasonable. Hence, for the 50–75 ka interval, seven chronological tie points of the onsets of Greenland Interstadials (GI) 13 to 19 based on NGRIP annual layer counting (GICC05; Svensson et al., 2008) and ss09sea age scale estimations (Wolff et al., 2010) have been transferred to midpoint transitions of defined peaks in total tree pollen percentages in the TP record (Fig. 12; Supplement 3). Because of increased dating uncertainties in the NGRIP chronology beyond 75 ka, we have integrated three original control points of Milner et al. (2016) for the 75–90 ka interval into the new TP-2005 age model by tuning the onset of GI 20/C19 and the transitions of the Lydia II (GI 21/C21) cold stage with the Mediterranean forest pollen signals of core MD95-2042 (Sánchez Goñi et al., 1999) (Supplement 3). These dates were derived by aligning the MD95-2042 planktonic $\delta^{18}O$ record (Shackleton et al., 2000) with the synthetic Greenland record of Barker et al. (2011).
- The chronology of the MIS 5c–MIS 5e section (*c*. 90–130 ka) is based on three imported

tephra ages, two of them derived from sanidine $^{40}Ar/^{39}Ar$ dating and one from the Lago Grande di Monticchio varve chronology. In addition to these independent time markers, tephrochronologically confirmed Monticchio varve ages (Martin-Puertas et al., 2014; Wulf et al., 2012) for five palynological tie points were transferred to the new TP-2005 chronology (Fig. 12). These represent palynologically and sedimentologically well-defined transitions at the ends and onsets of cold stages MON3/GS-24/C23 (103,000 ± 5,150 and 105,500 ± 5,275 varve yr) and MON2/GS-25/C24 (108,630 ± 5,431 and 110,429 ± 5,521 varve yr), and the MIS 6/MIS 5 boundary at 127,750 ± 6,388 varve yr (Martin-Puertas et al., 2014).

Consequently, the new age-depth model of the MIS 1–MIS 5 interval of the TP-2005 sequence synthesises a total of 61 independent time markers and 20 palynological alignment points (Supplement 3). Linear interpolation of these chronological markers, however, suggests a virtual hiatus at *c*. 25 m depth (Fig. 11c), which is not reflected in the sedimentological and/or palynological data. Therefore, an alternative age-depth model was generated using the Bayesian statistical software OxCal ver. 4.3 (Bronk Ramsey, 2017) (Figs. 11d, e), which is more consistent than the linear interpolation (Fig. 11c) with credible estimates of mean peat accumulation rates of *c*. 1 mm/a and 0.4 mm/a during the late/middle and early Holocene, respectively. For the core interval representing MIS 2 to MIS 5, mean accumulation rates were relatively constant at *c*. 0.2–0.3 mm/a, being in agreement with previous studies (Christanis, 1983; Kalaitzidis, 2007).

One of the highlights of establishing a partly independent, high-precision chronology for the TP-2005 sequence is the potential it provides for yielding more precise age estimates for currently poorly dated tephra layers (Table 1). For example, the age of TP05-13.34 (TM-18-1d) is estimated to between 40,900 and 41,660 cal yr BP based on our new chronology, which is slightly older than the age of 40,440 cal yr BP approximated from incremental varve counting for its counterpart in the Lago Grande die Monticchio record. Moreover, tephras TP05-25.195 (POP1/TM-23-11) and TP05-31.255 (TM33-1a) have been re-dated to 93,250–98,430 yr and 117,780–123,970 yr, respectively; these new ages are, however, still within the 2σ error range

of previously determined radiometric ages and/or varve-count estimates. All of the other Bayesian modelled TP tephra ages, E1, Y-2, Y-3, CI and X-6, are in very close agreement with published radiometric ages.

6.3 Re-evaluation of regional tephra deposition patterns

The (crypto)tephra results for the TP-2005 sequence show that some Italian tephras that are prominent in, for example, nearby lake records in the western Balkans (e.g., Lakes Ohrid and Prespa; *c*. 270–300 km from the TP site) are either not represented at all or are present in trace amounts only in the TP-2005 record (Fig. 12). This does not appear to be the result of chemical degradation, since glass shards in the visible tephra layers in the TP sequence are very well preserved.

These different distribution patterns can be explained by a number of factors. First of all, they may be due to differences in the depositional processes that were at work in the environmental settings of the respective archives. Such processes include hydrological focussing of tephra particles via fluvial transportation from the terrestrial catchment into the depocentres of Lakes Ohrid and Prespa, whereas the mire setting at TP predominantly captured the direct air fall. On the other hand, the variations in tephra thicknesses and occurrences can also be related to differences in atmospheric tephra dispersal caused by variations in local wind and precipitation patterns. Lakes Ohrid, Lake Prespa and Tenaghi Philippon are positioned in a climatic transition zone that is influenced by the complex interplay between moist Westerlies, cold-dry Etesian air masses from the North, warm-humid air from the south and cyclonic/anticyclonic atmospheric circulation patterns in the Aegean region (e.g., Hamann et al., 2008; Koutsodendris et al., 2017; Kutiel and Benaroch, 2002; Maheras et al., 2000; Wagner et al., 2017). It is particularly noteworthy that precipitation patterns differ substantially in the western and eastern Balkans: whereas mean annual precipitation in the Lake Ohrid and Lake Prespa region was *c*. 1000–1600 mm/yr during the 1940–1995 period, it was merely *c*. 500–800 mm/yr at Tenaghi Philippon (Fotiadi et al., 1999; Hijmans et al., 2005; https://www.eea.europa.eu). The two times higher rainfall received in the western part of the

Balkans results partially from orographic forcing of the moist Westerlies by the Dinarides and Pindos mountain ranges (Metaxas, 1978; Xoplaki et al., 2000). This enhanced precipitation results in a higher likelihood for atmospheric fallout of eastward-transported fine-grained Italian tephra in the western Balkans. Differences in precipitation between the western Balkans and TP may have played an even more important role during the last glacial, when a generally drier climate prevailed across the Balkan Peninsula compared to the warmer/moist conditions during MIS 1 and MIS 5 (e.g., Milner et al., 2012, 2013, 2016; Sadori et al., 2016; Tzedakis et al., 2002).

Furthermore, moist southerly winds during spring, summer and autumn can also enhance the dispersal and fallout of Aegean Arc tephras in the eastern Balkans and western Black Sea region. This is reflected, for example, by the striking thickness of the Y-2 tephra at TP (4-15 cm; St. Seymour et al., 2004; this study) and in the Sea of Marmara (1-7 cm; Wulf et al., 2002), approximately 530 km from the Santorini source volcano. Other Santorini eruptions of comparable magnitude such as the Late Holocene Minoan eruption are recorded in the Black Sea (e.g., Kwiecien et al., 2008) but not in sediments from the northern Aegean Sea, the Sea of Marmara (e.g., Aksu et al., 2008; Çağatay et al., 2015; Wulf et al., 2002) or at TP. This may indicate a stronger influence of westerly winds during the time of that eruption.

These considerations highlight the important influence of atmospheric and climatic conditions on tephra dispersal in the greater Balkan region. Additional dispersal complexities may arise from atmospheric circulation contrasts between glacial/stadial and interglacial/interstadial times.

6.4 Climatostratigraphic context of tephras in Eastern Mediterranean records

The identification of eight primary tephra layers in the MIS 1 to MIS 5 section of the TP-2005 sequence allows climate-proxy datasets from TP to be correlated with those from other long terrestrial and marine records in the Mediterranean region that have been analysed for their tephra content (Figs. 12, 13). For the time being, the terrestrial climate-proxy archives comprise mainly pollen data from lacustrine sediments, such as Lago Grande di Monticchio in

southern Italy and Lake Ohrid in Albania/Macedonia. Lago Grande di Monticchio provides a continuous high-resolution (decadal- to centennial-scale) vegetation and tephra record for the MIS 1-5 interval (e.g., Allen et al., 1999; Brauer et al., 2007; Martin-Puertas et al., 2014; Wulf et al., 2004, 2012), and therefore is the most suitable for comparison with the TP record (Figs., 12, 13). In the case of Lake Ohrid, high-resolution pollen data are presently only available for the MIS 5 interval (Sinopoli et al., 2018), while the generation of a continuous high-resolution pollen and cryptotephra record is still in progress (e.g., Leicher et al., 2016; Sadori et al., 2016; Wagner et al., 2017) (Figs. 1, 12, 13). Other valuable terrestrial tephra archives include the Sulmona and Fucino basins in central Italy (Fig. 1), although these are either incomplete for the MIS 1 to MIS 5 interval (Sulmona; Giaccio et al., 2012; 2013; Regattieri et al., 2015, 2017) or lack a comprehensive palaeoenvironmental dataset (Fucino; Giaccio et al., 2015, 2017b) (Fig. 13). A recent study has, however, provided a high-resolution oxygen isotope record for the MIS 5 interval in Sulmona (Regattieri et al., 2017) enabling a detailed comparison of precipitation data for the Central Mediterranean with the TP vegetation record for this time period (Fig. 12). The palaeoclimatic record from Ioannina in southwestern Greece (e.g., Tzedakis et al., 2003; Fig. 1) also offers the potential for detailed comparison with the TP record, but lacks a detailed tephrochronology.

Mediterranean deep-sea records, on the other hand, have rarely been examined for their (crypto)tephra content so far. The only marine records in the Central Mediterranean with detailed tephrostratigraphies spanning the MIS1 to MIS 5 time period are cores PRAD 1-2 from the Adriatic Sea (Bourne et al., 2010, 2015) and KC01B from the Ionian Sea (Insinga et al., 2014; Lourens, 2004); these cores register a number of tephra layers in common with TP (e.g. Y-3, CI, TM-23-11, and X-6; Fig. 13) but lack high-resolution proxy data. Aegean Sea core LC21, on the other hand, provides temporally highly resolved proxy datasets (Grant et al., 2012) and a detailed (crypto)tephrochronology (Satow et al., 2015); however the only common tephra is the CI, and proxy data from core LC21 are not available for this time interval (Satow et al., 2015) (Figs. 1, 13).

Hence detailed comparisons of Mediterranean palaeoclimatic records spanning the MIS-1

to MIS-5 interval are presently restricted to few terrestrial records (Figs. 1, 12, 13). Nevertheless, progress is being made in the identification of tephra isochrons that can aid these comparisons, and some of the key points to emerge from the new results presented here are as follows.

E1 tephra. The early Holocene E1 tephra from Lipari, Aeolian Islands, only occurs in the TP record and has been re-dated by the new TP-2005 age model to 8,255 ± 95 cal yr BP, which is in close agreement with the marine-reservoir corrected, calibrated ^{14}C ages of its marine tephra equivalents (Caron et al., 2012; Siani et al., 2004). The climatostratigraphic position of the E1 tephra in the TP record is *c*. 120 years prior to the onset of the palynologically well-defined 8.2 ka-event, which is dated in TP to 8140 ± 90 cal yr BP.

Y-2 tephra. The Santorini Y-2 tephra also only occurs in TP and is dated by the new TP-2005 age model to 21,885 ± 625 cal yr BP. This age accords with the age constrained by Lee et al. (2013) and Bronk Ramsey et al. (2015) based on two deposition records and proximal ^{14}C dates. In TP, the Y-2 tephra occurs within MIS 2, *c*. 530 years after the onset of Greenland Interstadial GI2.

Y-3 tephra. The Campanian Y-3 tephra, re-dated in TP-2005 to 29,040 ± 280 cal yr BP, occurs at TP and Lago Grande di Monticchio in a similar palynostratigraphic position within Greenland Stadial (GS) 5 and Heinrich Stadial H3. More specifically, the new TP-2005 chronology places the Y-3 deposition *c*. 2400 years after the onset of GS5/H3 (*c*. 31.44 cal ka BP) and 930 years prior to the onset of GI4 (*c*. 28.1 cal ka BP) (Fig. 12). The timing at TP differs from varve counts and sedimentation rate estimates at Lago Grande di Monticchio; here, deposition of the Y-3 tephra occurred *c*. 3430 years after the onset of GS5/H3 and 590 years before the onset of GI4, but is within 2σ uncertainties of both chronologies.

CI tephra. The new TP-2005 chronology re-dates the Campanian Ignimbrite to 39,680 ± 140 cal yr BP and places it at *c*. 1000 years after the onset of GS9/H4 (*c*. 40.58 cal ka BP) and 3280 years before the onset of GI8 (*c*. 36.3 cal ka BP). The resulting total duration of *c*. 4280 years for H4, however, strongly deviates from the *c*. 2000 years obtained through high-

precision incremental varve dating at Lago Grande di Monticchio (Wutke et al., 2015); there, the CI was deposited *c*. 820 years after the onset and *c*. 1170 years before the end of GS9/H4 (Wutke et al. (2015).

***TM-18-1d tephra*.** This tephra occurs in Lago Grande di Monticchio *c*. 590 years prior to the deposition of the CI and therewith *c*. 230 years after the onset of GS9/H4 (Wutke et al., 2015). In TP, where the TM-18-1d tephra correlative is newly dated to 41,280 ± 380 cal yr BP, the time difference between the GS9/H4 onset and tephra deposition is estimated to *c*. 720 years.

TM-23-11/POP1. The climatostratigraphic position of the TM-23-11 tephra in Monticchio is roughly defined within MIS 5c and *c*. 6800 years after the end of GS24/C23 (Martin-Puertas et al., 2014). The new TP-2005 age model re-dates this tephra to 95,840 ± 2,590 yr and allows a more precise palynostratigraphical placement *c*. 4,800 years after the decline of GS24/C23 and *c*. 2,690 years prior to the onset of GS23/C22. The position of TM-23-11 in TP at the onset of a short decline in total tree pollen percentages within the GI23 warm/wet interval coincides with the position of the POP1 tephra equivalent in the Sulmona Basin at the onset of a brief drier event during GI23 (Giaccio et al., 2012; Regattieri et al., 2015, 2017).

X-6 tephra. The X-6 tephra was first reported from MIS 5d deep-sea cores from the Eastern Mediterranean Sea by Keller et al. (1978). Its stratigraphic position was subsequently more tightly constrained in the Lago Grande di Monticchio records, where it occurs during cold event GS25/C24, *c*. 740 years before the onset of GI24 (Brauer et al., 2007; Martin Puertas et al., 2014). High-resolution oxygen isotope and new high-resolution vegetation data for the MIS 5 intervals in the Sulmona Basin and Lake Ohrid sediments (Regattieri et al., 2017; Sinopoli et al., 2018) allow a more detailed assessment of the climatostratigraphic position of the X-6 tephra and hence a direct comparison with the MIS 5 pollen record from TP. In Sulmona, the X-6 (POP4) tephra is positioned at the end of a brief wetter period that occurs in the middle of the arid interval correlated with the North Atlantic C24 cooling event (Regattieri et al., 2017). This position is in striking agreement with the occurrence of the X-6 tephra in the pollen records from Lago Grande di Monticchio, Lake Ohrid and TP at the end of a short event of increased

total pollen percentages, interpreted as a wetter incursion during the C24 dry period (Fig. 12). The age of the X-6 tephra has been re-modelled by the new TP-2005 chronology to 109,380 ± 860 yr, which is in accordance with the Lago Grande di Monticchio varve age and previous radiometric dates.

TM-33-1a tephra. This tephra is placed in the Lago Grande di Monticchio record within MIS 5e, *c*. 11,050 years after the MIS 6/5e transition (Martin Puertas et al., 2014). In TP, its tephra equivalent is re-dated to 120,875 ± 3095 yr, which makes it *c*. 4000 years older than its age estimate based on varve counting at Monticchio. The timing of the MIS 6/5e boundary is re-dated by the new TP-2005 age model to 129,040 ± 4170 yr, hence placing the deposition of TM-33-1a in TP *c*. 9,170 years after the onset of the Last Interglacial.

The comparison of the climatostratigraphic positions of tephras in the Monticchio and TP pollen records indicates similarities in the relative positions of tephras, but some divergence in absolute ages as they would derive from the pollen records (e.g., tephras Y-3, CI, TM-23-11, TM-33-1a). These differences do most likely not represent temporal leads or lags of vegetation responses to climate changes, but rather reflect resolution issues and chronological uncertainties of the different dating methods, namely varve counting at Monticchio *versus* radiometric dating and palynological tuning at TP. Hence, for a more robust assessment of the proposed climatostratigraphic positions of tephras, additional well-dated MIS 1-5 records from the Mediterranean region are much needed.

7. Summary and Conclusions

Examination of the 1–34 m interval of the TP-2005 core for cryptotephra content has led to the detection of five new cryptotephra layers that represent new primary fall events, adding to the Y-2, Y-3 and Campanian Ignimbrite volcanic ash layers previously identified. The new cryptotephras, which represent the most distal findings with regard to their sources, are the early Holocene E1 tephra from the Aeolian Islands, the Campanian POP1/TM-23-11 (92.4 ka) and X-6 tephras (109.5 ka), and two Italian tephras that have so far only been identified at

Lago Grande di Monticchio, namely tephras TM-18-1d (c. 41.3 cal ka BP) and TM-33-1a (116.7 ka). Integration of tephra ages, additional ^{14}C dates on TP sediments and high-resolution palynological alignments resulted in an improved age-depth model of the MIS 1-5 interval of the TP-2005 sequence, and is a major step towards increasing the number of well-dated, long and temporally highly resolved palaeoclimate records in the Eastern Mediterranean region. The new cryptotephra data provide additional isochrons for improving the correlation of long terrestrial and marine palaeoenvironmental records in the eastern Mediterranean region.

The tephra results furthermore imply that the Tenaghi Philippon record is key to further refining atmospheric circulation patterns for the Eastern Mediterranean and adjacent regions for the MIS 1-5 interval. It is located in an ideal position for receiving tephra from both Italian and Aegean Arc volcanoes, and modern atmospheric patterns hold the potential to transport volcanic ash also from East Carpathian and central Anatolian volcanic centres towards TP. This makes TP an important reference archive for correlating palaeoenvironmental sequences from sites in the central Mediterranean with those in the Eastern Mediterranean region.

Our new cryptotephra investigation at TP has also provided new insight into the factors that can affect the preservation of volcanic glass shards in peat-dominated sedimentary sequences. The evidence for extensive displacement/re-deposition of tephra shards in the TP-2005 core can provide additional information about past environmental influences, such as potential changes in ground water level.The identification of potentially redeposited tephra glass shards versus *in situ* components critically hinges on the detailed major and trace element geochemical characterisation of a high number of shards, which requires elaborated shard extraction techniques and the application of high-precision micro-analytical techniques. Hence, detailed cryptotephra studies may help to better understand post-depositional taphonomic processes in peat bogs, but potentially also in other terrestrial and marine sediments.

Acknowledgments

SW and JP acknowledge support through the Senckenberg Gesellschaft für Naturforschung

and Heidelberg University. MH was funded by the Natural Environment Research Council (NERC) via the RESET consortium (project number NE/E015905/1). RS is supported by an Early Career Fellowship from the Leverhulme Trust (ECF-2015-396). AK, JP and GS acknowledge support through the German Research Foundation (DFG; grant KO4960/3 to AK and JP, and grant PR651/3 to JP and GS). The Heidelberg Ion Microprobe (HIP) facility at Heidelberg University is operated under the auspices of the DFG Scientific Instrumentation and Information Technology programme. We are very grateful to Ilse Glass, Monika Doubrawa and Kai Uwe Käser for laboratory support during tephra sample processing, and Thomas Ludwig for help during SIMS measurements at Heidelberg University. Alexander Varychev was responsible for SEM sample mapping, and Johannes Grimm and Hans-Peter Meyer for the EPMA setup at Heidelberg University. Ralf Gertisser provided pumice samples of the Cape Tripiti tephra deposit from Santorini. We thank Biagio Giaccio and an anonymous reviewer for their constructive comments that helped to improve this contribution.

SUPPLEMENTARY FILES

Supplement 1: EPMA, LA-ICP-MS and SIMS glass analytical data of TP-2005 tephra layers.

Supplement 2: EPMA and LA-ICP-MS glass data of distal (Lago Grande di Monticchio) and proximal Santorini tephra deposits.

Supplement 3: Revised age-depth model of the TP-2005 sequence (0–135 ka BP) and palynological data re-calibrated on the new time scale.

References

Aksu, W.E., Jenner, G., Hiscott, R.N., İşler, E.B., 2008. Occurrence, stratigraphy and geochemistry of Late Quaternary tephra layers in the Aegean Sea and the Marmara Sea. Marine Geology 252, 174-192.

Albert, P.G., Hardiman, M., Keller, J., Tomlinson, E.L., Smith, V.C., Bourne, A.J., Wulf, S., Zanchetta, G., Sulpizio, R., Müller, U.C., Pross, J., Ottolini, L., Matthews, I.P., Blockley, S.P.E., Menzies, M.A., 2015. Revisiting the Y-3 tephrostratigraphic marker: a new diagnostic glass geochemistry, age estimate, and details on its climatostratigraphical context. Quaternary Science Reviews 118, 105-121.

Albert, P.G., Tomlinson, E.L., Smith, V.S., Di Traglia, F., Pistolesi, M., Morris, A., Donato, P., De Rosa, R., Sulpizio, R., Keller, J., Rosi, M., Menzies, M., 2017. Glass geochemistry of pyroclastic deposits from the Aeolian Islands in the last 50 ka: A proximal database for tephrochronology. Journal of Volcanology and Geothermal Research 336, 81-107.

Albert, P.G., Tomlinson, E.L., Smith, V.C., Di Roberto, A., Todman, A., Rosi, M., Marani, M., Müller, W., Menzies, M.A., 2012. Marine-continental tephra correlations: Volcanic glass geochemistry from the Marsili Basin and the Aeolian Islands, Southern Tyrrhenian Sea, Italy. Journal of Volcanology and Geothermal Research 229-230, 74-94.

Allen, J.R.M., Brandt, U., Brauer, A., Hubberten, H.-W., Huntley, B., Keller, J., Kraml, M., Mackensen, A., Mingram, J., Negendank, J.F.W., Nowaczyk, N.R., Oberhänsli, H., Watts, W.A., Wulf, S., Zolitschka, B., 1999. Rapid environmental changes in southern Europe during the last glacial period. Nature 400, 740-743.

Barker, S., Knorr, G., Edwards, R.L., Parrenin, F., Putnam, A.E., Skinner, L.C., Wolff, E., Ziegler, M., 2011. 800,000 years of abrupt climate variability. Science 334, 347-351.

Bjarnason, Á.H., 1991. Vegetation on lava fields in the Hekla area, Iceland, Acta Phytogeographica Suecica. PhD Thesis, University of Uppsala, p. 110.

Blockley, S., Pyne-O'Donnell, S.D.F., Lowe, J.J., Matthews, I.P., Stone, A., Pollard, M., Turney, C.S.M., Molyneux, E.G., 2005. A new and less destructive laboratory procedure for the physical separation of distal glass tephra shards from sediments. Quaternary Science Reviews 24, 1952-1960.

Bourne, A.J., Albert, P.G., Matthews, I.P., Trincardi, F., Wulf, S., Asioli, A., Blockley, S.P.E., Keller, J., Lowe, J.J., 2015. Tephrochronology of core PRAD 1-2 from the Adriatic Sea: insights into Italian explosive volcanism for the period 200-80 ka. Quaternary Science Reviews 116, 28-43.

Bourne, A.J., Lowe, J.J., Trincardi, F., Asioli, A., Blockley, S., Wulf, S., Matthews, I.P., Piva, A., Vigliotti, L., 2010. Distal tephra record for the last ca 105,000 years from core PRAD 1-2 in the central Adriatic Sea: implications for marine tephrostratigraphy. Quaternary Science Reviews 29, 3079-3094.

Brauer, A., Allen, J.R.M., Mingram, J., Dulski, P., Wulf, S., Huntley, B., 2007. Evidence for last

interglacial chronology and environmental change from Southern Europe. Proceedings of the National Academy of Science, 104, 450-455.

Bronk Ramsey, C., 2008. Deposition models for chronological records. Quaternary Science Reviews 27, 42-60.

Bronk Ramsey, C., 2009a. Bayesian analysis of radiocarbon dates. Radiocarbon 51, 337-360.

Bronk Ramsey, C., 2009b. Dealing with outliers and offsets in radiocarbon dating. Radiocarbon 51, 1023-1045.

Bronk Ramsey, C., 2017. OxCal ver.4.3, in: https://c14.arch.ox.ac.uk/oxcal/OxCal.html (Ed.).

Bronk Ramsey, C., Albert, P.G., Blockley, S.P.E., Hardiman, M., Housley, R.A., Lane, C.S., Lee, S., Matthews, I.P., Smith, V.C., Lowe, J.J., 2015. Improved age estimates for key Late Quaternary European tephra horizons in the RESET lattice. Quaternary Science Reviews 118, 18-32.

Bronk Ramsey, C., Dee, M., Lee, S., Nakagawa, T., Staff, R.A., 2010. Developments in the calibration and modelling of radiocarbon dates. Radiocarbon 52, 953-961.

Bronk Ramsey, C., Lee, S., 2013. Recent and planned developments of the program OxCal. Radiocarbon 55, 720-730.

Çağatay, M.N., Wulf, S., Sancar, Ü., Özmaral, A., Vidal, L., Henry, P. Appelt, O., Gasperini, L., 2015. The tephra record from the Sea of Marmara for the last ca. 70 ka and its palaeoceanographic implications. Marine Geology 361, 96-110.

Caron, B., Siani, G., Sulpizio, R., Zanchetta, G., Paterne, M., Santacroce, R., Tema, E., Zanella, E., 2012. Late Pleistocene to Holocene tephrostratigraphic record from the Northern Ionian Sea. Marine Geology 311-314, 41-51.

Christanis, K., 1983. Genese und Fazies der Torf-Lagerstätte von Philippi (Griechisch-Mazedonien) als Beispiel der Entstehung einer Braunkohlen-Lagerstätte vom stark telmatischen Typ. PhD Thesis, University of Braunschweig, p. 170.

Christanis, K., 1987. Philippi/Greece: a peat deposit awaiting development. International Peat Journal 2, 45-54.

Christanis, K., 2016. The Philippi Peatland (Greece). In: C.M. Finlayson et al. (eds.), The Wetland Book, Springer Science+Business Media Dordrecht. doi: 10.1007/978-94-007-6173-5_147-1.

Cullen, V.L., Smith, V.C., Arz, H.W., 2014. The detailed tephrostratigraphy of a core from the south-east Black sea spanning the last ~60 ka. Journal of Quaternary Science 29, 675-690.

Damaschke, M., Sulpizio, R., Zanchetta, G., Wagner, B., Böhm, A., Nowaczyk, N., Rethemeyer, J., Hilgers, A., 2013. Tephrostratigraphic studies on a sediment core from Lake Prespa in the Balkans. Climate of the Past 9, 267-287.

de Beaulieu, J.-L., Brugiapaglia, E., Joannin, S., Guiter, F., Zanchetta, G., Wulf, S., Peyron,

O., Bernardo, L., Didier, J., Stock, A., Rius, D., Magny, M., 2017. Lateglacial-Holocene abrupt vegetation changes at Lago Trifoglietti in Calabria, southern Italy: The setting of ecosystems in a refugial zone. Quaternary Science Reviews 158, 44-57.

De Rosa, R., Donato, P., Gioncada, A., Masetti, M., Santacroce, R., 2003. The Monte Guardia eruption (Lipari, Aeolian Islands): an example of a reversely zoned magma mixing sequence. Bulletin of Volcanology 65, 530-543.

Di Vito, M., Isaia, R., Orsi, G., Southon, J., di Vita, S., D' Antonio, M., Pappalardo, L., Piochi, M., 1999. Volcanism and deformation since 12,000 years at the Campi Flegrei caldera (Italy). Journal of Volcanology and Geothermal Research 91, 221-246.

Druitt, T.H., Brenchley, P.J., Gökten, Y.E., Francaviglia, V., 1995. Late Quaternary rhyolitic eruptions from the Acigöl Complex, central Turkey. Journal of the Geological Society of London 152, 655-667.

Druitt, T.H., Edwards, L., Mellors, R.M., Pyle, D.M., Sparks, R.S.J., Lanphere, M., Davies, M., Barriero, B., 1999. Santorini Volcano. Geological Society, London, Vol. 19, p. 165.

Druitt, T.H., Francalanci, L., Fabbro, G., 2015. Field guide to Santorini volcano. MeMoVolc short course, Santorini, p. 56.

Druitt, T.H., Mellors, R.A., Pyle, D.M., Sparks, R.S.J., 1989. Explosive volcanism on Santorini, Greece. Geological Magazine 126, 95-126.

Eastwood, W.J., Pearce, N.J.G., Westgate, J.A., Perkins, W.T., Lamb, H.F., Roberts, N., 1999. Geochemistry of Santorini tephra in lake sediments from Southwest Turkey. Global and Planetary Change 21, 17-29.

Fabbro, G.N., Druitt, T.H., Scaillet, S., 2013. Evolution of the crustal magma plumbing system during the build-up to the 22-ka caldera-forming eruption of Santorini (Greece). Bulletin of Volcanology 75, 767-788.

Federman, A.N., Carey, S.N., 1980. Electron microprobe correlation of tephra layers from Eastern Mediterranean abyssal sediments and the island of Santorini. Quaternary Research 13, 160-171.

Fletcher, W.J., Müller, U.C., Koutsodendris, A., Christanis, K., Pross, J., 2013. A centennial-scale record of vegetation and climate variability from 312 to 240 ka (Marine Isotope Stages 9c-a, 8 and 7e) from Tenaghi Philippon, NE Greece. Quaternary Science Reviews 78, 108-125.

Fotiadi, A.K., Metaxas, A.D., Bartzokas, A., 1999. A statistical study of precipitation in northwest Greece. International Journal of Climatology 19, 1221-1232.

Georgakopoulos, A., Femández-Turiel, J.L., Christanis, K., Kalaitzidis, S., Kassoli-Foumaraki, A., Llorens, J.F., Filippidis, A., Gimeno, D., 2001. The Drama basin water: quality and peat/lignite interaction. Environmental Geology 41, 121-127.

Giaccio, B., Castorina, F., Nomade, S., Scardia, G., Voltaggio, M., Sagnotti, L., 2013. Revised chronology of the Sulmona lacustrine succession, central Italy. Journal of Quaternary

Science 28, 545-551.

Giaccio, B., Hajdas, I., Isaia, R., Deino, A., Nomade, S., 2017a. High-precision ^{14}C and $^{40}Ar/^{39}Ar$ dating of the Campanian Ignimbrite (Y-5) reconciles the time-scale of climatic cultural processes at 40 ka. Scientific Reports 7, 45940.

Giaccio, B., Niespolo, E.M., Pereira, A., Nomade, S., Renne, P.R., Albert, P.G., Arienzo, I., Regattieri, E., Wagner, B., Zanchetta, G., Gaeta, M., Galli, P., Mannella, G., Peronace, E., Sottili, G., Florindo, F., Leicher, N., Marra, F., Tomlinson, E.L., 2017b. First integrated tephrochronological record for the last ~190 kyr from the Fucino Quaternary lacustrine succession, central Italy. Quaternary Science Reviews 158, 211-234.

Giaccio, B., Nomade, S., Wulf, S., Isaia, R., Sottili, G., Cavuoto, G., Galli, P., Messina, P., Sposato, A., Sulpizio, R., Zanchetta, G., 2012. The late MIS 5 Mediterranean tephra markers: a reappraisal from peninsular Italy terrestrial records. Quaternary Science Reviews 56, 31-45.

Giaccio, B., Regattieri, E., Zanchetta, G., Wagner, B., Galli, P., Mannella, G., Niespolo, E., Peronace, E., Renne, P.R., Nomade, S., Cavinato, G.P., Messina, P., Sposato, A., Boschi, C., Florindo, F., Marra, F., Sadori, L., 2015. A key continental archive for the last 2 Ma of climatic history of the central Mediterranean region: A pilot drilling in the Fucino Basin, central Italy. Scientific Drilling 20, 13-19.

Gillot, P.Y., Chiesa, S., Pasquare, G., Vezzoli, L., 1982. <33.000 yr K/Ar dating of the volcano-tectonic horst of the isle of Ischia, Gulf of Naples. Nature 299, 242-245.

Giorgi F, Lionello P, 2008. Climate change projections for the Mediterranean region. Global and Planetary Change 63, 90-104.

Glais, A., López-Sáez, J.A., Lespez, L., Davidson, R., 2016. Climate and human-environment relationships on the edge of the Tenaghi-Philippon marsh (Northern Greece) during the Neolithization process. Quaternary International 403, 237-250.

Grant, K.M., Rohling, E.J., Bar-Matthews, M., Ayalon, A., Medina-Elizalde, M., Bronk Ramsey, C., Satow, C., Roberts, A.P., 2012. Rapid coupling between ice volume and polar temperature over the past 150,000 years. Nature 491, 744-747.

Hamann, Y., Ehrmann, W., Schmiedl, G., Krüger, S., Stuut, J.-B., Kuhnt, T., 2008. Sedimentation processes in the Eastern Mediterranean Sea during the Late Glacial and Holocene revealed by end-member modelling of the terrigenous fraction in marine sediments. Marine Geology 248, 97-114.

Hamann, Y., Wulf, S., Ersoy, O., Ehrmann, W., Aydar, E., Schmiedl, G., 2010. First evidence of a distal early Holocene ash layer in Eastern Mediterranean deep-sea sediments derived from the Anatolian volcanic province. Quaternary Research 73, 497-506.

Harangi, S., Lukács, R., Schmitt, A.K., Dunkl, I., Molnár, K., Kiss, B., Seghedi, I., Novothny, Á., Molnár, M., 2015. Constraints on the timing of Quaternary volcanism and duration of magma residence at Ciomadul volcano, east-central Europe, from combined U-Th/He and U-Th zircon geochronology. Journal of Volcanology and Geothermal Research 301, 66-80.

Hardiman, J.C., 1999. Deep sea tephra from Nisyros Island, eastern Aegean Sea, Greece, in: Firth, C.R., McGuire, W.J. (Eds.), Volcanoes in the Quaternary. Geological Society of London, London, pp. 69-88.

Hijmans, R.J., Cameron, S.E., Parra, J.L., Jones, P.G., Jarvis, A., 2005. Very high resolution interpolated climate surfaces for global land areas. International Journal of Climatology 25, 1965-1978.

Hunt, J.B., Hill, P.G., 1996. An inter-laboratory comparison of the electron probe microanalysis of glass geochemistry. Quaternary International 34-36, 229-241.

Insinga, D.D., Tamburrino, S., Lirer, F., Vezzoli, L., Barra, M., De Lange, G.J., Tiepolo, M., Vallefuoco, M., Mazzola, S., Sprovieri, M., 2014. Tephrochronology of the astronomically-tuned KC01B deep-sea core, Ionian Sea: insights into the explosive activity of the Central Mediterranean area during the last 200 ka. Quaternary Science Reviews 85, 63-84.

IPCC, 2014. Climate Change 2014: Synthesis Report. Contribution of Working Groups I, II and III to the Fifth Assessment Report of the Intergovernmental Panel on Climate Change, Core Writing Team, Pachauri RK, Meyer LA (eds.). IPCC, Geneva, Switzerland, 151 pp.

Jochum, K.P., Stoll, B., Herwig, K., Willbold, M., Hofmann, A.W., Amini, M., Aarburg, S., et al., 2006. MPI-DING reference glasses for in situ microanalysis: New reference values for element concentrations and isotope ratios. Geochemistry, Geophysics, Geosystems 7, Q02008.

Kalaitzidis, S., 2007. Peatification and evolution of peatlands in Greece. Ph.D. Thesis, Department of Geology, University of Patras, Greece, 532 p.

Kalaitzidis, S., Christanis, K., 2004. Peat petrography as a tool to interpret peat-accumulation features – case studies from Greece. In J. Päivänen (ed.), Wise use of Peatlands, Proc. 12th Int. Peat Congress (June 2004, Tampere, Finland), vol. 1, 42-47.

Karátson, D., Wulf, S., Veres, D., Magyari, E.K., Gertisser, R., Timar-Gabor, A., Novothny, Á., Telbisz, T., Szalai, Z., Anechitei-Deacu, V., Appelt, O., Bormann, M., Jánosi, C., Hubay, K., Schäbitz, F., 2016. The latest explosive eruptions of Ciomadul (Csomád) volcano, East Carpathians – a tephrostratigraphic approach for the 51–29 ka BP time interval. Journal of Volcanology and Geothermal Research 319, 29-51.

Keller, J., Ryan, W.B.F., Ninkovich, D., Altherr, R., 1978. Explosive volcanic activity in the Mediterranean over the past 200,000 yr as recorded in deep-sea sediments. Geological Society of America Bulletin 89, 591-604.

Kotthoff, U., Müller, U.C., Pross, J., Schmiedl, G., Lawson, I.T., van de Schootbrugge, B., Schulz, H., 2008a. Lateglacial and Holocene vegetation dynamics in the Aegean region: an integrated view based on pollen data from marine and terrestrial archives. The Holocene 18, 1019-1032.

Kotthoff, U., Pross, J., Müller, U.C., Peyron, O., Schmiedl, G., Schulz, H., Bordon, A., 2008b. Climate dynamics in the borderlands of the Aegean Sea during formation of sapropel S1 deduced from a marine pollen record. Quaternary Science Reviews 27, 832-845.

Koutsodendris, A., Brauer, A., Reed, J.M., Plessen, B., Friedrich, O., Hennrich, B., Zacharias, I., Pross, J., 2017. Climate variability in SE Europe since 1450 AD based on a varved sediment record from Etoliko Lagoon (Western Greece). Quaternary Science Reviews 159, 63-76.

Kuehn, S.C., Froese, D.G., Shane, P.A.R., INTAV Inter-comparison Participants, 2011. The INTAV inter-comparison of electron-beam microanalysis of glass by tephrochronology laboratories: Results and recommendations. Quaternary International 246, 19-47.

Kutiel, H., Benaroch, Y., 2002. North Sea-Caspian Pattern (NPC) – an upper level atmospheric teleconnections affecting the Eastern Mediterranean: Identification and definition. Theoretical and Applied Climatology 71, 17-28.

Kuzucuoglu, C., Pastre, J.F., Black, S., Ercan, T., Fontugne, M., Guillou, H., Hatté, C., Karabiyikoglu, M., Orth, P., Türkecan, A., 1998. Identification and dating of tephra layers from Quaternary sedimentary sequences of Inner Anatolia, Turkey. Journal of Volcanology and Geothermal Research 85, 153-172.

Kwiecien, O., Arz, H.W., Lamy, F., Wulf, S., Bahr, A., Röhl, U., Haug, G.H., 2008. Estimated reservoir ages of the Black Sea since the Last Glacial. Radiocarbon 50, 1-20.

Laskar, J., Robutel, P., Joutel, F., Gastineau, M., Correia, A.C.M., Levrard, B., 2004. A long-term numerical solution for the insolation quantities of the Earth. Astronomy & Astrophysics 428, 261-285.

Lee, S., Bronk Ramsey, C., Hardiman, M., 2013. Modeling the age of the Cape Riva (Y–2) tephra. Radiocarbon 55, 3-4.

Leicher, N., Zanchetta, G., Sulpizio, R., Giaccio, B., Wagner, B., Nomade, S., Francke, A., Del Carlo, P., 2016. First tephrostratigraphic results of the DEEP site record from Lake Ohrid (Macedonia and Albania). Biogeosciences 13, 2151-2178.

Lionello, P., Malanotte-Rizzoli, P., Boscolo, R., Alpert, P., Artale, V., Li, L., Luterbacher, J., May, W., Trigo, R., Tsimplis, M., Ulbrich, U., Xoplaki, E., 2006. The Mediterranean climate: An overview of the main characteristics and issues, in: Lionello, P., Malanotte-Rizzoli, P., Boscolo, R. (Eds.), Mediterranean climate variability. Elsevier, Amsterdam, pp. 1-26.

Lourens, L.J., 2004. Revised tuning of Ocean Drilling Program Site 964 and KC01B (Mediterranean) and implications for the $\delta^{18}O$, tephra, calcareous nannofossil, and geomagnetic reversal chronologies of the past 1.1 Myr. Paleoceanography 19, PA3010.

Lowe, D.J., 2011. Tephrochronology and its application: A review. Quaternary Geochronology 6, 107-153.

Lowe, J.J., Bronk Ramsey, C., Housley, R.A., Lane, C.S., Tomlinson, E.L., Team, R., Associates, R., 2015. The RESET project: constructing a European tephra lattice for refined synchronisation of environmental and archaeological events during the last c. 100 ka. Quaternary Science Reviews 118, 1-17.

Lowe, J., Barton, N., Blockley, S.P.E., Bronk Ramsey, C., Cullen, V.L., Davies, W., Gamble, C., Grant, K., Hardiman, M., Housley, R., Lane, C.S., Lee, S., Lewis, M., Macleod, A., Menzies,

M., Müller, W., Pollard, M., Price, C., Roberts, A.P., Rohling, E.J., Satow, C., Smith, V.C., Stringer, C.B., Tomlinson, E.L., White, D., Albert, P., Arienzo, I., Barker, G., Bori_C, D., Carandente, A., Civetta, L., Ferrier, C., Guadelli, J.L., Karkanas, P., Koumouzelis, M., Müller, U.C., Orsi, G., Pross, J., Rosi, M., Shalamanov-Korobar, L., Sirakov, N., Tzedakis, P.C., 2012. Volcanic ash layers illuminate the resilience of Neanderthals and early modern humans to natural hazards. Proceedings of the National Academy of Science 109, 13532-13537.

Lucchi, F., Tranne, C.A., De Astis, G., Keller, J., Losito, R., Morche, W., 2008. Stratigraphy and significance of Brown Tuffs on the Aeolian Islands (southern Italy). Journal of Volcanology and Geothermal Research 177, 49-70.

Maheras, P., Patrikas, I., Karacostas, T., Anagnostopoulou, C., 2000. Automatic classification of circulation types in Greece: methodology, description, frequency, variability and tend analysis. Theoretical and Applied Climatology 67, 205-223.

Margari, V., Pyle, D.M., Bryant, C., Gibbard, P.L., 2007. Mediterranean tephra stratigraphy revisited: Results from a long terrestrial sequence on Lesvos Island, Greece. Journal of Volcanology and Geothermal Research 163, 34-54.

Martin-Puertas, C., Brauer, A., Wulf, S., Ott, F., Lauterbach, S., Dulski, P., 2014. Annual proxy data from Lago Grande di Monticchio (southern Italy) between 76 and 112 ka: new chronological constraints and insights on abrupt climatic oscillations. Climate of the Past 10, 2099-2114.

Metaxas, A.D., 1978. Evidence on the importance of diabatic heating as a divergence factor in the Mediterranean. Archiv für Meteorologie, Geophysik und Bioklimatologie, Serie A 27, 69-80.

Milner, A.M., Collier, R.E.L., Roucoux, K.H., Müller, U.C., Pross, J., Christanis, K., Tzedakis, P.C., 2012. Enhanced seasonality of precipitation in the Mediterranean during the early part of the Last Interglacial. Geology 40, 919-922.

Milner, A.M., Müller, U.C., Roucoux, K.H., Collier, R.E.L., Pross, J., Kalaitzidis, S., Christanis, K., Tzedakis, P.C., 2013. Environmental variability during the last Interglacial: A new high-resolution pollen record from Tenaghi Philippon, Greece. Journal of Quaternary Science 28, 113-117.

Milner, A.M., Roucoux, K.H., Collier, R.E.L., Müller, U.C., Pross, J., Tzedakis, P.C., 2016. Vegetation responses to abrupt climatic changes during the Last Interglacial Complex (Marine Isotope Stage 5) at Tenaghi Philippon, NE Greece. Quaternary Science Reviews 154, 169-181.

Molnár, K., Harangi, S., Lukács, R., Dunkl, I., Schmitt, A.K., Kiss, B., Garamhegyi, T., Seghedi, I., 2018. The onset of the volcanism in the Ciomadul Volcanic Dome Complex (Eastern Carpathians): Eruption chronology and magma type variation. Journal of Volcanology and Geothermal Research, https://doi.org/10.1016/j.jvolgeores.2018.01.025.

Müller, U.C., Pross, J., Tzedakis, P.C., Gamble, C., Kotthoff, U., Schmiedl, G., Wulf, S., Christanis, K., 2011. The role of climate in the spread of modern humans into Europe. Quaternary Science Reviews 30, 273-279.

Müller, W., Shelley, M., Miller, P., Broude, S., 2009. Initial performance metrics of a new custom-designed ArF eximer LA-ICP-MS system coupled to a two-volume laser ablation cell. Journal of Analytical Atomic Spectrometry 24, 209-214.

Narcisi, B., Vezzoli, L., 1999. Quaternary stratigraphy of distal tephra layers in the Mediterranean – an overview. Global and Planetary Change 21, 31-50.

Neugebauer, I., Wulf, S., Schwab, M.J., Serb, J., Plessen, B., Appelt, O., Brauer, A., 2017. Implications of S1 tephra findings in Dead Sea and Tayma palaeolake sediments for marine reservoir age estimation and palaeoclimate synchronisation. Quaternary Science Reviews 170, 269-275.

NGRIP members, 2004. High-resolution record of Northern Hemisphere climate extending into the last interglacial period. Nature 431, 147-151.

Paillard, D., Labeyrie, L., Yiou, P., 1996. Macintosh program performs time-series analysis. Eos Trans. AGU 77, 379.

Panagiotopoulos, K., Böhm, A., Leng, M.J., Wagner, B., Schäbitz, F., 2014. Climate variability over the last 92 ka in SW Balkans from analysis of sediments from Lake Prespa. Climate of the Past 10, 643-660.

Paterne, M., Guichard, F., Duplessy, J.C., Siani, G., Sulpizio, R., Labeyrie, J., 2008. A 90,000-200,000 yrs marine tephra record of Italian volcanic activity in the Central Mediterranean Sea. Journal of Volcanology and Geothermal Research 177, 187-196.

Paterne, M., Guichard, F., Labeyrie, J., 1988. Explosive activity of the South Italian volcanoes during the past 80,000 years as determined by marine tephrochronology. Journal of Volcanology and Geothermal Research 34, 153-172.

Payne, R., Gehrels, M., 2010. The formation of tephra layers in peatlands: An experimental approach. Catena 81, 12-23.

Payne, R.J., Kilfeather, A.A., van der Meer, J.J.M., Blackford, J.J., 2005. Experiments on the taphonomy of tephra in peat. Suoseuro 56, 147-156.

Pearce, N.J.G., Perkins, W.T., Westgate, J.A., Gorton, M.P., Jackson, S.E., Neal, C.R., Chenery, S.P., 1997. A compilation of new and published major and trace element data for NIST SRM 610 and NIST SRM 612 glass reference materials. Geostandards Newsletter 21, 115-144.

Peyron, O., Goring, S., Dormoy, I., Kotthoff, U., Pross, J., de Beaulieu, J.-L., Drescher-Schneider, R., Vannière, B., Magny, M., 2011. Holocene seasonality changes in the central Mediterranean region reconstructed from the pollen sequences of Lake Accesa (Italy) and Tenaghi Philippon (Greece). Holocene 21, 131-146.

Pichler, H., Friedrich, W., 1976. Radiocarbon dates of Santorini volcanics. Nature 262, 373-374.

Pross, J., Kotthoff, U., Müller, U.C., Peyron, O., Dormoy, I., Schmiedl, G., Kalaitzidis, S., Smith, A.M., 2009. Massive perturbation in terrestrial ecosystems of the Eastern Mediterranean

region associated with the 8.2 kyr B.P. climatic event. Geology 37, 887-890.

Pross, J., Koutsodendris, A., Christanis, K., Fischer, T., Fletcher, W.J., Hardiman, M., Kalaitzidis, S., Knipping, M., Kotthoff, U., Milner, A.M., Müller, U.C., Schmiedl, G., Siavalas, G., Tzedakis, P.C., Wulf, S., 2015. The 1.35-Ma-long terrestrial climate archive of Tenaghi Philippon, northeastern Greece: Evolution, exploration, and perspectives for future research. Newsletters on Stratigraphy 48, 253-276.

Pross, J., Tzedakis, P.C., Schmiedl, G., Christanis, K., Hooghiemstra, H., Müller, U.C., Kotthoff, U., Kalaitzidis, S., Milner, A.M., 2007. Tenaghi Philippon (Greece) revisited: Drilling a continuous lower-latitude terrestrial climate archive of the last 250,000 years. Scientific Drilling 5, 44-46.

Regattieri, E., Giaccio, B., Nomade, S., Francke, A., Vogel, H., Drysdale, R.N., Perchiazzi, N., Wagner, B., Gemelli, M., Mazzini, I., Boschi, C., Galli, P., Peronace, E., 2017. A Last Interglacial record of environmental changes from the Sulmona Basin (central Italy). Palaeogeography, Palaeoclimatology, Palaeoecology 472, 51-66.

Regattieri, E., Giaccio, B., Zanchetta, G., Drysdale, R.N., Galli, P., Nomade, S., Peronace, E., Wulf, S., 2015. Hydrological variability over the Apennines during the Early Last Glacial precession minimum, as revealed by a stable isotope record from Sulmona basin, Central Italy. Journal of Quaternary Science 30, 19-31.

Reimer, P.J., Bard, E., Bayliss, A., J.W., B., Blackwell, P.G., Bronk Ramsey, C., Buck, C.E., Cheng, H., Edwards, R.L., Friedrich, M., Grootes, P.M., Guilderson, T.P., Haflidason, H., Hajdas, I., Hatté, C., Heaton, T.J., Hoffmann, D.L., Hogg, A.G., Hughen, K.A., Kaiser, K.F., Kromer, B., Manning, S.W., Niu, M., Reimer, R.W., Richards, D.A., Scott, E.M., Southon, J.R., Staff, R.A., Turney, S.M., van der Plicht, J., 2013. INTCAL13 and MARINE13 radiocarbon age calibration curves 0-50,000 years cal BP. Radiocarbon 55, 1869-1887.

Rohling, E.J., 1994. Review and new aspects concerning the formation of eastern Mediterranean sapropels. Marine Geology 122, 1-28.

Roucoux, K.H., Shackleton, N.J., de Abreu, L., 2001. Combined marine proxy and pollen analyses reveal rapid Iberian vegetation response to north Atlantic millennial-scale climate oscillations. Quaternary Research 56, 128-132.

Saaroni, H., Bitan, A., Alpert, P., Ziv, B., 1996. Continental polar outbreaks into the Levant and Eastern Mediterranean. International Journal of Climatology 16, 1175-1191.

Sadori, L., Koutsodendris, A., Panagiotopoulos, K., Masi, A., Bertini, A., Combourieu-Nebout, N., Francke, A., Kouli, K., Joannin, S., Mercuri, A.M., Peyron, O., Torri, P., Wagner, B., Zanchetta, G., Sinopoli, G., and Donders, T.H., 2016. Pollen-based paleoenvironmental and paleoclimatic change at Lake Ohrid (south-eastern Europe) during the past 500 ka. Biogeosciences 13, 1423–1437.

Sánchez Goñi, M.F., Bard, E., Landais, A., Rossignol, L., d'Errico, F., 2013. Air-sea temperature decoupling in western Europe during the last interglacial-glacial transition. Nature Geoscience 6, 837-841.

Sánchez Goñi, M.F., Cacho, I., Turon, J.L., Guiot, J., Sierro, F.J., Peypouquet, J.-P., Grimalt, J.O., Shackleton, N.J., 2002. Synchroneity between marine and terrestrial responses to millennial scale climate variability during the last glacial period in the Mediterranean region. Climate Dynamics 19, 95-105.

Sánchez Goñi, M.F., Desprat, S., Daniau, A.-L., Bassinot, F.C., Polanco-Martínez, J.M., Harriso, S.P., Allen, J.R.M., Anderson, R.S., Behling, H., Bonnefille, R., Burjachs, F., Carrión, J.S., Cheddadi, R., Clark, J.S., Combourieu-Nebout, N., Courtney-Mustaphi, C.J., Debusk, G.H., Dupont, L.M., Finch, J.M., Fletcher, W.J., Giardini, M., González, C., Gosling, W.D., Grigg, L.D., Grimm, E.C., Hayashi, R., Helmens, K., Heusser, L.E., Hill, T., Hope, G., Huntley, B., Igarashi, Y., Irino, T., Jacobs, B., Jiménez-Moreno, G., Kawai, S., Kershaw, P., Kumon, F., Lawson, I.T., Ledru, M.-P., Lézine, A.-M., Liew, P.M., Magri, D., Marchant, R., Margari, V., Mayle, F.E., McKenzie, M., Moss, P., Müller, S., Müller, U.C., Naughton, F., Newnham, R.M., Oba, T., Pérez-Obiol, R., Pini, R., Ravazzi, C., Roucoux, K.H., Rucina, S.M., Scott, L., Takahara, H., Tzedakis, P.C., Urrego, D.H., van Geel, B., Valencia, B.G., Vandergoes, M.J., Vincens, A., Whitlock, C.L., Willard, D.A., Yamamoto, M., 2017. The ACER pollen and charcoal database: a global resource to document vegetation and fire response to abrupt climate changes during the last glacial period. Earth System Science Data. DOI: http://dx.doi.org/10.5194/essd-2017-4.

Sánchez Goñi, M.F., Eynaud, F., Turon, J.L., Shackleton, N.J., 1999. High resolution palynological record off the Iberian margin: direct land-sea correlation for the last interglacial complex. Earth and Planetary Science Letters 171, 123-137.

Santacroce, R., Cioni, R., Marianelli, P., Sbrana, A., Sulpizio, R., Zanchetta, G., Donahue, D.J., Joron, J.L., 2008. Age and whole rock-glass compositions of proximal pyroclastics from the major explosive eruptions of Somma-Vesuvius: A review as a tool for distal tephrostratigraphy. Journal of Volcanology and Geothermal Research 177, 1-18.

Sarikaya, A.M., Çiner, A., Sen, E., Ersoy, O., Zreda, M., 2017. Dating Young Lava Flows with Cosmogenic ^{36}Cl: AN Example from the Late Pleistocene-Early Holocene Erciyes Monogenetic Lava Domes in Central Turkey. EGU General Assembly Conference Abstracts, 19, 3937.

Satow, C., Tomlinson, E.L., Grant, K.M., Albert, P.G., Smith, V.C., Manning, C.J., Ottolini, L., Wulf, S., Rohling, E.J., Lowe, J.J., Blockley, S.P.E., Menzies, M.A., 2015. A new contribution to the Late Quaternary tephrostratigraphy of the Mediterranean: Aegean Sea core LC21. Quaternary Science Reviews 117, 96-112.

Schemmel, F., Niedermeyer, E.M., Koutsodendris, A., Pross, J., Fiebig, J., Mulch, A., 2017. Paleohydrological changes in the Eastern Mediterranean region during the early Holocene recorded in plant wax *n*-alkane distributions and $\delta^{13}C_{TOC}$ – new data from Tenaghi Philippon, NE Greece. Organic Geochemistry 110, 100-109.

Schemmel, F., Niedermeyer, E.M., Schwab-Lavrič, V., Gleixner, G., Pross, J., Mulch, A., 2016. Plant-wax δD values record changing Eastern Mediterranean atmospheric circulation patterns during the 8.2 ka BP climatic event. Quaternary Science Reviews 133, 96-107.

Schmiedl, G., Hemleben, C., Keller, J., Segl, M., 1998. Impact of climatic changes on the benthic foraminiferal fauna in the Ionian Sea during the last 330,000 years. Paleoceanography 13, 447-458.

Schmitt, A.K., Danišík, M., Evans, N.J., Siebel, W., Kiemele, E., Aydin, F., Harvey, J.C., 2011. Acigöl rhyolite field, Central Anatolia (part 1): high-resolution dating of eruption episodes and zircon growth rates. Contributions to Mineralogy and Petrology, 162, 1215-1231.

Schwarz, M., 2000. Tephrakorrelation im östlichen Mittelmeer (Meteor M40/4 Kerne). Diploma Thesis, Albert-Ludwigs-Universität Freiburg, p. 257.

Sevink, J., van Bergen, M.J., van der Pflicht, J., Feiken, H., Anastasia, C., Huizinga, A., 2011. Robust date for the Bronze Age Avellino eruption (Somma-Vesuvius): 3945 +/- 10 cal BP (1995 +/- 10 cal BC). Quaternary Science Reviews 30, 1035-1046.

Shackleton, N.J., Hall, M.A., Vincent, E., 2000. Phase relationships between millennial-scale events 64,000–24,000 years ago. Paleoceanography 15, 565-569.

Siani, G., Paterne, M., Michel, E., Sulpizio, R., Sbrana, A., Arnold, M., Haddad, G., 2001. Mediterranean Sea surface radiocarbon reservoir age changes since the last glacial maximum. Science 294, 1917-1920.

Siani, G., Sulpizio, R., Paterne, M., Sbrana, A., 2004. Tephrostratigraphy study for the last 18,000 ^{14}C years in a deep-sea sediment sequence for the South Adriatic. Quaternary Science Reviews 23, 2485-2500.

Sinopoli, G., Masi, A., Regattieri, E., Wagner, B., Francke, A., Peyron, O., Sadori, L., 2018. Palynology of the Last Interglacial Complex at Lake Ohrid: palaeoenvironmental and palaeoclimatic inferences. Quaternary Science Reviews 180, 177-192.

Smith, V.C., Isaia, R., Engwell, S.L., Albert, P.G., 2016. Tephra dispersal during the Campanian Ignimbrite (Italy) eruption: implications for ultra-distal ash transport during the large caldera-forming eruption. Bulletin of Volcanology 78, 45-59.

Smith, V.C., Isaia, R., Pearce, N.J.G., 2011. Tephrostratigraphy and glass compositions of post-15 kyr Campi Flegrei eruptions: implications for eruption history and chronostratigraphic markers. Quaternary Science Reviews 30, 3638-3660.

St. Seymour, K., Christanis, K., Bouzinos, A., Papazisimou, S., Papatheodorou, G., Moran, E., Dénès, G., 2004. Tephrostratigraphy and tephrochronology in the Philippi peat basin, Macedonia, Northern Hellas (Greece). Quaternary International 121, 53-65.

Sulpizio, R., Van Welden, A., Caron, B., Zanchetta, G., 2010a. The Holocene tephrostratigraphic record of Lake Shkodra (Albania and Montenegro). Journal of Quaternary Science 25, 633-650.

Sulpizio, R., Zanchetta, G., D'Orazio, M.D., Vogel, H., Wagner, B., 2010b. Tephrostratigraphy and tephrochronology of lakes Ohrid and Prespa, Balkans. Biogeosciences, 3273-3288.

Sulpizio, R., Zanchetta, G., Paterne, M., Siani, G., 2003. A review of tephrostratigraphy in central and southern Italy during the last 65 ka. Il Quaternario 16, 91-108.

Svensson, A., Andersen, K.K., Bigler, M., Clausen, H.B., Dahl-Jensen, D., Davies, S.M., Johnsen, S.J., Muscheler, R., Parrenin, F., Rasmussen, S.O., Röthlisberger, R., Seierstad, I., Steffensen, J.P., Vinther, B.M., 2008. A 60,000 year Greenland stratigraphic ice core

chronology. Climate of the Past 4, 47-57.

Thorarinsson, S., 1944. Tefrokronologiska studier pa Island. Geogr. Analer, 1-215.

Tomlinson, E.L., Arienzo, I., Civetta, L., Wulf, S., Smith, V.C., Hardiman, M., Lane, C.S., Carandente, A., Orsi, G., Rosi, M., Müller, W., Menzies, M.A., 2012a. Geochemistry of the Phlegrean Fields (Italy) proximal sources for major Mediterranean tephras: Implications for the dispersal of Plinian and co-ignimbritic components of explosive eruptions. Geochimica et Cosmochimica Acta 93, 102-128.

Tomlinson, E.L., Kinvig, H.S., Smith, V.C., Blundy, J.D., Gottsmann, J., Müller, W., Menzies, M.A., 2012b. The Upper and Lower Nisyros Pumices: Revisions to the Mediterranean tephrostratigraphic record based on micron-beam glass geochemistry. Journal of Volcanology and Geothermal Research 243-244, 69-80.

Tomlinson, E.L., Smith, V.C., Albert, P.G., Aydar, E., Civetta, L., Cioni, R., Cubukcu, E., Gertisser, R., Isaia, R., Menzies, M.A., Orsi, G., Rosi, M., Zanchetta, G., 2015. The major and trace element glass compositions of the productive Mediterranean volcanic sources: tools for correlating distal tephra layers in and around Europe. Quaternary Science Reviews 118, 48-66.

Tomlinson, E.L., Thordarson, T., Müller, W., Thirlwall, M.F., Menzies, M.A., 2010. Micro analysis of tephra by LA-ICP-MS - strategies, advantages and limitations assessed using the Thorsmork ignimbrite (Southern Iceland). Chemical Geology 279, 73-89.

Turney, C.S.M., 1998. Extraction of rhyolitic component of Vedde microtephra from minerogenic lake sediments. Journal of Paleolimnology 19, 199-206.

Tzedakis, P.C., Frogley, M.R., Heaton, T.H.E., 2003. Last Interglacial conditions in southern Europe: evidence from Ioannina, northwest Greece. Global and Planetary Change 36, 157-170.

Tzedakis, P.C., Hooghiemstra, H., Pälike, H., 2006. The last 1.35 million years at Tenaghi Philippon: revised chronostratigraphy and long-term vegetation trends. Quaternary Science Reviews 25, 3416-3430.

Tzedakis, P.C., Lawson, I.T., Frogley, M.R., Hewitt, G.M., Preece, R.C., 2002. Buffered tree population changes in a Quaternary refugium: evolutionary implications. Science 297, 2044-2047.

van der Wiel, A.M., Wijmstra, T.A., 1987a. Palynology of the lower part (78–120 m) of the core Tenaghi Philippon II, Middle Pleistocene of Macedonia, Greece. Review of Palaeobotany and Palynology 52, 73-88.

van der Wiel, A.M., Wijmstra, T.A., 1987b. Palynology of the 112.8–197.8 m interval of the core Tenaghi Philippon III, Middle Pleistocene of Macedonia, Greece. Review of Palaeobotany and Palynology 52, 89-117.

van Hout, R., Katz, J., 2004. A method for measuring the density of irregularly shaped biological aerosols such as pollen. Journal of Aerosol Science 35, 1369-1384.

Vinci, A., 1985. Distribution and chemical composition of tephra layers from Eastern Mediterranean abyssal sediments. Marine Geology 64, 143-155.

Wagner, B., Wilke, T., Francke, A., Albrecht, C., Baumgarten, H., Bertini, A., Combourieu-Nebout, N., Cvetkoska, A., D´Addabbo, M., Donders, T.H., Föller, K., Giaccio, B., Hauffe, T., Holtvoeth, J., Joannin, S., Jovanovska, E., Just, J., Kouli, K., Koutsodendris, A., Krastel, S., Lacey, J.H., Leicher, N., Leng, M.J., Levkov, Z., Lindhorst, K., Masi, A., Mercuri, A.M., Nomade, S., Nowaczyk, N., Panagiotopoulos, K., Peyron, O., Reed, J.M., Regattieri, E., Sadori, L., Sagnotti, L., Stelbrink, B., Sulpizio, R., Tofilovska, S., Torri, P., Vogel, H., Wagner, T., Wagner-Cremer, F., Wolff, G.A., Wonik, T., Zanchetta, G., Zhang, X.S., 2017. The environmental and evolutionary history of Lake Ohrid (FYROM/Albania): Interim results from the SCOPSCO deep drilling project. Biogeosciences 14, 2033-2054.

Wijmstra, T.A., 1969. Palynology of the first 30 m of a 120 m deep section in northern Greece. Acta Botanica Neerlandica 18, 511-527.

Wijmstra, T.A., Smit, A., 1976. Palynology of the middle part (30–78 meters) of a 120 m deep section in northern Greece (Macedonia). Acta Botanica Neerlandica 25, 297-312.

Wijmstra, T.A., Groenhart, M.C., 1983. Record of 700,000 years vegetational history in Eastern Macedonia (Greece). Revista de la Academia Colombiana Ciencias Exactas, Fı´sicas y Naturales 15, 87-98.

Wijmstra, T.A., Young, R., 1992. Vegetational and climatic transitions between interglacial and glacial periods during the last 1 million years in northern Greece. In: Kukla, G.J., Went, E. (eds), Start of a Glacial. NATO ASI Series 13, 97-112.

Wolff, E.W., Chappellaz, J., Blunier, T., Rasmussen, S.O., Svensson, A., 2010. Millennial-scale variability during the last glacial: The ice core record. Quaternary Science Reviews 29, 2828-2838.

Wulf, S., Brauer, A., Kraml, M., Keller, J., Negendank, J.F.W., 2004. Tephrochronology of the 100 ka lacustrine sediment record of Lago Grande di Monticchio (southern Italy). Quaternary International 122, 7-30.

Wulf, S., Brauer, A., Mingram, J., Zolitschka, B., Negendank, J.F.W., 2006. Distal tephras in the sediments of Monticchio maar lakes, in: Principe, C. (Ed.), La geologia del monte Vulture. Consiglio Nazionale delle Ricerche, pp. 105-122.

Wulf, S., Fedorowicz, S., Veres, D., Lanczont, M., Karátson, D., Gertisser, R., Bormann, M., Magyari, E.K., Appelt, O., Hambach, U., Gozhyk, P.F., 2016. The 'Roxolany Tephra' (Ukraine) – new evidence for an origin from Ciomadul volcano, East Carpathians. Journal of Quaternary Science 31, 565-576.

Wulf, S., Keller, J., Paterne, M., Mingram, J., Lauterbach, S., Opitz, S., Sottili, G., Giaccio, B., Albert, P.G., Satow, C., Tomlinson, E.L., Viccaro, M., Brauer, A., 2012. The 100–133 ka record of Italian explosive volcanism and revised tephrochronology of Lago Grande di Monticchio. Quaternary Science Reviews 58, 104-123.

Wulf, S., Kraml, M., Kuhn, T., Schwarz, M., Inthorn, M., Keller, J., Kuscu, I., Halbach, P., 2002.

Marine tephra from the Cape Riva eruption (22 ka) of Santorini in the Sea of Marmara. Marine Geology 183, 131-141.

Wutke, K., Wulf, S., Tomlinson, E.L., Hardiman, M., Dulski, P., Luterbacher, J., Brauer, A., 2015. Geochemical properties and environmental impacts of seven Campanian tephra layers deposited between 40 and 38 ka BP in the varved lake sediments of Lago Grande di Monticchio, southern Italy. Quaternary Science Reviews 18, 67-83.

Xoplaki, E., González-Rouco, J.F., Luterbacher, J., Wanner, H., 2004. Wet season Mediterranean precipitation variability: influence of large-scale dynamics and trends. Climate Dynamics 23, 63-78.

Xoplaki, E., Luterbacher, J., Burkard, R., Patrikas, I., Maheras, P., 2000. Connection between the large-scale 500 hPa geopotential height fields and precipitation over Greece during wintertime. Climate Research 14, 129-146.

Zanchetta, G., Sulpizio, R., Roberts, N., Cioni, R., Eastwood, W.J., Siani, G., Caron, B., Paterne, M., Santacroce, R., 2011. Tephrostratigraphy, chronology and climatic events of the Mediterranean basin during the Holocene: An overview. Holocene 21, 33-52.

Table 1: Overview of occurrences, glass shard counts, chemical characteristics, published radiometric and new Bayesian modelled ages of (crypto)tephra layers in the 1–34 m depth interval of Tenaghi Philippon core TP-2005. Primary tephras are highlighted in bold and grey shading. The references for tephra radiometric ages are: [1] Caron et al. (2012); [2] Bronk Ramsey et al. (2015); [3] Giaccio et al. (2017a); [4] Wutke et al. (2015), this study; [5] Giaccio et al. (2012); [6] Martin-Puertas et al. (2014), Wulf et al. (2012); [7] Regattieri et al. (2017); [8] Gillot et al. (1982). * total number of glass shards in investigated sediment volume.

Tephra	TP-2005 full depth interval (m)	Peak shards/ g_{dwt}	Glass chemistry	Tephra source	Published age of tephra correlative with 2σ error (cal yr BP)	TP-2005 Bayesian modelled age range (cal yr BP) 95.4% uncertainty, this study
TP05-2.625	2.62-2.63	19	Tr/P	*re-deposited CI*		*5,550 – 5,790*
TP05-3.375	3.37-3.38	5* (1)	Tr/P	*re-deposited CI*		*6,430 – 6,630*
TP05-5.075	**5.05-5.10**	**5* (2)**	**Tr/P + R**	**E-1 (Aeolian Islands)** *re-deposited CI*	**8,270 ± 96** [1]	**8,160 – 8,350**
TP05-7.07	7.03-7.14	>10,000	R	*re-deposited Y-2*		*17,710 – 18,270*
TP05-7.26	7.22-7.33	>10,000	R	*re-deposited Y-2*		*20,120 – 20,880*
TP05-7.61	**7.43-7.61**	**visible**	**R**	**Cape Riva/Y-2 (Santorini)**	**22,024 ± 642** [2]	**21,260 – 22,510**
TP05-8.90	8.88-8.92	275	-	unidentified		27,330 – 27,840
TP05-8.96	8.95-9.00	65	-	unidentified		27,430 – 27,960
TP05-9.23	9.20-9.26	56	Tr	*re-deposited Y-3*		*27,880 – 28,510*
TP05-9.36	9.34-9.43	1258	Tr	*re-deposited Y-3*		*28,120 – 28,760*
TP05-9.51	9.44-9.56	1028	Tr (+R)	*re-deposited Y-3* *Y-2 contamination*		*28,400 – 29,000*
TP05-9.70	**9.68-9.76**	**2060**	**Tr + R**	**Y-3 (Campi Flegrei)** *Y-2 contamination*	**29,059 ± 356** [2]	**28,760 – 29,320**
TP05-9.78	9.76-9.81	952	R	*Y-2 contamination*		*28,860 – 29,450*
TP05-12.87	**12.50-12.87**	**visible**	**Tr/P**	**Campanian Ignimbrite (Campi Flegrei)**	**39,850 ± 140** [3]	**39,540 – 39,820**
TP05-13.25	13.24-13.27	1311	Tr/P	*CI contamination*		*40,670 – 41,310*
TP05-13.28	13.27-13.30	1191	Tr/P	*CI contamination*		*40,760 – 41.400*
TP05-13.34	**13.31-13.35**	**3092**	**Tr/P**	**TM-18-1d (Campi Flegrei)** *CI contamination*	*c. 40,440* [4]	**40,900 – 41,660**
TP05-13.54	13.50-13.55	1582	Tr/P	*CI contamination*		*41,770 – 42,530*
TP05-13.92	13.90-13.93	2038	Tr/P	*CI contamination*		*43,720 – 44,700*
TP05-14.50	14.46-14.54	40	Tr/P	*CI contamination*		*46,030 – 47,310*
TP05-17.91	17.90-17.92	749	-	unidentified		63,940 – 66,350
TP05-19.915	19.91-19.93	144	Tr	*CI contamination*		*72,860 – 75,110*
TP05-21.045	21.03-21.05	76	Tr	*CI and Y-2 contamination*		*77,210 – 79,530*
TP05-22.065	22.05-22.07	64	Tr/P (+R)	*CI and Y-2 contamination*		*80,710 – 83,270*
TP05-23.055	23.05-23.07	73	Tr/P	*CI contamination*		*84,930 – 88,060*
TP05-24.055	24.04-24.06	217	Tr/P	*CI contamination*		*88,820 – 92,910*
TP05-24.915	24.91-24.92	234	Tr/P (+R)	*CI and Y-2 contamination*		*92,160 – 97,070*
TP05-25.085	25.05-25.10	22	Tr/P (+R)	*CI and Y-2 contamination*		*92,820 – 97,890*
TP05-25.135	25.11-25.15	83	Tr/P	*CI contamination*		*93,020 – 98,140*
TP05-25.195	**25.18-25.20**	**39**	**Tr**	**TM-23-11/POP1 (Campania)** *CI contamination*	**92,400 ± 4600** [5] **96,210 ± 4810** [6]	**93,250 – 98,430**
TP05-25.465	25.46-25.47	956	Tr/P (+R)	unknown Campanian *CI and Y-2 contamination*		94,890 – 100,030
TP05-26.055	26.04-26.06	41	Tr/P	*CI contamination*		*98,430 – 103,430*
TP05-26.35	26.30-26.40	8	Tr/P	*Re-deposited X-6*		*100,000 – 104,770*
TP05-26.915	26.91-26.92	34	Tr/P (+R)	X-5 (Campania)? *Re-deposited X-6, CI and Y-2 contamination*		*102,960 – 107,150*
TP05-27.035	27.02-27.04	110	Tr/P	*CI, X-5(?) contamination*		*103,570 – 107,600*
TP05-27.915	**27.91-27.93**	**92**	**Tr/P**	**X-6/TM-27 (Campania),** *CI contamination*	**109,500 ± 900** [7] **109,370 ± 5470** [6]	**108,520 – 110,240**
TP05-27.995	27.98-28.00	128	Tr/P	*X-6 and CI contamination*		*108,670 – 110,660*
TP05-31.255	**31.24-31.26**	**11**	**Tr/P**	**TM-33-1a (Ischia),** *CI contamination*	**113,100 – 126,900** [8] **116,700 ± 5825** [6]	**117,780 – 123,970**
TP05-31.95	31.91-32.00	7*	Tr/P - R	unknown Campanian *CI and Y-2 contamination*		120,290 – 127,240
TP05-32.225	32.21-32.23	13	Tr/P – R	*CI and Y-2 contamination*		*121,280 – 128,530*
TP05-32.265	32.26-32.27	21	Tr/P	*CI contamination*		*121,430 – 128,720*
TP05-32.53	32.52-32.54	4* (2)	Tr/P	unknown Campanian *CI contamination*		122,380 – 129,960

Sample	**TP05-5.075**	**TP05-7.61**	**TP05-9.70**	**TP05-12.87 A**	**TP05-12.87 B**	**TP05-13.34**	**TP05-25.195**	**TP05-27.915 A**	**TP05-27.915 B**	**TP05-31.255**
Correlative	E1	Y-2	Y-3	CI fall	CI flow	TM-18-1d	TM-23-11	X-6/TM-27	X-6/TM-27	TM-33-1a
(wt%)										
SiO_2	75.38	70.79	60.94	60.23	58.80	59.29	61.04	59.89	59.83	61.44
TiO_2	0.13	0.47	0.35	0.40	0.34	0.37	0.36	0.41	0.45	0.31
Al_2O_3	12.44	14.31	17.65	18.15	17.75	17.96	18.69	19.55	18.88	18.50
FeO	1.52	3.11	2.70	2.98	3.43	3.05	3.55	3.09	3.00	3.01
MnO	0.01	0.13	0.09	0.18	0.14	0.22	0.23	0.11	0.19	0.11
MgO	0.05	0.40	0.48	0.30	0.68	0.31	0.65	0.34	0.33	0.56
CaO	0.67	1.67	2.27	1.74	2.55	1.65	2.61	1.56	1.63	1.18
Na_2O	3.50	5.53	3.76	6.28	2.66	6.49	4.21	7.00	6.05	5.92
K_2O	4.54	2.92	8.82	6.88	9.53	6.98	8.03	6.68	6.81	6.49
P_2O_5	0.02	0.06	0.10	0.07	0.16	0.06	0.20	0.00	0.00	0.02
Cl	0.45	0.27	n.a.	0.88	0.34	n.a.	0.48	0.76	0.87	0.62
Total	98.71	99.65	97.15	98.09	96.37	96.37	100.02	99.38	98.04	98.17
(ppm)										
Rb	-	105	347	459	282	431	291	-	-	282
Sr	-	72	341	19	564	22	412	-	-	92
Y	-	48	28	55	20	63	20	-	-	22
Zr	-	301	307	660	177	793	186	-	-	231
Nb	-	11	48	118	28	136	31	-	-	36
Ba	-	472	182	16	657	18	381	-	-	60
La	-	28	63	124	46	160	44	-	-	45
Ce	-	58	116	238	86	275	80	-	-	88
Th	-	15	26	52	13	70	13	-	-	14
U	-	5	9	18	5	27	5	-	-	6

Table 2: Representative EPMA glass analyses (non-normalized data) of primary tephras of the TP-2005 sequence for the last 135 ka. The full dataset is provided in Supplement 1.

Figure 1: a) Location of Tenaghi Philippon (yellow star) and other palaeoclimatic archives mentioned in the text (circles) with respect to the positions of high-explosive Quaternary volcanoes (red symbols) in the Eastern Mediterranean region. Inset map shows the location of marine core MD95-2042 at the western Iberian Margin. **b)** Overview map of the Drama basin in NE Greece. **c)** Detailed map of the Philippi peatland showing the location of the TP-2005 borehole (yellow star) and of other drilling sites mentioned in the text (circles); modified after Pross et al. (2015).

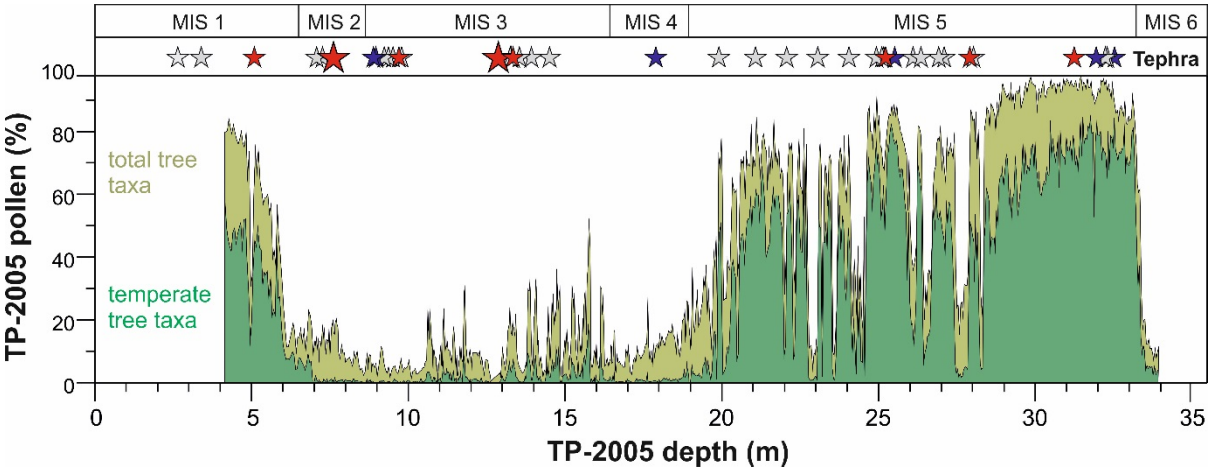

Figure 2: Positions of the tephra layers detected in the Tenaghi Philippon TP-2005 core plotted against total and temperate tree-pollen percentages (Milner et al., 2012, 2013, 2016; Müller et al., 2011). Stars indicate the positions of primary correlated tephras (red) and likely primary cryptotephra layers of unknown origin (blue); grey stars show the positions of reworked tephra material (see text for further detail); large red stars represent visible tephra layers. Positions of boundaries of marine isotope stages (MIS) after Müller et al. (2011) and Milner et al. (2016).

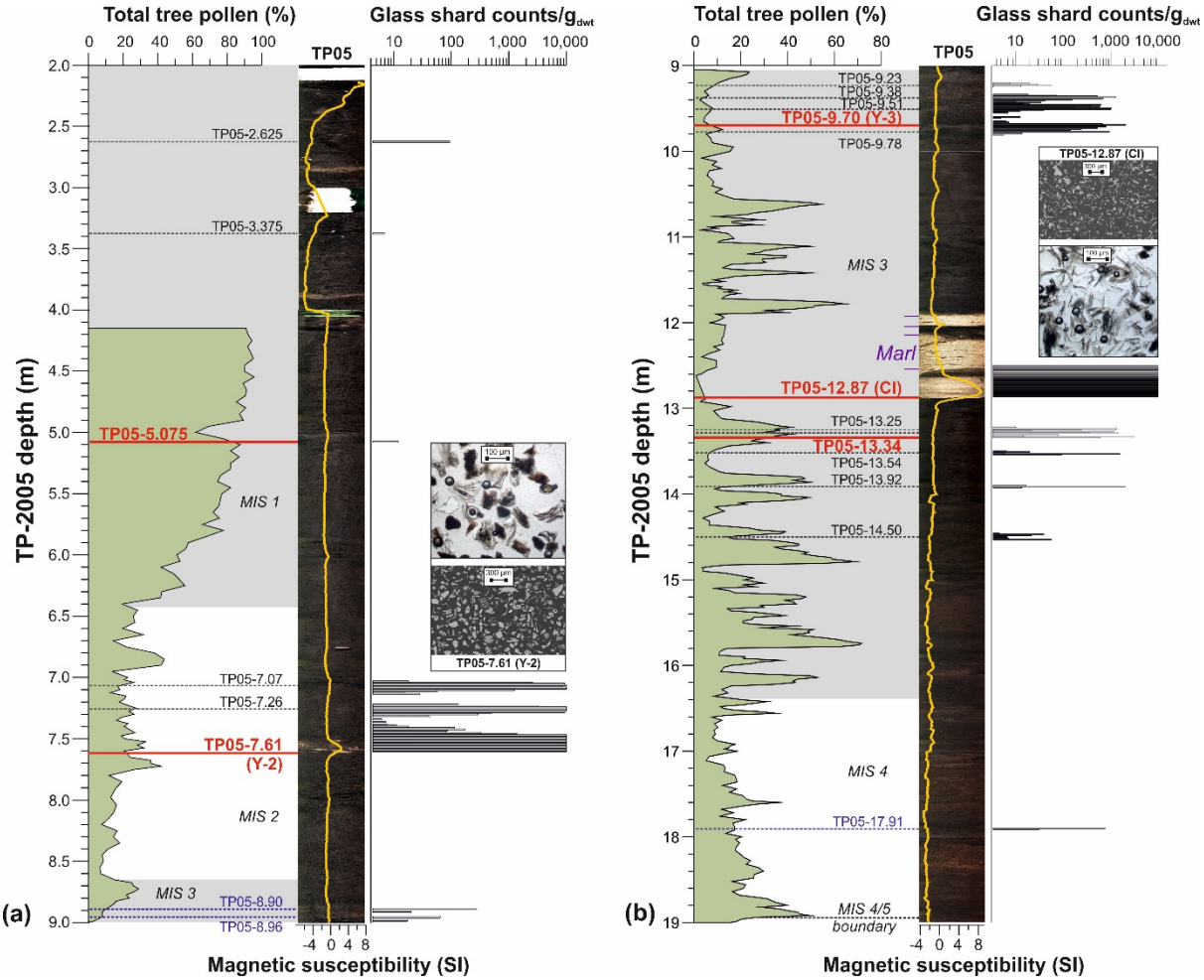

Figure 3: Composite of stratigraphic information for core TP-2005 for the intervals **(a)** MIS 1–MIS 2 and **(b)** MIS 3–MIS 4 comprising: total tree pollen curves (Müller et al., 2011; Pross et al., 2009); photographic images of lithostratigraphic changes; magnetic susceptibility (Pross et al., 2007); positions of detected tephras layers (dotted lines); glass shard counts; and transmitted light and backscattered electron (BSE) images of visible tephra layers. Note that visible tephras and some cryptotephras exceed 10,000 shards/g_{dwt}. Solid red lines indicate the positions of primary (crypto)tephra layers, dotted black and blue lines indicate reworked and yet unidentified tephra material, respectively. Grey shaded and white areas indicate warmer (MIS 1, 3) and cooler (MIS 2, 4) intervals, respectively.

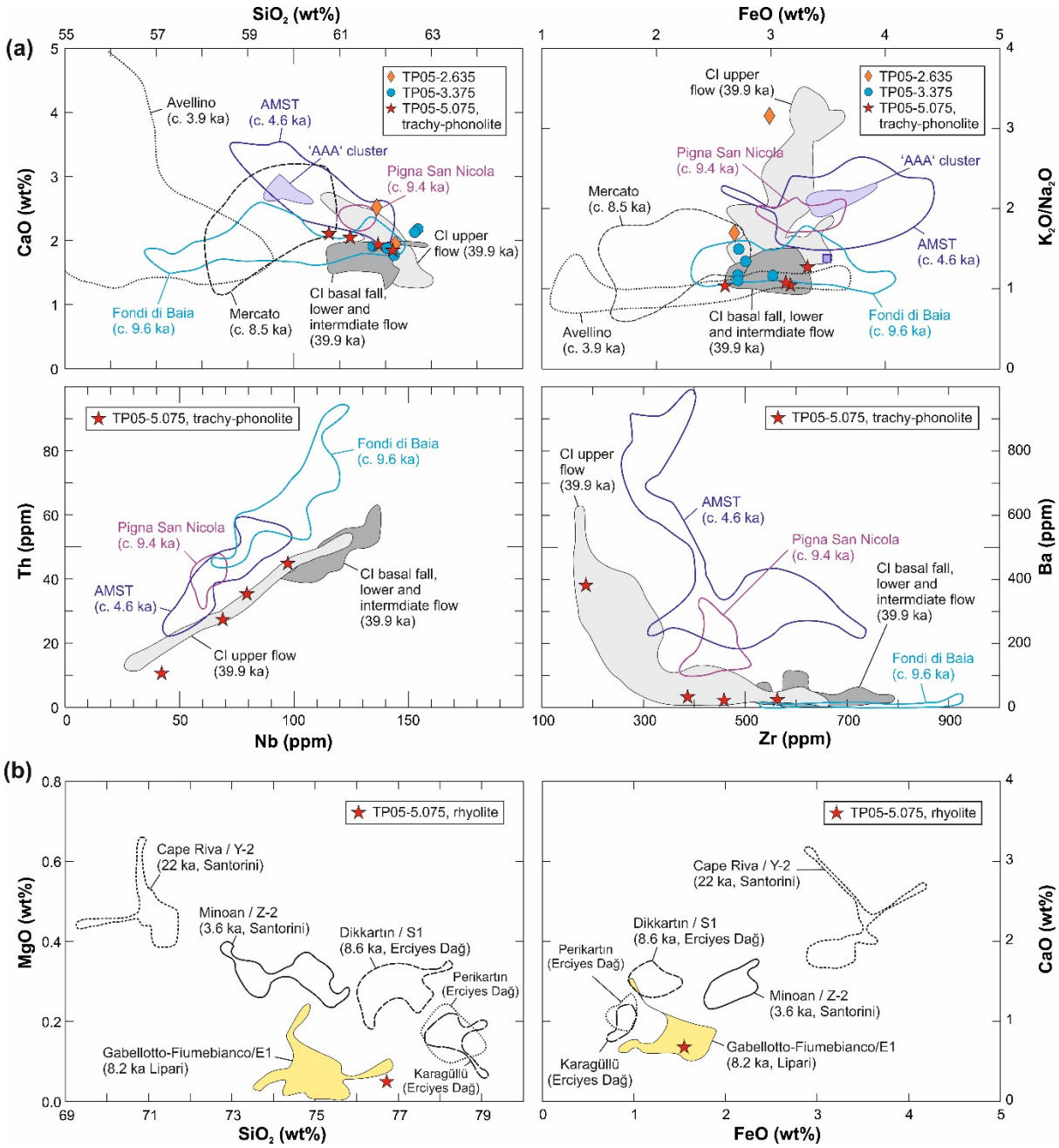

Figure 4: Bivariate plots of chemical components of cryptotephras TP05-2.625, TP05-3.375 and TP05-5.075 that discriminate **(a)** trachyphonolitic from **(b)** rhyolitic characteristics in Holocene Eastern Mediterranean tephras. The data are based on EPMA/SEM and LA-ICP-MS glass measurements obtained from proximal and distal tephra deposits of the following eruptions: **(a)** Agnano Monte Spina (AMST), Fondi di Baia, and Pigna San Nicola: Smith et al. (2011); 'AAA' cluster: Siani et al. (2004), Sulpizio et al. (2010a); Avellino and Mercato: Santacroce et al. (2008), Tomlinson et al. (2015), Wulf et al. (2004); Campanian Ignimbrite (CI): Smith et al. (2016), Tomlinson et al. (2012a). **(b)** Minoan: Kwiecien et al. (2008); Cape Riva/Y-2: Tomlinson et al. (2015); Dikkartin, Perikartin, Karagüllü: Hamann et al. (2010), Tomlinson et al. (2015); Gabellotto-Fiumebianco/E1: Albert et al. (2017), Caron et al. (2012), de Beaulieu et al. (2017), Siani et al. (2004).

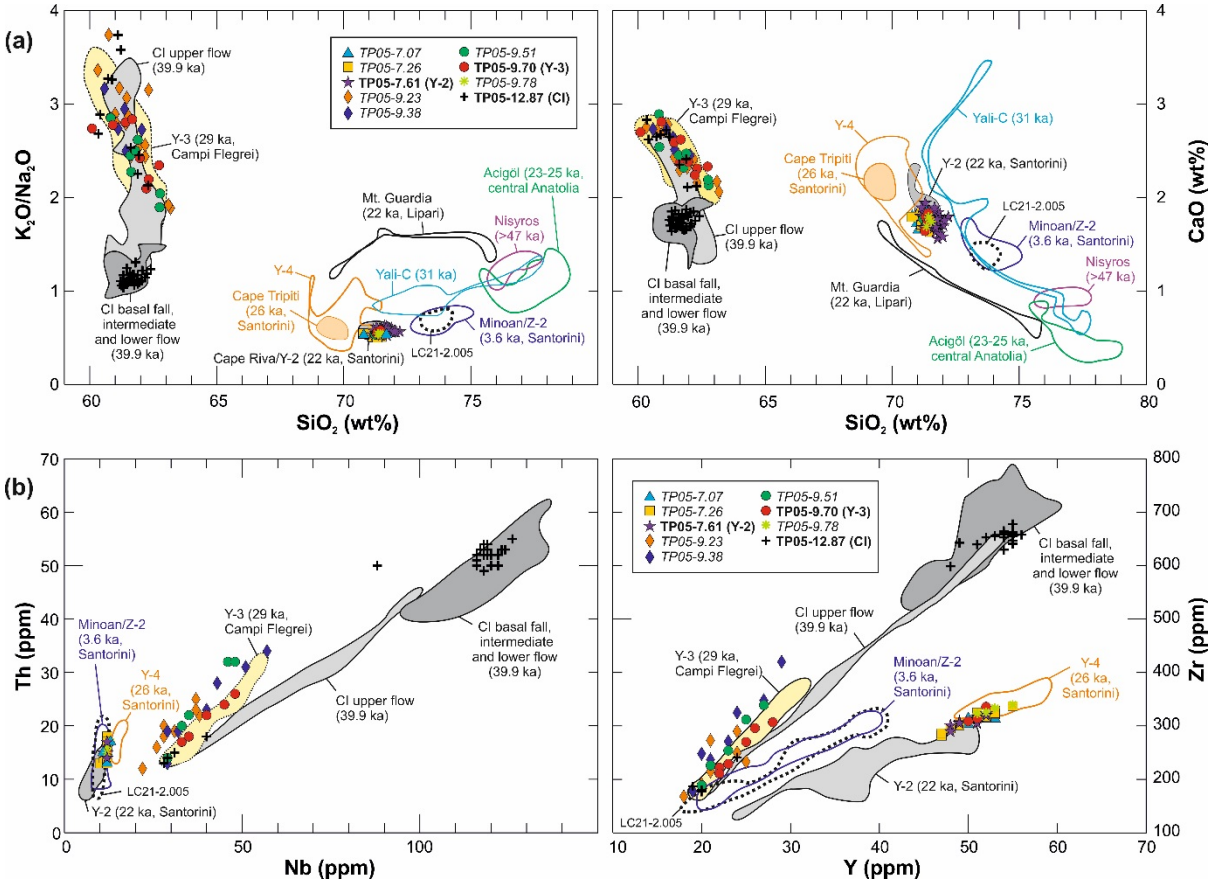

Figure 5: Bivariate plots of **(a)** EPMA major and **(b)** LA-ICP-MS/SIMS trace element glass composition of tephras detected in the 7-13 m depth interval of the TP-2005 sequence. Tephras in bold are interpreted as primary fall deposits, while tephras in italics indicate redeposited material. The reference data used are: Y-3: Albert et al. (2015), Wulf et al. (2004); Campanian Ignimbrite/CI: Smith et al. (2016), Tomlinson et al. (2012a); Mt. Guardia: De Rosa et al. (2003); Nisyros: Tomlinson et al. (2012b); Cape Riva/Y-2, Acigöl: Tomlinson et al. (2015); Yali: Hardiman (1999); Minoan/Z-2: Kwiecien et al. (2008), Satow et al. (2015); Y-4, LC21-2.005: Satow et al. (2015), Vinci (1985); Cape Tripiti: this study (see Supplement 2).

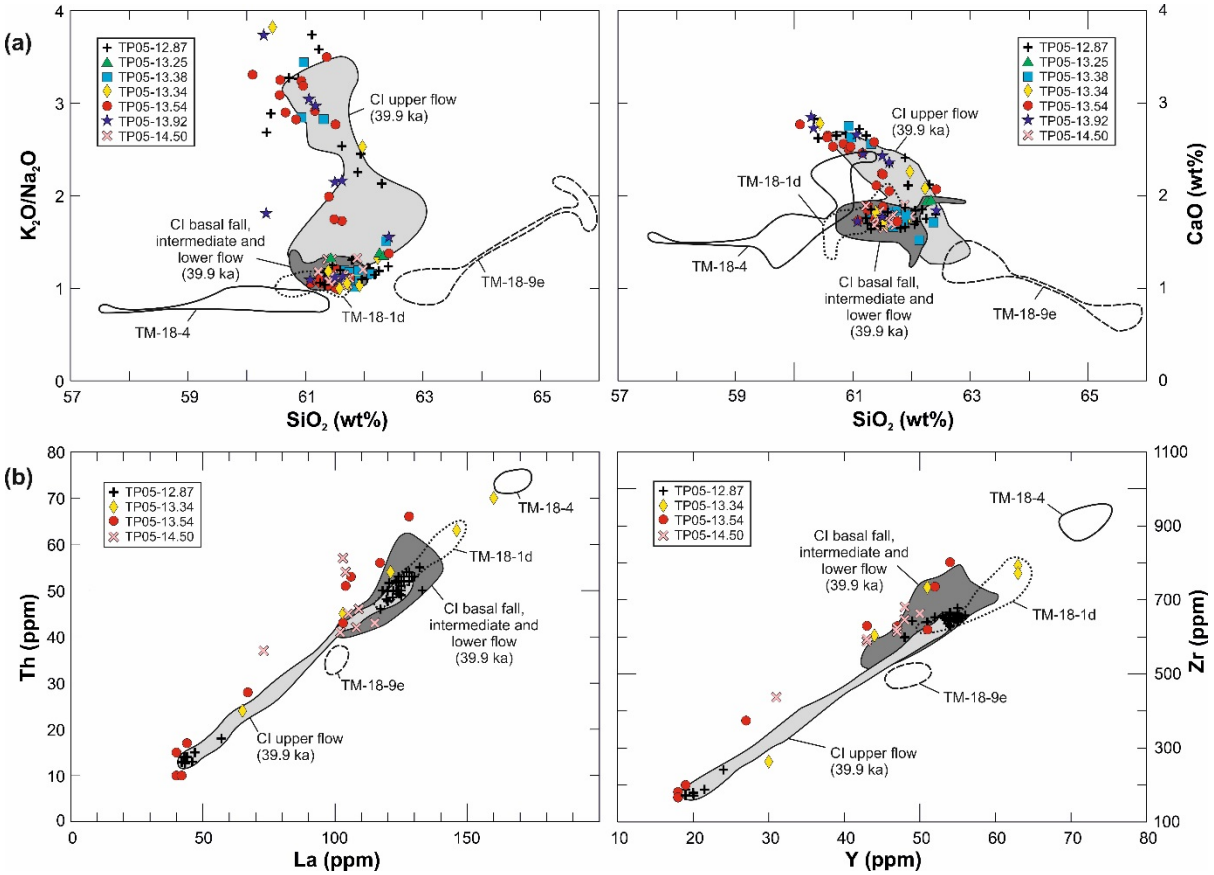

Figure 6: Bivariate plots of **(a)** EPMA major and **(b)** LA-ICP-MS/SIMS trace element chemical compositions of MIS 3 tephras deposited between 12 and 15 m depth in the TP-2005 core and potential proximal tephra equivalents. The data used for this comparison were: Campanian Ignimbrite (CI): Smith et al. (2016), Tomlinson et al. (2015); TM-18-1d, TM-18-4, TM-18-9e: this study (see Supplement 2).

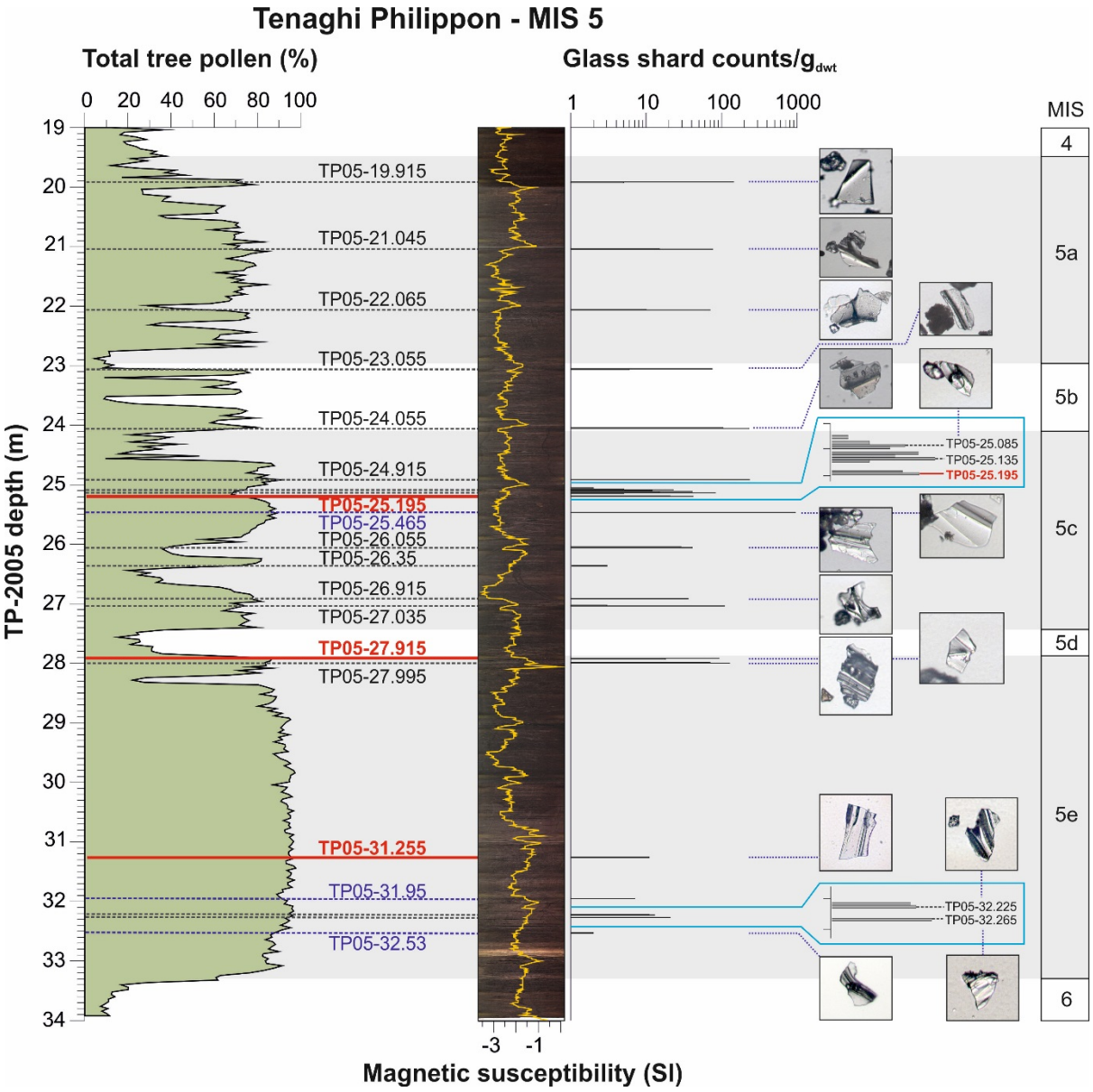

Figure 7: Composite stratigraphic profile of core TP-2005 for the MIS 5 interval showing: total tree pollen curve (Milner et al., 2012, 2013, 2016); photographic images of lithological variations; magnetic susceptibility (Pross et al., 2007); position of cryptotephras; glass shard counts; and transmitted light images of some typical glass shards in the cryptotephra layers. Solid red lines indicate the positions of primary (crypto)tephra layers, dotted black and blue lines indicate reworked and yet unidentified tephra material, respectively. Grey shaded and white areas indicate warmer (MIS 5a, 5c, 5e) and cooler (MIS 5b, 5d) intervals, respectively.

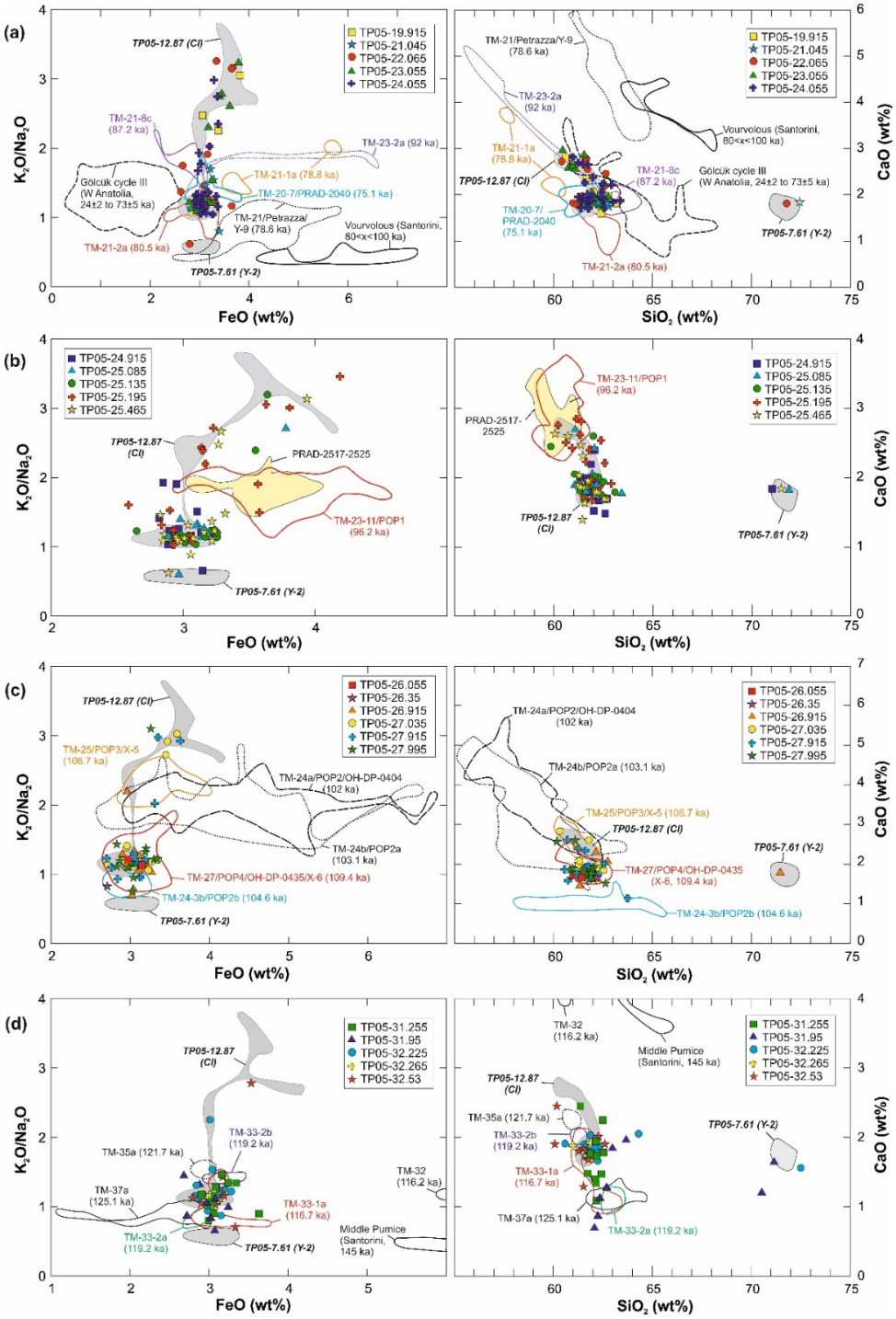

Figure 8: Bivariate plots of FeO *versus* alkali ratio K_2O/Na_2O and SiO_2 *versus* CaO for discriminating between MIS 5 tephras in the TP-2005 sequence. Tephra samples are shown in stratigraphic order: **(a)** TP05-19.915 to TP05-24.055; **(b)** TP05-24.915 to TP05-25.465; **(c)** TP05-26.055 to TP05-27.995; **(d)** TP05-31.255 to TP05-32.53. The reference data used are: Lago Grande di Monticchio tephras (TM): Wulf et al. (2004, 2006, 2012), this study (see Supplement 2); PRAD-2040: Bourne et al. (2010); POP1-POP3: Giaccio et al. (2012, 2013), Regattieri et al. (2017); OH-DP-0404, -0435: Leicher et al. (2016); Vourvoulos, Gölcük cycle III: Tomlinson et al. (2015); Middle Pumice: Druitt et al. (1999). Data of tephras TP05-7.61/Y-2 and TP05-12.87/CI (this study) are included for comparison.

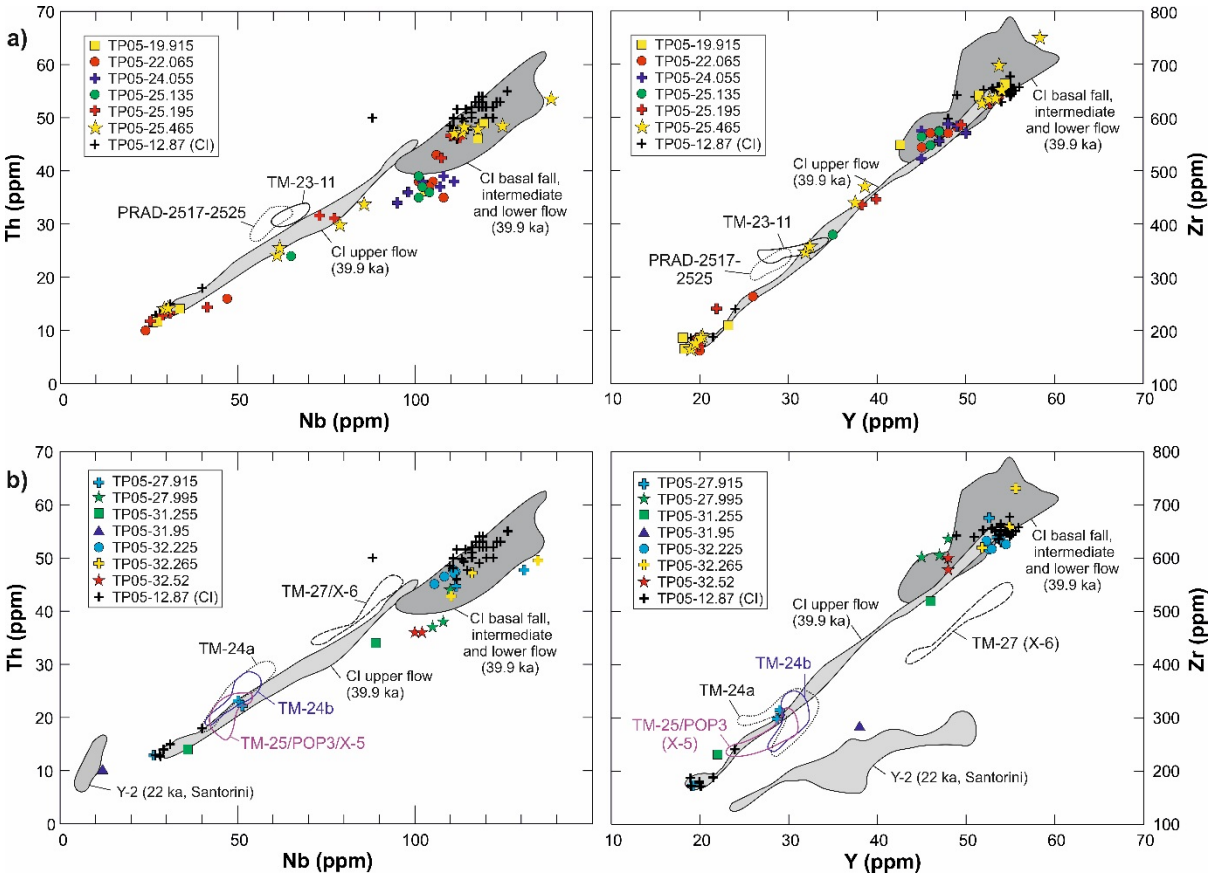

Figure 9: Bivariate plots of trace element ratios of MIS 5 tephras in the TP-2005 sequence, including data for tephra TP05-12.87/CI, shown for comparison. Tephra samples are shown in stratigraphic order: **(a)** TP05-19.915 to TP05-25.465; **(b)** TP05-27.915 to TP05-32.52. The reference data used: Campanian Ignimbrite/CI: Smith et al. (2016), Tomlinson et al. (2012a); Y-2: Tomlinson et al. (2015); PRAD-2517-2525: Bourne et al. (2010, 2015); TM-23-11, TM-27: Bourne et al. (2015); TM-24a, TM-24b, TM-25/POP3: Wulf et al. (2012); X-6: Giaccio et al. (2017b).

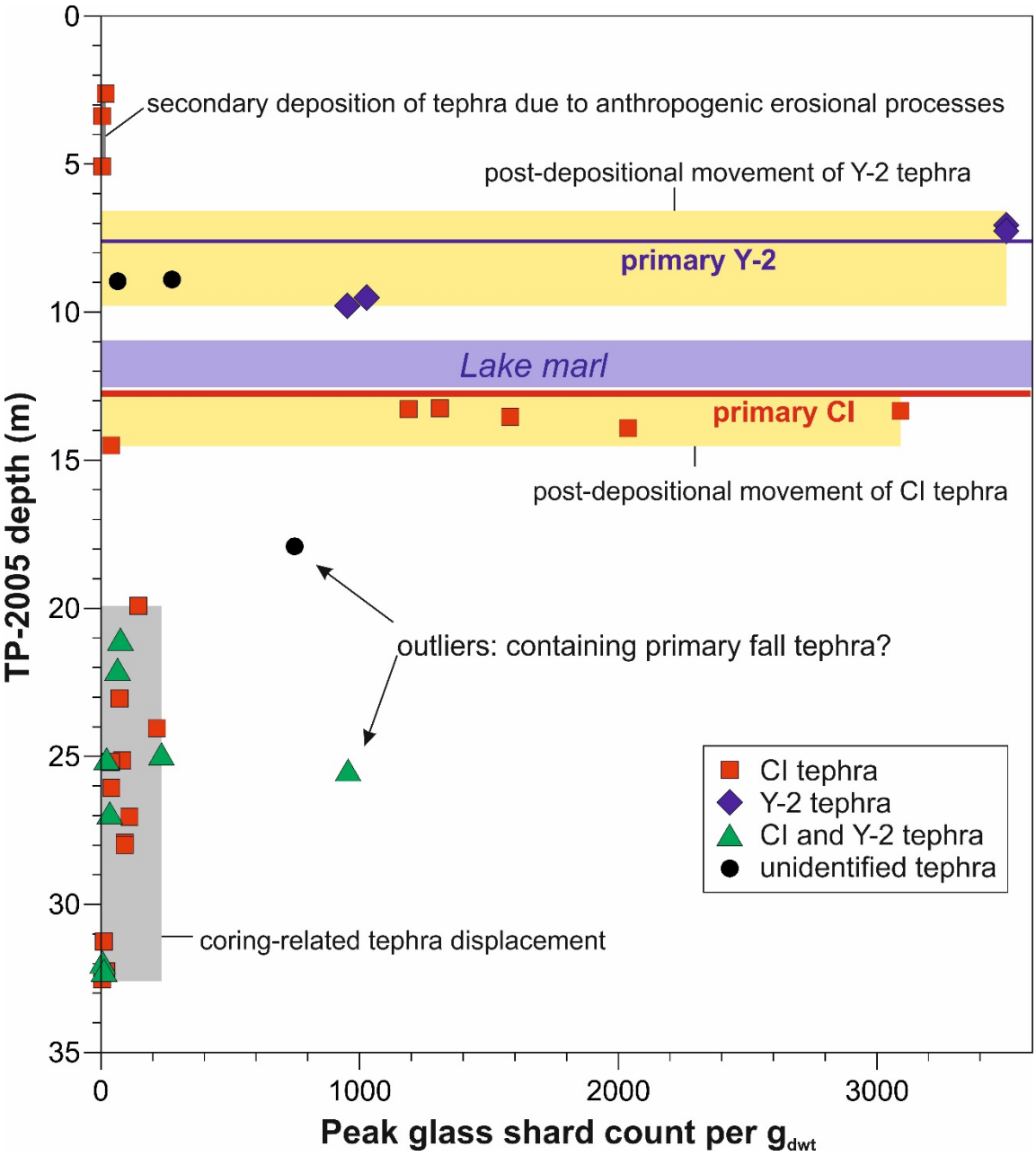

Figure 10: Numbers of glass shard peak concentrations of visible tephra and cryptotephra layers in the TP-2005 sequence that contain CI and/or Y-2 glass components and those of unknown origin. Three types of re-deposition patterns can be distinguished: (1) Post-depositional movement of tephra particles (yellow shaded area next to primary Y-2 and CI tephras); (2) secondary deposition of tephra particles (uppermost grey shaded area); and (3) coring-related displacement of tephra particles (lowermost grey shaded area). Two cryptotephras (TP05-17.91 and TP05-24.465) are outliers that most likely contain an additional primary tephra component.

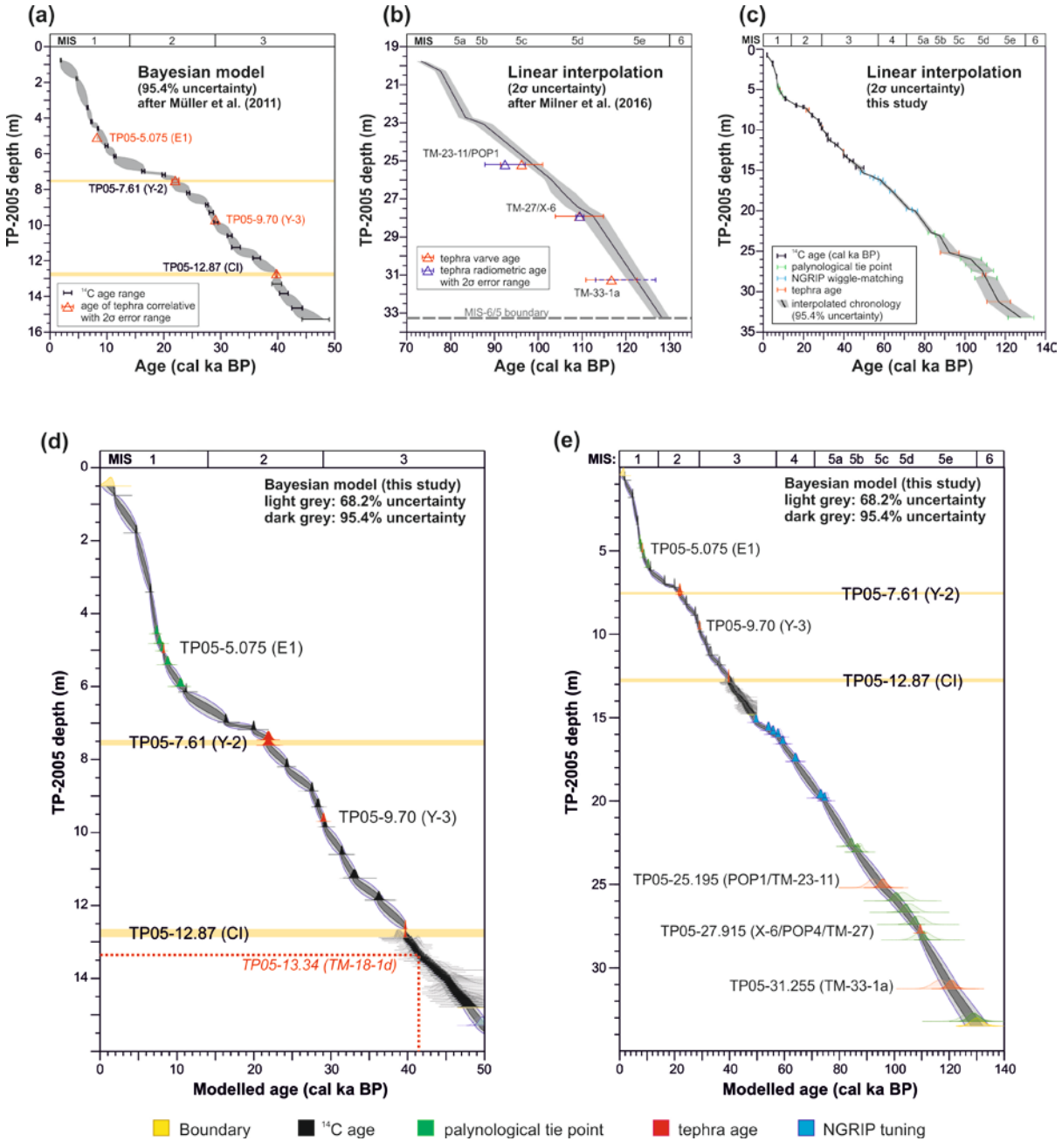

Figure 11: Age-depth plots for the TP-2005 record for the last 130 ka. **(a)** Re-modelled Bayesian radiocarbon chronology of the MIS 1-3 interval after Müller et al. (2011) using the OxCal v4.3 program (Bronk Ramsey, 2008, 2009a) and the IntCal13 calibration curve (Reimer et al., 2013) compared with 2σ-error ranges of ages of tephras identified in TP in this study (red triangles); yellow shading represents the 15-cm-thick Y-2 and 23-cm-thick CI tephras. **(b)** Palynologically tuned age model of the TP MIS 5 interval after Milner et al. (2016) compared with 2σ-error ranges of radiometric dates (blue triangles) and Lago Grande di Monticchio varve ages (red triangles, with 5 % dating error) of tephra correlatives. Dotted blue line represents the range of four K/Ar ages of the Ischia Punta Imperatore eruption (Gillot et al., 1982). **(c)** Linear-interpolated revised chronology of the TP-2005 sequence (this study). **(d)** and **(e)**: Best estimate Bayesian modelled age-depth plot of the last 50 ka (d) and 135 ka (e) of the TP-2005 core with symbol legend shown below; yellow shading represents the 15-cm-thick Y-2 and 23-cm-thick CI tephras. For details see Supplement 3.

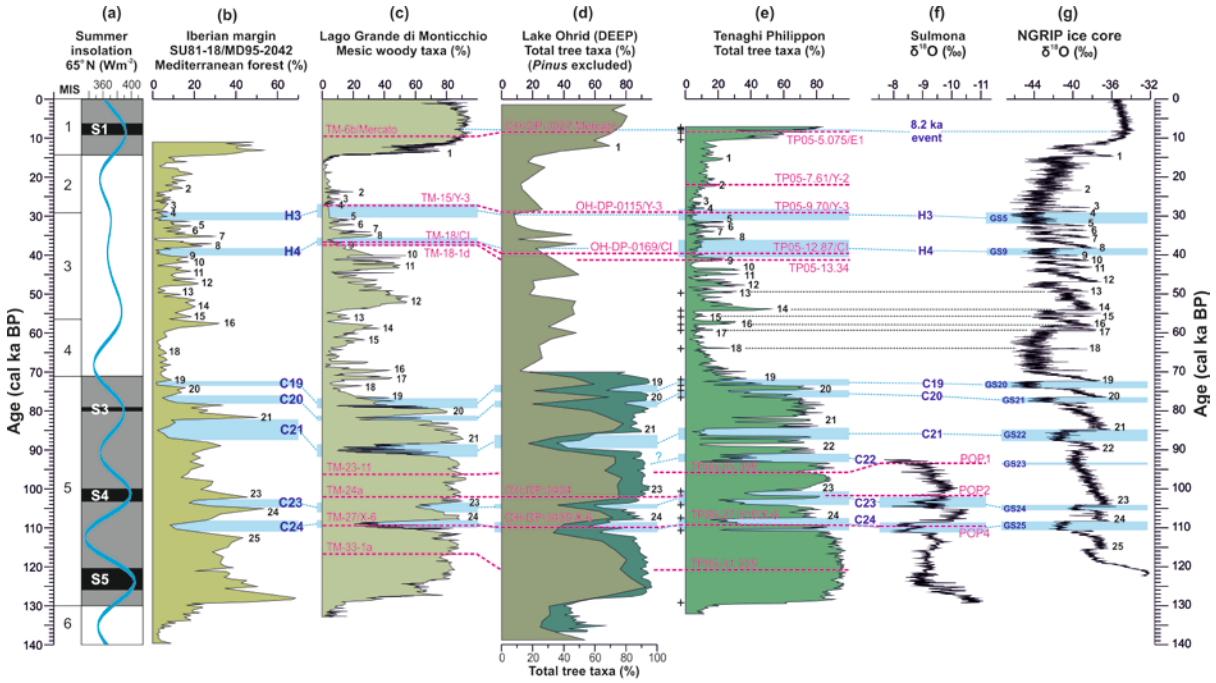

Figure 12: Correlation of Eastern Mediterranean pollen and oxygen isotope records with the NGRIP ice-core record for the last c. 140 ka. **(a)** Marine isotope stages, Eastern Mediterranean sapropel chronology (Schmiedl et al., 1998) and summer insolation curve for 65°N (Laskar et al., 2004). **(b)** Mediterranean forest pollen curve of marine core MD95-2042 from the Iberian Margin (Sánchez Goñi et al., 1999, 2013, 2017); note that the pollen data for the upper 23 ka of this sequence was obtained from surface core SU81-18. **(c)** Record of mesic woody pollen taxa from Lago Grande di Monticchio, southern Italy (Brauer et al., 2007; Martin-Puertas et al., 2014). **(d)** Lake Ohrid low-resolution total tree (excluding *Pinus*) pollen taxa (Sadori et al., 2016) and high-resolution AP curve for MIS 5 (Sinopoli et al., 2018). **(e)** total tree-pollen taxa record of Tenaghi Philippon core TP-2005 re-calibrated to the new time scale (this study, see Supplement 3). Original pollen data are from Milner et al. (2012, 2013, 2016), Müller et al. (2011) and Pross et al. (2009). Crosses mark the positions of palynological tie-points. Note that assignments of stadials and interstadials of the MIS 5 pollen record (Milner et al., 2016) have been revised in this study. **(f)** Oxygen isotope data for the MIS 5 interval from Sulmona basin, central Italy (Regattieri et al., 2017). **(g)** NGRIP oxygen isotope temperature record (NGRIP members, 2004). All records are plotted on their own independent time scales. Pink dotted lines indicate positions of tephra layers; black dotted lines show the tie-points of DO events (black numbers) for tuning the TP vegetation record to the NGRIP oxygen isotope curve. Blue fields and dotted lines indicate cold events/stadials mentioned in the text.

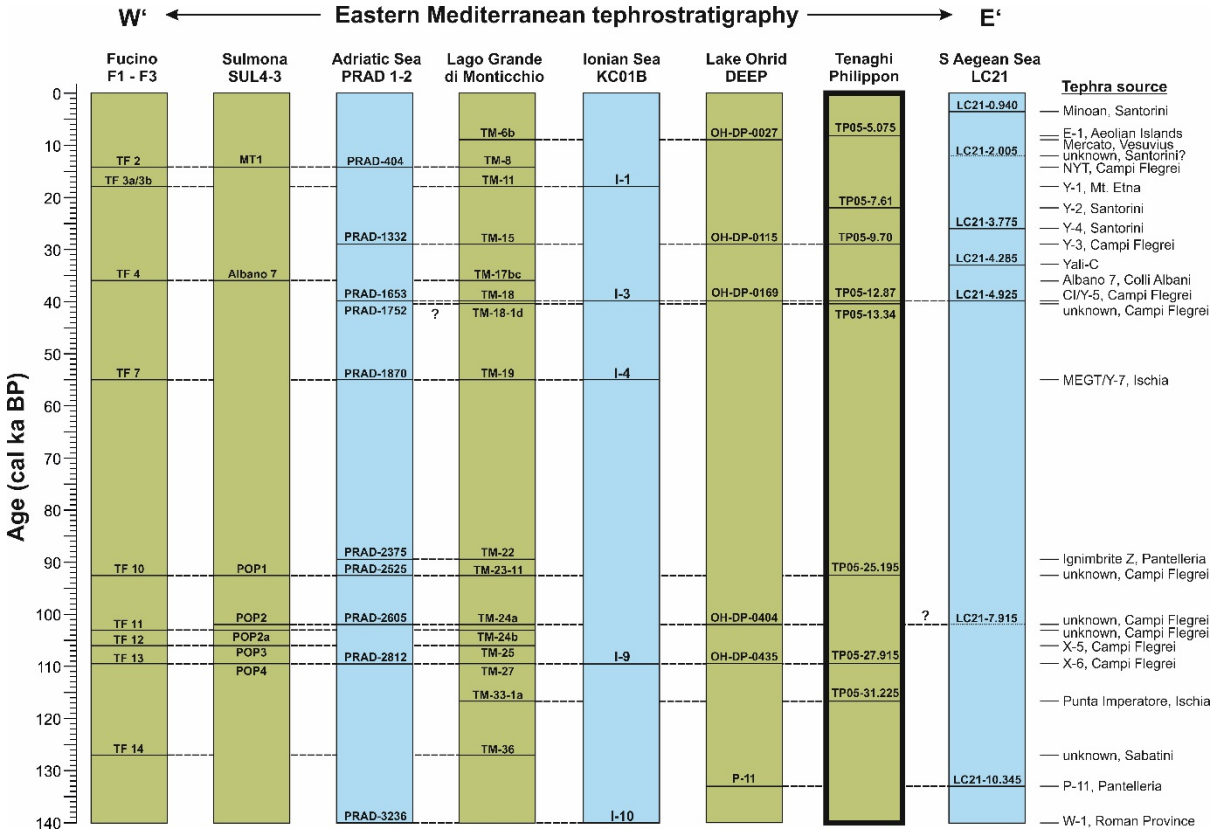

Figure 13: Generalised tephrostratigraphic framework for the Eastern Mediterranean region for the past 140 ka. Green and blue columns indicate archives from terrestrial and marine environments, respectively. The archives included are (from west to east): Fucino (Giaccio et al., 2017b); Sulmona (Giaccio et al., 2012); core PRAD 1-2, Adriatic Sea (Bourne et al., 2010, 2015); Lago Grande di Monticchio (Wulf et al., 2004, 2012); core KC01B, Ionian Sea (Insinga et al., 2014); Lake Ohrid (Leicher et al., 2016); Tenaghi Philippon (core TP-2005; Albert et al., 2015; Müller et al., 2011; Pross et al., 2015; this study); core LC21, South Aegean Sea (Satow et al., 2015).